FINITE ELEMENT ANALYSIS OF BOX GIRDER BRIDGES

A thesis submitted for the degree of
Doctor of Philosophy in the
Faculty of Engineering of
the University of London

by

Kevin Robert Moffatt, B.E.

Imperial College of Science and Technology
London

January 1974

ABSTRACT

A finite element computer program, developed for the linear static analysis of one, two, and three dimensional structures, is briefly described. The program contains several new elements which are especially suitable for use in the analysis of box girder bridges. Details of these elements are given. Model test results are used as a basis for demonstrating the accuracy and efficiency of the elements.

Two parametric studies which were carried out using the program are reported. The first study was concerned with the effect of plan dimensions, cross-sectional properties, support condition, and type of load on shear lag action in steel box girder bridges. The second study was concerned with the effect of the transverse distribution of shear connectors on the longitudinal bending behaviour of simply supported composite box girder bridges. The results of these studies are used as a basis for the formulation of design rules.

A C K N O W L E D G E M E N T S

The investigation described herein was undertaken in the Civil Engineering Department of Imperial College with the kind permission of Professor S.R. Sparkes.

During the course of the investigation, the writer received assistance from many persons. In particular, thanks are due to:

- Dr J.C. Chapman for acting as the writer's immediate supervisor; in this capacity he provided much appreciated guidance and encouragement throughout the course of the investigation
- Dr P.J. Dowling for his guidance over the last year or so of the investigation
- Dr P.T.K. Lim for his advice and especially for his unfailing cooperation in the development of the computer program employed in the investigation
- Mrs J.E. Slatford for her help with the computational aspect of the work
- Mrs A.Lim and Mrs M.Frieze for typing the manuscript
- Mrs M. Rathbone for tracing the tables and figures

Finally, the finacial support received by the writer from Ove Arup and Partners, the British Ship Research Association, and the Department of the Environment is gratefully acknowledged.

CONTENTS

Page

NOTATION

A_F	total cross-sectional area of a flange plate and the associated longitudinal stiffeners
A_W	total cross-sectional area of web plates at a section of a bridge
A_s	cross-sectional area of a stiffener
a,b	dimensions of an element in the x and y directions, respectively
B	half the distance between web centre lines or the distance between a web centre line and the free edge of a flange at the level of the mid-plane of the flange under consideration
B_s	breadth of a stiffener
$[C]$	matrix relating $\{\delta\}$ to $\{\alpha\}$
C^k_{ij}	elastic constant of the k th layer of a laminated element
C_x, C_y	extensional rigidities of a plate in the x and y directions, respectively
C_{xy}	shear rigidity of a plate
C_1	coupling rigidity associated with C_x and C_y
$[D]$	rigidity matrix
D	depth of a box girder
D_s	depth of a stiffener
D_x, D_y	flexural rigidities of a plate in the x and y directions, respectively
D_{xy}	twisting rigidity of a plate
D_1	coupling rigidity associated with D_x and D_y
E	modulus of elasticity in tension and compression for an isotropic material

E_x, E_y — moduli of elasticity in tension and compression for an orthotropic material in the x and y directions, respectively

F — force in a shear connector

F_{TC} — total longitudinal shear force in a transverse row of shear connectors of a composite girder assuming complete interaction

G — modulus of elasticity in shear

h_k — distance from the reference plane of a laminated element to the outer surface of the k th layer of the element

I — second moment of area

I_{cp} — second moment of area of a unit width of composite plate with respect to the neutral axis of the plate (steel units)

I_s — second moment of area of a stiffener with respect to the neutral axis of a stiffener-flange plate assembly

J — determinant of a Jacobian matrix

K — elastic stiffness of a support

K_s — slip modulus of a shear connector

K_{rs} — total slip modulus of a row of shear connectors

$[k]$ — element stiffness matrix

$[\bar{k}]$ — generalized coordinate element stiffness matrix

k — non-dimensional factor depending on D_s/B_s; slip modulus of a shear connexion per unit length of a composite girder

L — length of a girder; distance between adjacent points at which the bending moment is zero

L_w — length of a uniformly distributed load

M — longitudinal bending moment

M_x, M_y	bending moments per unit length of sections of a plate perpendicular to the x and y axes, respectively
M_{xy}	twisting moment per unit length of section of a plate perpendicular to the x axis
m	modular ratio = E_s/E_c
N_x, N_y	normal forces per unit length of sections of a plate perpendicular to the x and y axes, respectively
N_{xy}	shearing force in the direction of the y axis per unit length of section of a plate perpendicular to the x axis
n	number of longitudinal mesh divisions; number of layers in a laminated element
P	magnitude of a point load
$[Q]$	matrix relating $\{\varepsilon\}$ to $\{\alpha\}$
R_{ij}, S_{ij}, T_{ij}	elastic properties of a laminated element
S	spacing of stiffeners
$[S]$	element stress matrix
t	thickness of a plate
t_f	thickness of a flange plate
t_w	thickness of a web plate
U,V	components of displacement in x and y directions, respectively, of a point at a distance z from the reference plane of a laminated element
U,V,W	components of displacement in the X,Y,and Z directions, respectively
u,v,w	components of displacement in the x, y, and z directions, respectively
w_B	deflexion due to the bending component of a load

X,Y,Z	rectangular cartesian global coordinates (right-handed system of coordinates)
x,y,z	rectangular cartesian local coordinates (right-handed system of coordinates)
Z_p	distance from the middle plane of a flange plate to the neutral axis of a stiffener-flange plate assembly
$\{\alpha\}$	vector of α_i coefficients
α	ratio of the cross-sectional area of the longitudinal stiffeners within a breadth B of flange to the cross-sectional area of the associated flange plate within the same breadth
α_i	displacement function coefficient
β	non-dimensional factor $= 2A_F/A_W$
γ	non-dimensional factor $= F\ K_{rs}/F_{TC}\ K_s$
γ_{xy}	shearing component of strain in the xy-plane
$\{\delta\}$	vector of nodal parameters
$\{\varepsilon\}$	strain vector
$\varepsilon_x, \varepsilon_y$	normal components of strain in the x and y directions, respectively
$\theta_x, \theta_y, \theta_z$	components of rotation about the x, y, and z axes, respectively (positive direction determined by right-hand screw rule)
ν	Poisson's ratio for an isotropic material
ν_{xy}	Poisson's ratio for induced strain in the y direction due to a strain in the x direction for an orthotropic material
ν_{yx}	Poisson's ratio for induced strain in the x direction due to a strain in the y direction for an orthotropic material
ξ, η	generalized cartesian coordinates

$\{\sigma\}$	vector of stress resultants and stress couples
σ_B	bending stress
σ_{DB}	distortional bending stress
σ_{DW}	distortional warping stress
σ_x, σ_y	normal components of stress parallel to the x and y axes, respectively
τ	shearing stress
τ_{xy}	shearing component of stress in the xy-plane
ψ	effective breadth ratio

Superscripts

BEF	solution by beam on elastic foundation analogy
c	reference to concrete slab
ETB	solution by elementary theory of bending
FE	solution by finite element method
k	k th layer of a laminated element
P	point load condition
s	reference to steel plate
U	uniform load condition

Subscripts

C	complete interaction condition
c	property of concrete
I	incomplete interaction condition
i	i th nodal point of an element
i,j	i th row and j th column of a matrix
s	property of steel

CHAPTER 1.

GENERAL INTRODUCTION

1.1 INTRODUCTORY REMARKS

In recent years there has been an increasing tendency for designers to adopt box girder construction for medium and long span bridges. This trend has been primarily due to the economic, functional, and aesthetic advantages of the box girder bridge over other types of bridge, coupled with the development of a wider understanding of the behaviour of this structural form.

Box girder bridges have been analysed using techniques based on orthotropic plate theory,[1] the grillage analogy,[2] thin-walled beam theory,[3,4,5] folded plate theory,[6,7] the finite strip method,[8] and the finite element method.[9,10] Of these approaches, the finite element method has proved to be the most versatile and effective. It requires a minimum of simplifying assumptions in the idealization of the bridge and can be readily used for bridges having such features as curved boundaries, irregularly-spaced column supports, and complex variations in material properties. For these reasons, the finite element method has been employed exclusively for the work described in this thesis.

The basic theory of the finite element method and the application thereof to the analysis of structures is now well established, especially in the case of static linear behaviour. However, some detailed development of the method is still required in respect of this behaviour for certain structural types. For example, in the case of some box girder bridges, existing elements may not be able to represent the structural behaviour efficiently or may not permit a sufficiently refined idealization of the structure. Accordingly, part of the work described in this thesis has been concerned with the development and testing of elements that are especially applicable to box girder bridges. These elements have been incorporated into a general purpose finite element program which was developed jointly by Lim[11] and the writer.

In the early design stages of a bridge structure it is not practicable to analyse all the possible structural systems and simple design procedures must be used to identify those systems which warrant a detailed investigation. In the case of box girder bridges there are relatively few simple design procedures available. Accordingly, a further part of the work described in this thesis has been concerned with using the finite element program to obtain the necessary information for the formulation of some such simplified procedures.

1.2 OUTLINE OF THESIS

The thesis consists of seven chapters. This first chapter indicates the general objectives and presentation of the work.

Chapter 2 describes the general purpose finite element computer program which was used for all the finite element analyses reported in this thesis. The program was developed for the linear static analysis of one, two, and three dimensional structures. A level of experimental verification is established for the program by use of results from several model tests.

Chapter 3 describes three higher order elements that are efficient in representing the behaviour of box girder bridges. The practical application of the elements is demonstrated by reference to several single cell box girders and two box girder bridge models.

Chapter 4 describes several elements which are suitable for use in the analysis of box girder bridges having composite top flanges. The analysis may take into account incomplete interaction at the concrete-steel interface. Model test results for a composite box girder bridge, a composite beam, and a composite plate are used as a basis for demonstrating the accuracy of the elements.

Chapter 5 describes a numerical investigation into the influence of in-plane shear strain on the effectiveness of steel box girder bridge flanges. The results of the investigation are used to formulate design rules that enable effective breadths for deflexion and stress calculations to be estimated.

Chapter 6 describes a numerical investigation into the effect of the transverse distribution of shear connectors on the longitudinal bending behaviour of simply supported composite box girder bridges. The implications of the results are noted with respect to the formulation of design rules.

Chapter 7 summarizes the work that was undertaken and draws some conclusions of a general nature.

CHAPTER 2.

DESCRIPTION OF COMPUTER PROGRAM

2.1 INTRODUCTION

The finite element method has proved to be a powerful analytical technique having application to a wide range of structural types. Further, in the application of the method to each different structural type, there is a similarity in the necessary computer code. Thus the method is especially suitable for use as a basis for the development of general purpose structural analysis programs.

A recent survey by Gallagher[12] identified two such types of general purpose program, namely:

(i) programs having an extensive selection of elements, permitting virtually unrestricted modelling capabilities, but restricted to linear static analysis

(ii) programs incorporating, at least to some extent, the capabilities of programs of the first type but more particularly directed towards the representation of certain aspects of non-linear and dynamic behaviour.

This chapter briefly describes a program of the first type and the application thereof to the analysis of five models. The program, developed jointly by Lim[11] and the writer, is referred to as ICSAS which is the acronym for Imperial College Structural Analysis System.

2.2 SCOPE OF PROGRAM

ICSAS has been developed for the linear static analysis of one, two, and three dimensional structures. The elements in the ICSAS system which can be used for the analysis of various types of structure are shown in Table 2.1.

2.3 ORGANIZATION OF PROGRAM

A simplified flow diagram for an analysis by ICSAS is given in Fig.2.1. Each processor in the flow diagram represents a number of subroutines. A simple main routine calls the various subroutines in a sequence appropriate to the problem being solved.

Briefly the functions performed by the various processors are as follows:

(i) The Data Processor reads the input cards and generates arrays of nodal coordinates, element topology, material properties, matrix partitioning information, boundary conditions, and load conditions.

(ii) The Assembly Processor generates the upper half of the overall stiffness matrix in tridiagonalized form and the stress matrices for the elements.

(iii) The Restraint Processor modifies the overall stiffness matrix and the load vectors in accordance with the restraints imposed on the structure.

(iv) The Solution Processor solves for the displacements of the nodes in the global coordinate system. A forward elimination and backward substitution procedure is used with the inverse of each submatrix being obtained by means of the Cholesky square root method.

(v) The Stress Processor evaluates the stresses in each element with respect to their local coordinate system.

(vi) The Output Processor produces the results in a form specified by the user.

The modularity of the ICSAS system enables new facilities to be introduced quickly and easily. Furthermore, it allows the computer core storage requirements to be minimized by means of one of the following procedures:

(i) The program may be stored on tape or disc and only the subroutines applicable to a particular problem are loaded into the computer core storage. This process involves assembling a control deck for each different type of problem and is only useful if the necessary subroutines do not exceed the capacity of the computer core storage. For a typical analysis of a box girder bridge ICSAS requires between 45 and 60 K words of core storage when this procedure is used.

(ii) The program may be divided into several independent groups of subroutines which are called into the computer core storage from tape or disc as needed. Only the group of subroutines required at each stage of the computation of the problem are located in the computer core storage. This procedure requires an overlay facility which is provided by most present day computers. ICSAS can be implemented on a machine having a core storage of 32 K words when this procedure is used.

2.4 SOME FACILITIES OF PROGRAM

In addition to the usual facilities of a general purpose structural analysis system, ICSAS has a number of special facilities some of which are described below.

2.4.1 Machine independence

A high degree of machine independence has been achieved by using ANSI[a] Fortran for all but a very small part of the program.

(a) American National Standards Institute

ICSAS is intended for use on a computer having a core storage of at least 32 K words and has been implemented on the CDC 6400, CDC 6600, IBM 7094, ICL Atlas, and Univac 1108 computers.

2.4.2 Flexible input facilities

ICSAS has been programmed to accept alphanumeric data, the meaning of which is to a large extent self-evident to the structural engineer. Free format facilities have been provided where it has been considered convenient for the user. Data generation facilities which enable the user to take full advantage of any repeated data pattern have been included.

Considerable choice is given in the manner in which loads may be applied, including a facility for specifying fictitious nodes and elements which may be loaded directly. These loads will then be automatically distributed on to the nodes defining the structure, in accordance with either static or virtual work principles. This facility is particularly useful for describing Type HA or HB loadings.

A comprehensive description of many of the ICSAS input facilities is given in Ref.13.

2.4.3 Flexible output facilities

The output may be in one or more of the following forms: computer paper, punch card, paper tape, and magnetic tape. Any particular set of results may be obtained by means of a selective output facility. Sectional plots may also be obtained.

2.4.4 User-program interface facility

By means of simple commands in the input data, ICSAS can be instructed to communicate with routines, supplied by the user, at various stages of execution of a problem. This facility may enable the user to adapt ICSAS, if necessary, to suit his own special requirements. For example, the user may employ this facility to generate special input data, to produce selective output, and to post-process the results.

2.4.5 Computer cost saving facilities

The computer time required for assembling the stiffness matrix of the overall structure may be reduced by means of a facility which enables those elements which have the same stiffness matrix to be declared as similar elements. The stiffness matrix for each set of similar elements need then be evaluated only once.

ICSAS considers multiple load cases in groups of five, say, at a time, but there is no limit on the number of such groups which can be treated serially. The forward elimination process is only performed once, the eliminated form of the stiffness matrix being stored on tape or disc for the next group of load cases or for future runs.

2.4.6 Post-processing facilities

By using simple commands in the input data, the user can create new load cases as combinations of other load cases. The newly formed load case may then be stored and treated exactly like any other load case in further combinations.

2.4.7 Special elements for analysis of box girder bridges

ICSAS contains several elements that have been especially developed for use in the analysis of box girder bridges. These are:

(i) A quadrilateral shell element Q33[b] which is efficient in representing the overall behaviour of box girder bridges[14]

(ii) A triangular shell element T33 which, in conjunction with rectangular elements of the type (i), is suitable for use in the analysis of skewed box girder bridges (see Section 3.2)

(iii) A quadrilateral shell element Q43 which, in addition to being efficient in representing the overall behaviour of box girder bridges, is particularly suitable for use in rapidly varying stress fields (see Section 3.2)

(iv) A triangular shell element T43 which, in conjunction with rectangular elements of the type (iii), is suitable for use in the analysis of skewed box girder bridges (see Section 3.2)

(b) For ease of identification, those elements which are referred to several times in this thesis have been given a name that consists of a letter followed by one or two numerals. The letter signifies the shape of the element. The following list of letters have been adopted: T (triangle), R (rectangle), and Q (quadrilateral). The numerals refer to the number of degrees of freedom at each node of the element. Where there are two numerals, the first indicates the number of extensional degrees of freedom while the second indicates the number of flexural degrees of freedom. Where there is one numeral only, it indicates the total number of extensional and flexural degrees of freedom. The summation of the extensional and flexural degrees of freedom signifies the fact that there is coupling between these two sets of degrees of freedom.

(v) Beam-type elements which enable multi-cell bridge decks to be idealized as two dimensional structures[11]

(vi) Shell elements which can be used to represent laminated materials such as those occurring in composite box girder bridges (see Section 4.2)

2.5 EXPERIMENTAL VERIFICATION OF PROGRAM

The verification of ICSAS has been made by reference to results obtained from classical theory, other programs, and experimentation. This section briefly describes some of the experimental verification work.

2.5.1 Curved slab bridge model

The curved slab bridge model shown in Fig.2.2 was analysed[15] using two subdivisions into basic triangular flexural elements[9] and a subdivision into quadrilateral flexural elements.[15] Figure 2.3 shows the coarse subdivision of the idealized model into triangular elements. The nodal points for the subdivision into quadrilateral elements corresponded with those shown in Fig.2.3. Some comparisons between the analytical and experimental results for the model under dead load are shown in Figs 2.4 to 2.7; further results are given in Ref.15. It can be seen that the theoretical and experimental results are in close agreement, except in the case of the bending moment values near the supports. This localized discrepancy is due to the limitations of classical thin plate theory on which the analyses are based.

Thin plate theory predicts infinite bending moments under point loads or point reactions and hence the theoretical moments obtained in the vicinity of the supports merely reflect the refinement of the mesh in these regions. Lim and the writer[15] presented a technique by means of which a mesh size can be selected to give good estimates of local bending moments. Application of this technique to the analyses under consideration indicates that the moment values in the region of the supports, as given by the subdivision into triangular and quadrilateral elements, should be below and above the experimental values, respectively. Reference to Figs 2.5 to 2.7 shows this to be the case.

2.5.2 Straight composite beam and slab bridge model

The beam and slab bridge model shown in Fig.2.8 was analysed using a finite difference program and ICSAS.[16] In the finite element analysis the slab was represented by basic rectangular shell elements[9] and the eccentric beams were represented by line elements.[17] Owing to symmetry only one half of the model was analysed with the finite element discretization shown in Fig.2.9. Some comparisons of the finite element, finite difference, and experimental results for the model under a point load placed eccentrically at the mid-span are given in Figs 2.10 to 2.12. It can be seen that the results are in satisfactory agreement.

2.5.3 Ship's double-bottom model

A one-eighth scale model of the double-bottom of one complete hold of a dry cargo ship was tested experimentally[18] and analysed using ICSAS.[19] In the test the model was simply supported along all four edges and uniformly loaded by means of a pressure bag. For the analysis the model was idealized as a two dimensional assemblage of elements of the type described by El-gaaly.[20] Owing to double symmetry only one quarter of the model was analysed with the mesh shown in Fig.2.13. Some comparisons between the finite element and experimental results are given in Figs 2.14 and 2.15. It can be seen that the results are all in close agreement.

2.5.4 Curved single cell box girder bridge model

The box girder bridge model shown in Fig.2.16 was analysed using various finite element idealizations.[14] The analytical results shown in Fig.2.18, for the model under a Type HB loading (Fig.2.16), were obtained using the element Q33 with the subdivision shown in Fig.2.17. It can be seen that the finite element and experimental results are in close agreement except in the region of the tapered side cantilevers which were simply represented by elements of constant thickness.

2.5.5 Straight single cell box girder model

The quarter scale steel box girder model shown in Fig.2.19 was tested experimentally[21] and analysed using ICSAS. For the analysis, the model was idealized as an assemblage of basic rectangular extensional elements[9] and bar elements. The element subdivision used in the analysis was derived by attempting to represent all the structural features of the model. Owing to double symmetry only one quarter of the model was analysed; a typical cross-sectional arrangement of nodes is shown in Fig.2.20. Some comparisons between the finite element and experimental results for a load of 10 tons in each jack are given in Figs 2.21 to 2.23. It can be seen that, in general, the results are in close agreement; the large discrepancy at the web-tension flange junction is possibly due to residual stresses induced in the plates during the welding of the box.

As a further part of the investigation, the value of the stress effective breadth ratio[c] at the mid-span in the tension flange was determined from the finite element solution as 0.59. The design rules proposed in Section 5.5 give a corresponding value of 0.61.

2.5.6 Other Models

Further models that have been analysed using ICSAS include a straight three cell box girder bridge (Sub-section 3.3.3), a skewed composite twin cell box girder bridge (Sub-section 4.3.1), a straight composite beam (Sub-section 4.3.2), a square composite plate (Sub-section 4.3.3), a multi-cell bridge deck,[11] an oil tanker,[22] and a shear wall.[23] The writer was not directly associated with the analyses of the last three mentioned models and therefore the work has not been reported in this thesis.

2.6 CONCLUSIONS

A general purpose finite element program (ICSAS) has been described briefly. Its practical application has been illustrated by reference to the analysis of five models.

(c) For the definition of stress effective breadth ratio, see Section 5.2.

CHAPTER 3.

SOME ELEMENTS HAVING PARTICULAR APPLICATION TO BOX GIRDER BRIDGES

3.1 INTRODUCTION

Early finite element analyses of box girder bridges[24,25,26] employed the basic rectangular shell element R23, the stiffness matrix of which is obtained from the stiffness matrices of the basic extensional and flexural elements.[9] This element has at each of its nodal points two in-plane degrees of freedom u and v and three out-of-plane degrees of freedom w, θ_x, and θ_y (Fig.3.1), but no in-plane rotational degree of freedom θ_z. A large number of these elements must be used in the analysis of a box girder bridge since the element is not well suited to representing the predominate in-plane bending action of the webs.

Lim et al.[14] and Sisodiya et al.[27] have achieved more economical solutions by using a quadrilateral shell element Q33, the stiffness matrix of which is formed from the stiffness matrices of a higher order extensional element Q30 and the basic flexural element.[15] This shell element has a biased, beam-type, in-plane displacement field by virtue of the presence of a further in-plane degree of freedom $\partial v/\partial x$ at each node in place of the "free" in-plane rotation θ_z. This displacement field can closely approximate the deformation of the webs of a box girder bridge and the overall behaviour of the bridge therefore can be obtained with the use of a relatively coarse mesh division in the longitudinal direction. However, as in the case of the element R23, this element has the disadvantage that the in-plane longitudinal strain cannot vary over the length of the element. Consequently, an accurate estimation of the local stresses in the region of an intermediate support or a wheel load would require the use of a localized fine mesh division and an extrapolation procedure.

The question arises, therefore, as to whether more economical solutions could be obtained by using elements having higher order displacement functions. The specification of higher order displacement functions requires the introduction of either additional nodal continuities or additional side nodes. For the same order of displacement functions, the introduction of additional continuities rather than additional nodes results in a smaller number of unknowns and a smaller bandwidth in the stiffness matrix of the overall structure. These observations have lead the writer to develop a higher order quadrilateral element Q43, which has a further degree of nodal continuity $\partial u/\partial x$ chosen to permit a variation of the in-plane longitudinal strain over the length of the element. A description of this element is given in this chapter.

In the idealization of skewed box girder bridges it is often convenient to use rectangular elements and to adjust the mesh to the skewed boundaries using triangular elements (see the example of Subsection 4.3.1). Also, studies have shown that for a given number of nodes more accurate results are obtained when rectangular and triangular elements are used instead of parallelogrammic elements to idealize a skewed region.[28] For these reasons, two triangular elements T33 and T43, that are suitable for use with the elements Q33 and Q43 respectively, are also presented in this chapter.

In parallel with the development of higher order elements there is a need for comparative studies of the effect of element type and size on accuracy in order that recommendations may be made on the use of the elements. Several theoretical and model test results are used as a basis for such a study in this chapter.

3.2 DESCRIPTION OF ELEMENTS

This section describes a quadrilateral extensional element Q40, and two triangular extensional elements T30 and T40. The stiffness matrices for the shell elements Q43, T33, and T43 are formed from those of the elements Q40, T30, and T40, respectively, and from the basic quadrilateral flexural element[15] or the basic triangular flexural element,[9] as appropriate.

3.2.1 Quadrilateral element Q40

The element Q40 has four nodes, each of which has a nodal parameter vector $\{\delta\}_i$ defined as

$$\{\delta\}_i = \begin{Bmatrix} u \\ v \\ \partial v/\partial x \\ \partial u/\partial x \end{Bmatrix}_i$$

where u and v are translations parallel to the x and y axes of the element, respectively. Such a choice of nodal parameters enables the element displacement functions to be specified as follows:

$$u = \alpha_1 + \alpha_2\xi + \alpha_3\eta + \alpha_4\xi^2 + \alpha_5\xi\eta + \alpha_6\xi^3 + \alpha_7\xi^2\eta + \alpha_8\xi^3\eta$$

$$v = \alpha_9 + \alpha_{10}\xi + \alpha_{11}\eta + \alpha_{12}\xi^2 + \alpha_{13}\xi\eta + \alpha_{14}\xi^3 + \alpha_{15}\xi^2\eta + \alpha_{16}\xi^3\eta$$

where ξ and η are the generalized coordinates of the element (Fig.3.2), and α_1 to α_{16} are arbitrary coefficients. These displacement functions satisfy the compatibility condition for continuous displacement between adjacent elements and the constant strain criterion for rectangular, parallelogrammic, and trapezoidal elements but not for a general quadrilateral element. (A similar comment can be made in respect of the element Q30. However, Sisodiya et al.[27] have shown that good results can be obtained when the element Q30 is used as a general quadrilateral.) Details of the formulation of the stiffness matrix for the element Q40 are given in Appendix A.

The following points refer to the use of the element Q40:

(i) Each element should be orientated such that its x-axis is in a direction parallel to the direction of the predominant bending stresses in the structure.

(ii) In the assembly of the stiffness matrix of the overall structure, the element stiffness terms corresponding to the strain component $\partial u/\partial x$ may be treated as a local degree of freedom, for which no transformation to the global coordinate system is necessary.

(iii) The element should, in general, not be used in cases where an abrupt change of a plate property gives rise to a discontinuity in the strain component $\partial u/\partial x$.

3.2.2 Triangular element T30

The element T30 has three degrees of freedom u, v, and $\partial v/\partial x$ at each of its three nodes and has the following displacement functions:

$$u = \alpha_1 + \alpha_2 x + \alpha_3 y$$

$$v = \alpha_4 + \alpha_5 x + \alpha_6 y + \alpha_7 x^2 + \alpha_8 xy + \alpha_9 x^3$$

These displacement functions satisfy the constant strain criterion, while the compatibility condition for continuous displacement between this element and the element Q30 will be satisfied when the elements are assembled as shown in Fig.3.3. The stiffness matrix for the element T30 therefore has been derived for the limiting case of a right-angled triangle; details of the formulation are given in Appendix B.

3.2.3 Triangular element T40

The element T40 has four degrees of freedom u, v, $\partial v/\partial x$, and $\partial u/\partial x$ at each of its three nodes and has the following displacement functions:

$$u = \alpha_1 + \alpha_2 x + \alpha_3 y + \alpha_4 x^2 + \alpha_5 xy + \alpha_6 x^3$$
$$v = \alpha_7 + \alpha_8 x + \alpha_9 y + \alpha_{10} x^2 + \alpha_{11} xy + \alpha_{12} x^3$$

These displacement functions satisfy the constant strain criterion, while the compatibility condition for continuous displacement between this element and the element Q40 will be satisfied when the elements are assembled as shown in Fig.3.3. Again, the stiffness matrix for the element has been derived for the limiting case of a right-angled triangle; details of the formulation are given in Appendix B.

3.3 APPLICATIONS

In this section several single cell box girders, for which theoretical results are available, are used as a basis for comparing the accuracy of the shell elements referred to in this chapter. Following this, the elements Q33 and Q43 are used in the analysis of two box girder bridge models.

3.3.1 Straight single cell box girders

Details of the first box girder that was considered are given in Fig.3.4. The girder was analysed for both simply supported and fixed ended conditions. End diaphragms having infinite rigidity in their own plane were assumed. In the case of the simply supported condition it was assumed that there was no end restraint against warping. In the case of the fixed ended condition the ends of the box were fully restrained against warping.

The girder was considered to be loaded at the mid-span by a point load over one web. The bending and distortional components of the load (Fig.3.4) were treated separately in order that the results could be compared with those obtained using the elementary theory of bending (ETB) and the beam on elastic foundation analogy (BEF),[4] respectively. The torsional component of the load has not been considered here since the only stresses of any significance that it would induce are shearing stresses.

The girder was analysed using the elements R23, Q33, and Q43 with one mesh division over the width and depth, and from 2 to 64 mesh divisions in the longitudinal direction of the girder (Fig.3.5). (Since each cell wall was represented by a single row of elements, the solutions so obtained are consistent with the ETB and BEF solutions in that, in each case, the longitudinal strain distribution is assumed to vary linearly over the depth of the webs and across the width of the flanges.)

The values at the mid-span of the deflexion W_B and longitudinal stress σ_B, caused by the bending component of the load, and the distortional warping stress σ_{DW} and transverse distortional bending stress σ_{DB}, caused by the distortional component of the load, obtained using the various mesh divisions are given in Table 3.1. It can be seen that for each of W_B, σ_B, σ_{DW}, and σ_{DB}, the results obtained using the three elements converge to the same value, with the element Q43 giving the best convergence characteristics. The values given by the finite element analyses do not converge exactly to those given by the ETB and BEF because these techniques involve additional simplifying assumptions not made in the finite element analyses.

It should be noted that in the case of the two lower order elements, for which the longitudinal extensional strain is constant over the length of the element, the values of σ_B and σ_{DW} do not strictly pertain to the position directly under the load. An extrapolation procedure could be employed to obtain the peak values of σ_B and σ_{DW}. However, by using the element Q43 it is possible to obtain such peak values directly, for the same computer cost.

For example, the simply supported girder with a 4 by 1 by 1 division into Q43 elements gives differences between the finite element values and the simple theory values for W_B, σ_B, σ_{DW}, and σ_{DB} of 1, 1, 11, and 4 per cent, respectively, when non-dimensionalized using W_B^{ETB} for the deflexion and σ_B^{ETB} for the stresses. The corresponding values obtained using a 6 by 1 by 1 division into Q33 elements and an extrapolation formula of the highest possible order, namely a parabola, are 3, 3, 6, and 2. It should be emphasized that these two idealizations involved approximately the same computer cost.

In order that the effect of element aspect ratio on accuracy could be examined, simply supported girders having the same cross-sectional dimensions and material properties as the box shown in Fig.3.4 but of varying spans, were analysed using the elements R23, Q33, and Q43 with an 8 by 1 by 1 mesh division. The girders were considered to be loaded by a point load over each web at the mid-span. It is evident from Table 3.2 that the accuracies obtainable with the elements Q33 and Q43 are relatively independent of the aspect ratio of the elements; however, in the case of the element R23 the accuracy of the results deteriorates rapidly as the aspect ratio of the elements increases above unity. The same trends were obtained with other mesh divisions.

3.3.2 Skewed single cell box girder

The box girder shown in Fig.3.6 was used to investigate the effect of employing triangular and rectangular elements instead of parallelogrammic elements in the skewed regions of box girders. Idealizations based on the element Q33, the elements T33 and Q33, the element Q43, and the elements T43 and Q43 were considered. Figure 3.7 shows the finite element discretizations of the girder used in the investigation.

Some values of displacement for the girder under a point load P over each web at the free end are given in Table 3.3. The results indicate that an idealization based on a combination of triangular and rectangular elements is likely to give a slightly more flexible structure than the corresponding idealization based on parallelogrammic elements.

It is encouraging that such an observation may be made, since an idealization based on elements which employ displacement functions generally over-estimate the overall stiffness of box girder bridges.

3.3.3 Straight three cell box girder bridge model

Figure 3.8 shows the details of a straight three cell box girder bridge model which was analysed using the elements Q33 and Q43. The model, a 1/60th scale representation of an approach span to the Lower Yarra Bridge, Melbourne, was made of Perspex. Details of the instrumentation of the model are given in Fig.3.9. The results presented here are for a load placed eccentrically on the model by means of a cantilever at the mid-span (Fig.3.8).

Owing to symmetry only one half of the model was analysed with the finite element discretizations shown in Fig.3.10. In both idealizations the diaphragms were represented by Q33 elements and the support stiffnesses were transformed to the nodes at the outer webs assuming the diaphragms to be infinitely rigid in their own plane. The idealizations were selected so that the analyses involved approximately the same computer cost.

The experimental results of displacements and strains are given in Figs 3.11 to 3.13. These results compare well with the finite element results (Figs 3.12 to 3.14). In particular, it should be noted that good results have been obtained with the element Q43 notwithstanding the abrupt change in thickness of the inner webs.

3.3.4 Curved single cell box girder bridge model

Further experimental verification of the finite element analysis of box girder bridges using the elements Q33 and Q43 was provided by a comparison with some of the experimental results obtained from the model shown in Fig.2.16 and described in Ref.14.

The model was analysed using a 6 by 3 by 1 division into Q33 elements and a 4 by 3 by 1 division into Q43 elements (Fig.3.15). In both idealizations the diaphragms were represented by Q33 elements. The two analyses involved approximately the same computer cost.

The experimental results obtained for a point load of 100 lbf placed over the outer web at the mid-span are given in Fig.3.16. It can be seen from Fig.3.17 that the two sets of finite element results and the experimental results are in close agreement. It should be noted that in the case of the element Q33 it was necessary to use an extrapolation procedure in order to obtain the results shown, whereas in the case of the element Q43 it was possible to obtain the results directly.

3.4 CONCLUSIONS

(i) A shell element Q43 that is efficient in representing the behaviour of box girder bridges has been developed. The criteria for convergence are satisfied when the element is of rectangular, parallelogrammic, or trapezoidal shape, and it can therefore be used for the analysis of right, skewed, or curved box girder bridges having constant width and depth.

(ii) Theoretical results for several single cell box girders, and experimental results for two box girder bridge models, have been used as a basis for comparing the efficiency of this element with that of two elements (R23 and Q33) commonly employed in the analysis of box girder bridges. The comparisons showed that the element Q43 is much more efficient than the element R23, but only as efficient as the element Q33. However, the element Q43 has the advantage that the peak longitudinal stress values can be obtained directly. In particular, the comparisons showed that the accuracy of the results obtained using the element R23 deteriorates rapidly as the aspect ratio (length/depth) of the web elements increases above unity, whereas that obtained using the elements Q33 and Q43 is relatively independent of the element aspect ratio. Reliable results can be obtained using the elements Q33 and Q43 with as few as six and four mesh divisions, respectively, along the span and with one mesh division over the depth of the web.

(iii) Two triangular shell elements T33 and T43 have been developed for use with the elements Q33 and Q43, respectively. With the availability of these elements it is possible to analyse a skewed box girder bridge using a subdivision into triangular and rectangular elements.

(iv) A skewed single cell box girder was analysed using several different mesh schemes; the analyses were made using the elements T33 and Q33, the elements T43 and Q43, the element Q33 only, and the element Q43 only. It was found that, for the cases studied, an idealized structure based on a combination of triangular and rectangular elements was generally slightly more flexible than one based on parallelogrammic elements and having the same number of nodes.

CHAPTER 4.

SOME ELEMENTS HAVING PARTICULAR APPLICATION TO COMPOSITE BOX GIRDER BRIDGE DECKS

4.1 INTRODUCTION

A form of bridge construction that has been used in recent years is one in which a concrete deck slab is connected, by means of shear connectors, to one or more closed steel box girders (Fig.4.1). Generally, the connectors are distributed over the contact area between the concrete slab and the steel plate to ensure that these structural elements act as a composite plate.

In the analysis of this type of bridge it is commonly assumed that there is complete interaction between the concrete slab and steel plate, and that the composite plate may be transformed into an equivalent plate of one material. In a finite element analysis, such equivalent (homogeneous) plates could be idealized by means of elements of the type described in Chapter 3. However, such an approach would have the following disadvantages:

(i) The rigidity values for the equivalent plate would only approximate the true values.

(ii) Any variation in the level of the centroidal plane of the deck in the transverse direction would not be represented.

(iii) The stresses in each component of the deck would not be obtained directly, but would have to be estimated from those in the equivalent plate..

In the case of bridges having composite plates for which the assumption of complete interaction cannot be justified, an approach similar to the one mentioned in the previous paragraph would involve additional approximations. In particular, there is little or no information available on the effect of connector flexibility on the stiffness of a composite plate.

One method of overcoming these difficulties would be to develop elements for the discrete representation of the various components of a composite plate. Some such elements are described in this chapter. Model test results for a composite box girder bridge, a composite beam, and a composite plate are used as a basis for demonstrating the accuracy of the elements.

4.2 DESCRIPTION OF ELEMENTS

This section presents a procedure for formulating the stiffness matrix of a laminated shell element, each lamina of which may have different material properties and thickness. Such laminated shell elements could be used in the analysis of bridges having composite plates for which complete interaction may be assumed. The stiffness matrix is then given for a general linkage element. (The concept of a linkage element was first introduced by Ngo and Scordelis.[29]) It is subsequently noted how linkage elements may be used in conjunction with laminated shell elements to represent a composite plate for which the assumption of complete interaction cannot be justified.

4.2.1 Laminated shell elements

In the development of the stiffness matrices for the laminated shell elements it has been assumed that:

(i) The transverse deflexions of an element are small in comparison with its thickness.

(ii) Points of an element lying initially on a normal to the reference plane of the element remain on the normal to the reference surface of the element after deformation.

(iii) The normal stresses in a direction transverse to an element can be disregarded.

(iv) The principal directions of material orthotropy of each lamina are in the direction of the element axes.

It should be noted that the elements described in Chapter 3 are based on similar assumptions.

Consider the laminated shell element shown in Fig.4.2. Let u, v, and w be the displacement components of a point Q on the reference plane in the directions of the x, y, and z axes of the element and U, V, and W be the corresponding displacement components of a point P at a distance z from Q in the direction normal to the reference plane. Then, by virtue of assumptions (i) and (ii) the displacement components of P may be written as

$$U = u - z\frac{\partial w}{\partial x} \qquad (4.1(a))$$

$$V = v - z\frac{\partial w}{\partial y} \qquad (4.1(b))$$

$$W = w \qquad (4.1(c))$$

Equations 4.1(a) and 4.1(b) may be differentiated to give the strain-displacement relationship for the element as

$$\begin{Bmatrix} \varepsilon_x \\ \varepsilon_y \\ \gamma_{zy} \end{Bmatrix} = \begin{Bmatrix} \frac{\partial u}{\partial x} \\ \frac{\partial v}{\partial y} \\ \frac{\partial u}{\partial y}+\frac{\partial v}{\partial x} \end{Bmatrix} = \begin{bmatrix} 1 & 0 & 0 \\ 0 & 1 & 0 \\ 0 & 0 & 1 \end{bmatrix} \begin{Bmatrix} \frac{\partial u}{\partial x} \\ \frac{\partial v}{\partial y} \\ \frac{\partial u}{\partial y}+\frac{\partial v}{\partial x} \end{Bmatrix} + \begin{bmatrix} 1 & 0 & 0 \\ 0 & 1 & 0 \\ 0 & 0 & 1 \end{bmatrix} \begin{Bmatrix} -z\frac{\partial^2 w}{\partial x^2} \\ -z\frac{\partial^2 w}{\partial y^2} \\ -2z\frac{\partial^2 w}{\partial x \partial y} \end{Bmatrix} \quad (4.2)$$

By virtue of assumptions (ii) to (iv), the stress-strain relationship for the k th lamina may be written as

$$\begin{Bmatrix} \sigma_x \\ \sigma_y \\ \tau_{xy} \end{Bmatrix} = \begin{bmatrix} C_{11}^k & C_{12}^k & 0 \\ C_{21}^k & C_{22}^k & 0 \\ 0 & 0 & C_{33}^k \end{bmatrix} \begin{Bmatrix} \varepsilon_x \\ \varepsilon_y \\ \gamma_{xy} \end{Bmatrix} \quad (4.3)$$

where

$$C_{11}^k = E_x^k / (1 - \nu_{xy}^k \; \nu_{yx}^k)$$

$$C_{22}^k = E_y^k / (1 - \nu_{xy}^k \; \nu_{yx}^k)$$

$$C_{33}^k = G^k$$

$$C_{12}^k = C_{21}^k = \nu_{xy}^k \; E_y^k / (1 - \nu_{xy}^k \; \nu_{yx}^k)$$

In the above expressions E_x^k and E_y^k are the elastic moduli, G^k is the shear modulus, and ν_{xy}^k and ν_{yx}^k are the Poisson's ratios of the k th lamina, with respect to the x and y axes of the element.

Substitution of Eq.4.2 into Eq.4.3 gives

$$\begin{Bmatrix} \sigma_x \\ \sigma_y \\ \tau_{xy} \end{Bmatrix} = \begin{bmatrix} C_{11}^k & C_{12}^k & 0 \\ C_{21}^k & C_{22}^k & 0 \\ 0 & 0 & C_{33}^k \end{bmatrix} \begin{Bmatrix} \frac{\partial u}{\partial x} \\ \frac{\partial v}{\partial y} \\ \frac{\partial u}{\partial y} + \frac{\partial v}{\partial x} \end{Bmatrix} + \begin{bmatrix} C_{11}^k & C_{12}^k & 0 \\ C_{21}^k & C_{22}^k & 0 \\ 0 & 0 & C_{33}^k \end{bmatrix} \begin{Bmatrix} -z\frac{\partial^2 w}{\partial x^2} \\ -z\frac{\partial^2 w}{\partial y^2} \\ -2z\frac{\partial^2 w}{\partial x \partial y} \end{Bmatrix} \tag{4.4}$$

Integration of Eq.4.4 over the thickness of each lamina and summation of the resulting expressions over n laminae gives the stress resultants and stress couples in terms of the displacement as

$$\{\sigma\} = \begin{Bmatrix} N_x \\ N_y \\ N_{xy} \\ M_x \\ M_y \\ M_{xy} \end{Bmatrix} = \begin{bmatrix} R_{11} & R_{12} & 0 & T_{11} & T_{12} & 0 \\ R_{21} & R_{22} & 0 & T_{21} & T_{22} & 0 \\ 0 & 0 & R_{33} & 0 & 0 & T_{33} \\ T_{11} & T_{12} & 0 & S_{11} & S_{12} & 0 \\ T_{21} & T_{22} & 0 & S_{21} & S_{22} & 0 \\ 0 & 0 & T_{33} & 0 & 0 & S_{33} \end{bmatrix} \begin{Bmatrix} \frac{\partial u}{\partial x} \\ \frac{\partial v}{\partial y} \\ \frac{\partial u}{\partial y} + \frac{\partial v}{\partial x} \\ -\frac{\partial^2 w}{\partial x^2} \\ -\frac{\partial^2 w}{\partial y^2} \\ -2\frac{\partial^2 w}{\partial x \partial y} \end{Bmatrix} = [D]\{\varepsilon\} \tag{4.5}$$

where

$$R_{ij} = \sum_{k=1}^{n} C_{ij}^k \quad (h_k - h_{k-1})$$

$$S_{ij} = \frac{1}{3}\sum_{k=1}^{n} C_{ij}^k \quad (h_k^3 - h_{k-1}^3)$$

$$T_{ij} = \frac{1}{2}\sum_{k=1}^{n} C_{ij}^k \quad (h_k^2 - h_{k-1}^2)$$

In the above expressions h_k and h_{k-1} are the distances from the reference plane to the outer and inner surfaces of the k th lamina, respectively.

Following the derivation of Eq.4.5 and the selection of suitable displacement functions, the stiffness matrix for a laminated shell element may be derived using standard procedures.[9] Two such elements (R5 and R6) are presented in this thesis. The displacement functions of these elements correspond to those of the elements R23 and Q33 (see Chapter 3). Details of the formulation of the stiffness matrices for the elements are given in Appendix C.

4.2.2 Linkage elements

A linkage element has two nodal points and may be conceptually thought of as consisting of n linear springs, where n is the number of degrees of freedom at a node of the element. The element has no physical dimensions and hence its nodes may occupy the same point in space.

The stiffness matrix $[k]$ for a linkage element having the nodal degrees of freedom u, v, w, θ_x, θ_y, and θ_z would take the following form:

$$\left[\begin{array}{cccccccccccc}
k_x & 0 & 0 & 0 & 0 & 0 & -k_x & 0 & 0 & 0 & 0 & 0 \\
 & k_y & 0 & 0 & 0 & 0 & 0 & -k_y & 0 & 0 & 0 & 0 \\
 & & k_z & 0 & 0 & 0 & 0 & 0 & -k_z & 0 & 0 & 0 \\
 & & & k_{\theta x} & 0 & 0 & 0 & 0 & 0 & -k_{\theta x} & 0 & 0 \\
 & & & & k_{\theta y} & 0 & 0 & 0 & 0 & 0 & -k_{\theta y} & 0 \\
 & & & & & k_{\theta z} & 0 & 0 & 0 & 0 & 0 & -k_{\theta z} \\
 & & & & & & k_x & 0 & 0 & 0 & 0 & 0 \\
 & & \text{Symmetric} & & & & & k_y & 0 & 0 & 0 & 0 \\
 & & & & & & & & k_z & 0 & 0 & 0 \\
 & & & & & & & & & k_{\theta x} & 0 & 0 \\
 & & & & & & & & & & k_{\theta y} & 0 \\
 & & & & & & & & & & & k_{\theta z}
\end{array}\right] \qquad (4.8)$$

in which k_x, k_y, k_z, $k_{\theta x}$, $k_{\theta y}$, and $k_{\theta z}$ are the spring constants associated with the appropriate degrees of freedom. The stiffness matrices based on other sets of nodal degrees of freedom may be obtained by eliminating the appropriate rows and columns from Eq.4.8.

4.2.3 Eccentric shell elements

In order to allow for incomplete interaction in composite box girder bridges, it is necessary that the concrete slab and the steel plate should each be represented by a layer of shell elements and the shear connectors represented by linkage elements. The nodes of the shell elements must lie on adjoining element surfaces so that they may be connected by the linkage elements. Such eccentric shell elements are special cases of the laminated shell elements described in Sub-section 4.2.1.

4.3 APPLICATIONS

In this section the accuracy of the elements described in the preceeding section is demonstrated by reference to model test results.

4.3.1 Skewed composite twin cell box girder bridge model

The laminated shell elements were used in the analysis of the bridge model shown in Fig.4.3. Full details of the model and further results to those presented in this thesis are given in Ref.30.

Figure 4.4 shows the details of two finite element idealizations of the model used in the analyses. The webs and the diaphragms of the boxes were represented by Q33 elements and the bottom flanges by Q33 and T33 elements in both idealizations. The deck was represented by R6 and T33 elements in one idealization and by Q33 and T33 elements in the other.

For the latter case the rigidity values of the composite parts of the deck were obtained from the following expressions:

$$C_x = C_y = \frac{E_s\, t_s}{(1 - V_s^2)} + \frac{E_c\, t_c}{(1 - V_c^2)} \qquad D_x = D_y = \frac{E_s\, I_{cp}}{(1 - V_s V_c)}$$

$$C_{xy} = \frac{E_s\, t_s}{2(1 + V_s)} + \frac{E_c\, t_c}{2(1 + V_c)} \qquad D_{xy} = \left(\frac{1 - \sqrt{V_s\, V_c}}{2}\right) D_x$$

$$C_1 = V_s \frac{E_s\, t_s}{(1 - V_s^2)} + V_c \frac{E_c\, t_c}{(1 - V_c^2)} \qquad D_1 = \sqrt{V_s\, V_c}\; D_x$$

The reader is referred to the list of notation for the meaning of the above symbols. It should be noted that the boxes were firmly glued to the slab and no relative movement between these two components was observed during the tests.

The model was analysed for the load case shown in Fig.4.5. A comparison between the finite element and experimental values of displacement at the mid-span is given in Fig.4.6. It can be seen that all the results are in close agreement. (The greater stiffness exhibited by the idealization which employed homogeneous elements for representing the deck is to be expected because this idealization over-estimated the second moment of area of the model cross-section by 4 per cent whereas the other idealization over-estimated it by only 0.7 per cent.) Some comparisons between the finite element and experimental values of stress are given in Figs 4.7 to 4.9. It can be seen that these results are in satisfactory agreement. For the sake of clarity the stress plots obtained using the idealization which employed homogeneous elements for representing the deck have been omitted from Figs 4.7 to 4.9; these results also agreed satisfactorily with the experimental results.

4.3.2 Straight composite beam model

The technique proposed in Section 4.2 for considering incomplete interaction was used in the analysis of the model[31] shown in Fig.4.10.

Owing to double symmetry only one quarter of the model was analysed with the finite element discretization shown in Fig.4.11. The concrete slab was represented by R5 elements, the rolled steel joist by line elements,[17] and the shear connectors by linkage elements that allowed slip in the plane of the concrete-steel interface.

The model was analysed for a central point load of 3.36×10^4 lbf. Some results from the finite element analysis are compared with those of a finite difference analysis[31] and the model test in Figs 4.12 to 4.14. It can be seen that all the results are in good agreement.

4.3.3 Square composite plate model

The proposed technique for considering incomplete interaction was also used in the analysis of the model[32,33] shown in Fig.4.15.

Owing to double symmetry only one quarter of the model was analysed with the finite element discretization shown in Fig.4.16. The concrete slab and the steel plate were represented by R5 elements, and the shear connectors by linkage elements that allowed slip in the plane of the concrete-steel interface.

The model was analysed for a central 4 inch square patch load of 8325 lbf. Some values of slip obtained from the finite element analysis, a Fourier series analysis,[32] and the model test are given in Table 4.1. It can be seen that the two sets of theoretical results are in close agreement. However, the agreement between the theoretical and experimental results is only reasonable; some of the discrepancies are probably due to the cracking of the concrete and the non-linear behaviour of the shear connectors.

4.4 CONCLUSIONS

(i) The formulation of the stiffness matrix for homogeneous shell elements (Chapter 3) has been extended to the case of laminated shell elements.

(ii) Such laminated elements may be usefully employed in the analysis of composite box girder bridges having complete interaction at the concrete-steel interfaces; the use of these elements instead of homogeneous elements in the analysis has the advantage that the analytical model approximates the true physical structure more closely, and that the stresses in the various components of the structure are obtained directly.

(iii) Comparisons made between results obtained using the laminated elements and those obtained from a model test showed close agreement.

(iv) The use of laminated elements instead of homogeneous elements involves only a small increase in computer cost.

(v) A procedure is outlined for using laminated elements in conjunction with linkage elements for the analysis of composite bridges having incomplete interaction at the concrete-steel interfaces.

(vi) Comparisons made between results obtained using the procedure and those obtained from model tests showed close agreement.

(vii) The computer cost of an analysis which takes into account incomplete interaction can be significantly greater than that of a corresponding analysis which assumes complete interaction. (The increase in cost is largely due to the additional degrees of freedom required at each position where a linkage element is employed).

C H A P T E R 5.

PARAMETRIC STUDY OF THE SHEAR LAG PHENOMENON IN STEEL BOX GIRDER BRIDGES

5.1 INTRODUCTION

When girders with wide flanges are subjected to lateral bending loads the deflexions and stresses cannot be obtained accurately from the elementary theory of bending. This is because the assumption made by the elementary theory that cross-sections of the girder which were plane before bending remain plane after bending does not apply; owing to the action of shear strain in the flanges the parts of the flange remote from a web lag behind those near the web. If this effect, often termed shear lag, is ignored, the strength of the girder will be overestimated.

In particular, the action of shear strain in the flanges results in a non-uniform distribution of the direct stresses in the flanges with the peak values, at the web-flange intersection, being greater than the stress value given by the elementary theory of bending (see Fig.5.1). It is convenient, for design purposes, to introduce the concept of an effective breadth of plate which is considered to be uniformly stressed, thereby allowing the application of the elementary theory. The action of shear strain in the flanges also results in the deflexions obtained using the elementary theory being underestimated. So far as the writer is aware, the concept of an effective breadth for deflexion calculations has not been introduced in the literature. Such an approach is considered in this chapter.

The phenomenon of shear lag has been dealt with in many papers, some of which are noted in the list of references.[34-38] The work described in the papers has shown that the effective breadth for stress calculations varies along the span and depends on the load distribution, cross-sectional properties and boundary conditions, as well as the plan dimensions of the bridge. Since the application of the theoretical solutions given in the published works are too involved for design office practice, most of the investigators have presented values of effective breadths for variations in some of the parameters noted above. However, the papers, even as a collective group, do not provide sufficient information in a suitable form for the design engineer.

At present, the British Codes of Practice give only a limited amount of guidance on effective breadth values. There are no specific design clauses that deal with the effective breadths of steel or concrete bridge decks. In the code for the design of composite bridge girders (CP117: part 2: 1967)[39] a single expression for an effective breadth is given in terms of the ratio of the breadth B to the length L of the slab. Currently some British design engineers use the recommendations on effective breadth given in the draft of the German code for steel road bridges (DIN1073).[40] This code only considers uniformly loaded beams with various support conditions. No allowance is made for the cross-sectional properties.

The purpose of the work described in this chapter was to establish design rules for estimating the effective breadths of steel box girder bridge flanges. The data on which the rules have been based was obtained using the finite element program described in Chapter 2.

5.2 DEFINITION OF EFFECTIVE BREADTHS

In this thesis, unless otherwise stated, the following definitions hold:

(i) The stress effective breadth of a flange plate is that breadth of plate which, with a constant longitudinal stress across its middle plane equal to the stress in the related web[a] at the level of the middle plane of the flange plate, would sustain a force equal to the force in the flange plate as predicted by a theory that correctly allows for shear deformation of the flange (see Fig.5.1).

(ii) The deflexion effective breadth of a flange plate is that breadth of plate which, when used in conjunction with elementary theory of bending formulae, gives the same result for the deflexions at the webs of the cross-section under consideration as a theory that correctly allows for shear deformation of the flange.

(iii) An effective breadth ratio is the ratio of an effective breadth of a flange plate to the actual breadth of the plate.

5.3 FINITE ELEMENT IDEALIZATIONS

This section describes a preliminary investigation that was carried out in order to determine finite element idealizations that would be suitable for use in studying the shear lag phenomenon in box girder bridges. The box girders used in the investigation were based on cross-sections 1 and 8 (Fig.5.2, Table 5.1) and were analysed for a uniform load over the length of each web and for a point load over each web at the mid-span.

(a) According to thin plate theory, on which the finite element analyses used in this thesis were based, the stress in a web element is not necessarily equal to the stress in a flange element at a node defining the intersection of the two elements. The stress in the web element has been selected as the base stress since, in general, it will give smaller effective breadth values.

5.3.1 Type of element

The solutions given in this chapter were obtained using idealizations based on the element Q43 (see Section 3.2). This element was employed because it can efficiently represent the behaviour of box girder bridge structures and, in particular, it is suitable for use in rapidly varying stress fields such as those associated with the shear lag phenomenon.

5.3.2 Mesh size

To gain an appreciation of the mesh sizes required in the determination of effective breadths, simply supported box girders of cross-section 1 and having B/L values of 0.05, 0.20, and 0.40 were analysed using several different mesh schemes. End diaphragms which were infinitely rigid in the plane of the diaphragm and which provided no restraint against warping were assumed. In the case of the point loads at the mid-span, the loads were distributed uniformly over the depth of the webs in order to avoid any local stress concentrations. Such stresses are not accounted for by the effective breadth concept and are not fully realized in practice since all loads are distributed over some finite bearing length.

For each box a mesh of 6 elements over the depth of the webs, 16 elements over the breadth of the flanges, and 22 elements over the length of the box, graded as shown in Fig.5.3, was found to give practically the same effective breadth values as finer mesh schemes. It should be noted that it was necessary to specify a fine mesh division in the region of the point loads.

The subsequent results given in this chapter were all obtained using mesh divisions for the flanges of comparable grade to the one listed above; fine mesh divisions were used in the region of each point load, internal support reaction, and fixed end considered in the examples. It is shown in Sub-section 5.3.3 that only one element need be used over the depth of the webs.

5.3.3 Idealization of webs

Many of the published solutions which consider the effects of shear lag are based on the assumption that the elementary theory of bending applies to the webs. This assumption would have the advantage that the results of any numerical tests using these solutions would not be affected by the phenomenon of deep beam behaviour.

To investigate the possibility of using this assumption in the present study, the box girders described in Sub-section 5.3.2 were analysed with the in-plane properties of the web material set to values consistent with those implied by the elementary theory of bending.

The values of the effective breadth ratios at the mid-span obtained from the analyses described in this sub-section and the previous one are given in Table 5.2. It can be seen that each set of corresponding values are in close agreement, except for the deflexion effective breadth values when the ratio of depth to length (D/L) is equal to 0.4. Generally box girders will have a value of D/L less than 0.4. Also, for box girders having values of D/L greater than 0.4, the deflexion related to the normal stresses is only a small percentage of the total deflexion, and hence the deflexion effective breadth values would not be of practical importance.

From these observations, values for the in-plane properties of the web material consistent with those implied by the elementary theory of bending were chosen for the subsequent analyses described in this chapter. Such values have the additional advantage that only one element need be used over the depth of the webs.

5.3.4 Idealization of diaphragms

To investigate the effect of diaphragm stiffness on effective breadth values, the box girders described in Sub-section 5.3.2 were analysed with an additional diaphragm at the mid-span. In one set of tests the diaphragms were considered to be made of $\frac{1}{2}$ inch plate. In a second set of tests the diaphragms were considered to be infinitely rigid.

It was found that each set of corresponding effective breadth values obtained at the mid-span for the two types of diaphragm differed by less than 1.5 per cent. Further, these values and the corresponding values obtained for the box girders that did not have diaphragms at the mid-span all differed by less than 4 per cent.

Hence it may be concluded that the stiffness of any diaphragms present in a box girder bridge need not be represented accurately in respect of the determination of effective breadths when the girder is under symmetrical (bending) loads. The subsequent results given in this chapter were obtained assuming diaphragms which were infinitely rigid in the plane of the diaphragm and which provided no restraint against warping.

5.3.5 Idealization of flanges

In the finite element analysis of steel box girder bridges having stiffened flanges, the flanges could be represented by discrete plate and beam elements or by orthotropic plate elements with constant thickness. To gain an appreciation of the effect of the two types of idealization on effective breadth values, simply supported box girders of cross-section 8 and having B/L values of 0.05, 0.20, and 0.40 were analysed using both types of idealization.

In the case of the discrete component idealization, an eccentric beam element, similar to the one described in Ref. 17, was used to represent the stiffeners. In the case of the orthotropic plate idealization, the rigidity values were obtained from the following expressions:

$$C_x = \frac{Et_f}{(1-\nu^2)} + \frac{EA_s}{S} \qquad D_x = \frac{Et_f^3}{12(1-\nu^2)} + \frac{Et_f\,Z_p^2}{(1-\nu^2)} + \frac{EI_s}{S}$$

$$C_y = \frac{Et_f}{(1-\nu^2)} \qquad D_y = \frac{Et_f^3}{12(1-\nu^2)}$$

$$C_{xy} = G\,t_f \qquad D_{xy} = \frac{Gt_f^3}{12} + \frac{k\,D_s\,B_s^3\,G}{4S}$$

$$C_1 = \frac{\nu Et_f}{(1-\nu^2)} \qquad D_1 = \frac{\nu Et_f^3}{12(1-\nu^2)}$$

The reader is referred to the list of notation for the meaning of the above symbols. The expressions shown for the extensional rigidities were given by Morley[41] and those for the flexural rigidities by Sawko and Cope.[42]

It was found that each set of corresponding effective breadth values obtained at the mid-span using the two idealizations differed by less than 1 per cent. Thus it would appear that either of the two idealizations would have been suitable for use in the subsequent part of the study reported here. However, the orthotropic plate idealization was used since it provides results of a more general nature.

5.3.6 Comparison with available solutions

As a final check on the selected finite element idealizations, simply supported box girders of cross-sections 1 and 8 and having B/L values of 0.05, 0.10, 0.20, and 0.40 were analysed using the finite element method and techniques proposed by Kondo et al.[34] and Schade.[35] The values of the stress effective breadth ratios obtained at the mid-span are given in Table 5.3. It can be seen that the agreement between the values given by the various techniques is satisfactory.

5.4 INFLUENCE OF VARIOUS PARAMETERS ON EFFECTIVE BREADTH

In this section the influence of various significant parameters on effective breadth values is studied. The box girder bridges used in the investigation had the cross-sections shown in Fig.5.2. Except where specified otherwise, the bridges were analysed for a uniform load over the length of each web and for a point load over each web at the mid-span. The magnitudes of the loads were selected to give equal deflexions of the webs at the mid-span, the necessary calculations being based on Oden[43] in the case of multi-cell bridges. In the following discussion these two standard cases will be referred to as the uniform load case and the point load case.

5.4.1 Flange orthotropy

For the present study a convenient measure of the orthotropy of steel flanges is the stiffening factor α, which is defined as the ratio of the cross-sectional area of the longitudinal stiffeners within a breadth of flange B to the cross-sectional area of the associated flange plate within the breadth B. Figure 5.4 shows the variation of effective breadth ratios at the mid-span with stiffening factor for simply supported box girders having a B/L value of 0.20. It can be seen that the effective breadth ratios decrease by a significant amount, in practically a linear manner[b], as the stiffening factor increases. The reason for this mode of variation would be that as the stiffening factor increases, there is proportionally more extensional stiffness available for mobilization by the same shear stiffness.

Another measure of flange orthotropy is given by the ratio of longitudinal extensional rigidity C_x to shear rigidity C_{xy}. It can be seen that the plots in Fig.5.4 have been extended out of the range of realistic values of the stiffening factor by using the ratio C_x/C_{xy} as a scale variable. Points in this range could be of practical importance in the case of cracked reinforced concrete flanges since the concrete would contribute to the shear stiffness but not to the extensional stiffness of the flanges.

(b) The plot of stress effective breadth ratios for the point load case is in fact slightly curved. This would be due to the additional effect of the ratio of the flange to web cross-sectional areas, which will be discussed in Sub-section 5.4.2.

5.4.2 Cross-sectional dimensions

Simply supported box girder bridges of cross-sections 1 to 10 and 13 to 15, and having B/L values of 0.05, 0.20, and 0.40 were analysed for the two standard load cases. It was found that only the stress effective breadth values for the point load case were dependent on the cross-sectional dimensions.

It is possible to identify a non-dimensional constant β (the ratio of twice the cross-sectional area of the flange under consideration to the cross-sectional area of the webs) which may be used as a parameter for quantifying the dependency noted above. A similar factor was introduced by Schade.[35] Tables 5.4 and 5.5 give an indication of the influence of the factor β on effective breadth values.

5.4.3 Cross-sectional shape

It has been suggested by Kondo et al.[34] that the effective breadth values obtained for a deck plate supported by two main girders (Fig.5.5(a)) can be used to find effective breadth values for bridges of other cross-sectional shapes. The procedure involves applying the values for the simple cross-sectional shape to the breadths of plate B_1, B_2 ... associated with each web of the bridge, as indicated in Fig.5.5(b).

To investigate the accuracy of this approach, simply supported box girder bridges of cross-sections 13 and 16 and having B/L ratios of 0.05, 0.20, and 0.40 were analysed for the two standard test load cases. Table 5.6 gives the values obtained for the stress effective breadth ratios at the mid-span. Except in the case of the outer overhanging flanges, these values compare favourably with the corresponding values for single cell box girders (Table 5.3). In making the comparisons it is important to allow for the effect of the factor β described in Sub-section 5.4.2.

As a further part of the investigation, values of the deflexion effective breadth ratios at the mid-span were determined for the single cell box girders. These values were then used in conjunction with the elementary theory of bending to determine the mid-span deflexions of the box girder bridges described in this sub-section. In each case the average deflexion for the webs was slightly overestimated; these errors presumably arise because the outer overhanging flanges are not as efficient in resisting the lateral loads as the flanges of the single cell box girders.

The above observations indicate that the procedure suggested by Kondo et al.[34] (modified slightly in the case of outer overhanging flanges) would be suitable for design office calculations and it has been proposed in the design rules of Section 5.5.

5.4.4 Aspect ratio of flange

Values of effective breadth ratios for simply supported box girders of cross-sections 4 and 8 are given in Table 5.7, for a range of aspect ratios of flange (B/L). The previous results of this section indicate that these values could be used as a basis for estimating the corresponding values for box girder bridges having any typical cross-sectional properties. This generalization would, of course, necessitate the use of modification factors to take into account the effects of the cross-sectional dimensions and the cross-sectional shape on the effective breadth values. Some suitable values for these factors, based on the results presented in Sub-sections 5.4.2 and 5.4.3, are recommended in Section 5.5

The following examples considered in this section indicate how the values given in Table 5.7 may be used to estimate effective breadth values in cases where conditions are different from those considered so far.

5.4.5 Position of point load

Simply supported box girders of cross-sections 4 and 8 and having B/L values of 0.05, 0.20, and 0.40 were analysed for a point load over each web at various positions along the span. It was found that the stress effective breadth ratios at the position of the applied loads, obtained from the analyses, could be accurately estimated by using the values given in Table 5.7 in conjunction with a simple empirical formula (Fig.5.7, case 1). The values obtained from both the finite element analyses and the formula, for the examples described above, are given in Table 5.8.

5.4.6 Length of uniform load

Figure 5.6 shows the variation of stress effective breadth ratios at the mid-span of box girders of cross-section 8 with the length of centrally located uniform load over each web. It can be seen that for a girder having a B/L value less than 0.2, the effective breadth ratio is particularly sensitive to the loaded length when this length is less than a quarter of the span. These observations are of practical significance since, in general, loads (including those due to supports) are subject to some distribution.

5.4.7 <u>Support condition</u>

It would be hardly practicable to provide effective breadth values for all the support conditions that are likely to occur in practice. An alternative approximate approach would be to isolate portions of the bridge between adjacent points of zero moment and treat such portions as simply supported spans. Figure 5.8 shows that formulae[c] for stress effective breadth ratios based on such an approach give reliable values.

As a further part of the investigation, the deflexions at the mid-span of each span of the box girders shown in Fig.5.8 were calculated by applying the elementary theory of bending to a beam of varying cross-section, the properties of which were determined by considering an effective breadth ratio for each equivalent simply supported span. Values of the deflexion effective breadth ratios at the mid-span for the point load case given in Table 5.7 were used in the calculations. In each case the calculated value of the deflexion and the value given by a finite element analysis differed by less than 5 per cent.

(c) Appendix D demonstrates some of the detailed steps that were used in deriving the formulae, given in Fig.5.7, by reference to a propped cantilever.

In the case of statically indeterminant bridges the question arises as to what cross-sectional properties should be assumed for the purpose of evaluating the distribution of the longitudinal bending moments. Two simple approaches would be to use either an unreduced cross-section or a varying cross-section based on deflexion effective breadths. These approaches were investigated by reference to the box girders shown in Fig.5.8. The stresses in the webs were evaluated using the bending moment values obtained by assuming an unreduced cross-section and section moduli based on the values of the effective breadth ratios shown in Fig.5.8. For each girder the calculated values were within 3 per cent of the values obtained from the finite element analyses. Generally, an even better agreement between each set of values was achieved by using the second approach mentioned above for finding the distribution of bending moments.

5.4.8 Web curtailment

Fixed ended box girders of cross-section 8 over the central half span, cross-section 12 over the end quarter spans, and having B/L values of 0.05, 0.20, and 0.40 were analysed for a uniform load over the length of each outer web and for a point load over each web at the mid-span. The girders were analysed both with ½ inch thick disphragms at the cross-sections at which the middle webs were curtailed, and without these diaphragms present.

The values of the stress effective breadth ratios associated with the outer webs at the mid-span and at the supports are given in Table 5.9. It can be seen that the values at the mid-span are not affected by the presence of the curtailed webs and that the values at the supports are only affected when diaphragms are provided. The diaphragms have an influence on the results because they cause some of the shear forces to be transferred from the outer webs to the central webs.

5.4.9 Position in span

Figures 5.9 to 5.15 show longitudinal plots of effective breadth ratios for box girders of cross-section 8 having various support and load conditions. It can be seen that:

(i) The stress effective breadth ratios decrease rapidly in the region of point loads or near the support regions.

(ii) The stress effective breadth ratios are practically constant over the distance along which uniformly distributed loads are applied, except in a region of zero moment. In the case of the fixed ended uniformly loaded box girders, the plots of effective breadth ratios asymptote to non-realistic values in the region of the points of zero moment. Yuille[37] noted that this was basically due to anomalies in the concept of an effective breadth. In general, the stresses in such regions would not be of practical importance and the adoption of any sensible value for the effective breadths would suffice.

(iii) The deflexion effective breadth ratios are reasonably constant over the length of the girders irrespective of the type of loading.

5.5 PROPOSALS FOR DESIGN RULES

This section gives proposals for design clauses on the effective breadth of box girder bridge flanges.[d] The proposals are based on the results contained in this chapter.

Numbering systems separate from those used elsewhere in this thesis have been adopted for the proposed rules to enable them to be treated as a separate entity.

EFFECTIVE BREADTHS OF FLANGES

1. General

(i) Allowance for the action of in-plane shear strain[e] in flanges should be made by determining effective flange breadths to replace actual flange breadths, in calculations based on the elementary theory of bending, as follows.

(ii) The total effective breadth should be taken as the sum of the effective breadths of the portions of flange on each side of each web.[f] The effective breadth of each portion should be taken as:

ΨB for portions between webs

$0.85\ \Psi B$ for protions projecting beyond an outer web[g]

where

Ψ is an effective breadth ratio determined from the following clauses

---

(d) These clauses have been incorporated in the design rules issued by the Committee of Investigation into the Design and Erection of Steel Box Girder Bridges.[44]

(e) A description of the action of in-plane shear strain is given in Section 5.1.

(f) This recommendation is supported by the results presented in Sub-section 5.4.3.

(g) The value of 0.85 was obtained from a consideration of the results presented in Sub-section 5.4.3.

B is half the distance between web centre lines or the distance between a web centre line and the free edge of a flange at the level of the mid-plane of the flange under consideration

2. <u>Effective breadth ratios for stress calculations</u>

(i) For simply supported girders, the value of Ψ should be determined from Table EB1[h], subject to the provisions of other relevant clauses of this section.

Table EB1. Effective breadth ratios (ψ) for box girders

Loading condition	Point load at mid-span				Uniform load over L			
Section being considered	Mid-span		Quarter-span to support		Mid-span to quarter-span		Support of simple span	
B/L \ α	0	1	0	1	0	1	0	1
0	1·00	1·00	1·00	1·00	1·00	1·00	1·00	1·00
0·05	0·80	0·75	1·00	1·00	0·98	0·97	0·84	0·77
0·10	0·67	0·59	1·00	0·99	0·95	0·89	0·70	0·60
0·20	0·49	0·40	0·98	0·84	0·81	0·67	0·52	0·38
0·30	0·38	0·30	0·82	0·61	0·65	0·48	0·40	0·29
0·40	0·30	0·23	0·63	0·44	0·50	0·35	0·32	0·22
0·50	0·24	0·18	0·47	0·33	0·38	0·27	0·27	0·18
0·60	0·19	0·14	0·36	0·26	0·29	0·22	0·22	0·15
0·70	0·16	0·11	0·29	0·21	0·24	0·18	0·19	0·12
0·80	0·14	0·10	0·23	0·18	0·20	0·16	0·16	0·11
0·90	0·13	0·09	0·20	0·16	0·17	0·14	0·14	0·10
1·00	0·12	0·08	0·19	0·14	0·16	0·12	0·12	0·09

(h) The values of Ψ given in the first six columns of Table EB1 were obtained from Table 5.7, while those in the last two columns were obtained by means of plots of the type shown in Figs 5.9 and 5.10.

In Table EB1

B is as defined previously

L is the distance between adjacent points at which the bending moment is zero

α is the ratio of the cross-sectional area of the longitudinal stiffeners within a breadth B of flange to the cross-sectional area of the associated flange plate within the same breadth

(ii) Values of Ψ for B/L values[i] and α values[j] intermediate to those given in Table EB1 may be obtained by linear interpolation.

(iii) When a concrete deck acts in conjunction with a stiffened flange the α value should be based on an equivalent thickness of flange equal to the sum of the thickness of the steel plate and 1/m times the thickness of the concrete (where m is the modular ratio). The longitudinal reinforcement bars in the concrete should be treated in the same way as the longitudinal flange stiffeners.[k]

(i) The interval of the B/L values was selected so that it was possible to make this recommendation.

(j) This recommendation is supported by the results presented in Sub-section 5.4.1.

(k) This approach would always give a value of α greater than or equal to zero. In the case of cracked concrete it is possible to envisage conditions in which the value of the ratio of the longitudinal extensional rigidity C_x to the shear rigidity C_{xy} for the flange would be smaller than that corresponding to α equal to zero. Thus strict application of the clause would be conservative. The designer could allow for this by extrapolating the values given in Table EB1 out of the range of realistic values of α by using the ratio C_x/C_{xy} as a scale variable, as indicated in Fig.5.4.

(iv) Values of Ψ at the mid-span for a point load at the mid-span should be multiplied by the factor[l]

$$\left(1.08 - 0.04 \frac{A_F}{A_W}\right)$$

where

A_F is the total cross-sectional area of the entire flange plate being considered plus the cross-sectional area of the associated longitudinal stiffeners

A_W is the total cross-sectional area of the web plates at the same cross-section

(v) For point loads at positions other than the mid-span position the value of Ψ at the point of application of the load should be calculated according to the formula[m]

$$\Psi = \frac{1}{3}\left(2\Psi_{2x} + \Psi_{2(L-x)}\right)$$

where

Ψ_{2x} and $\Psi_{2(L-x)}$	are the values of Ψ, given by the preceeding clauses, at the mid-span for a point load at the mid-span with B/L equal to B/2x and B/2(L-x) respectively
x	is the shortest distance from an end of the span to the point of application of the load
B and L	are as defined previously

(l) This factor was obtained from a consideration of the results presented in Sub-section 5.4.2.
(m) This recommendation is supported by the results presented in Sub-section 5.4.5.

(vi) In the case of a uniformly distributed loading over the length of the span, the values of Ψ may be assumed as constant between the mid-span and the quarter-span positions. Values of Ψ between the quarter-span positions and the supports may be obtained by linear interpolation.[n]

(vii) In the case of a point loading, the values of Ψ may be assumed to vary linearly, over a distance equal to a quarter of the span on each side of the load, between the value obtained at the point of application of the load to the value given by the preceeding clauses for the quarter-span with a point load at the mid-span. This latter value may also be assumed to apply over the remainder of the span.[o]

(viii)Values of Ψ for a uniformly distributed loading over the length of the span, given by the preceeding clauses, may be used when loads are uniformly distributed over half the span or more. For loads uniformly distributed over less than half the span, the value of Ψ at any cross-section should be calculated according to the formula[p]

$$\Psi = \Psi^{P} + \frac{2L_W}{L}\left(\Psi^{U} - \Psi^{P} \right)$$

(n) This recommendation is supported by the results presented in Sub-section 5.4.9.

(o) This recommendation is supported by the results presented in Sub-section 5.4.9. It gives conservative values for positions near the point of application of the load for flanges having values of B/L less than 0.2.

(p) This recommendation is supported by the results presented in Sub-sections 5.4.6 and 5.4.9.

where

Ψ^P and Ψ^U are the values of Ψ given by the preceeding clauses for the uniform and point load cases, respectively, at the cross-section being considered

L_W is the length of the uniformly distributed load

L is as defined previously

(ix) The value of Ψ to be considered when different systems of loads exist at the same time, which, if they acted independently would cause bending moments M_1, M_2, ..., M_n and involve effective breadth ratios of Ψ_1, Ψ_2, ..., Ψ_n, should be calculated according to the formula(q)

$$\Psi = \frac{M_1 + M_2 + \dots + M_n}{\frac{M_1}{\Psi_1} + \frac{M_2}{\Psi_2} + \dots + \frac{M_n}{\Psi_n}}$$

(x) For other than simply supported girders, the preceeding clauses may be used to determine effective breadths by treating each portion of girder between adjacent points of zero moment as an equivalent simply supported span. In the special case of a portion of span between a fixed end and a point of zero moment, the position of an

---

(q) This recommendation is supported by the work presented in Appendix E. The formula can be particularly useful in the determination of effective breadths of girders that are not simply supported (see Clause 2(X) and Appendix D). It should be noted that in certain cases the application of this design rule can give values of Ψ that exceed unity. Consider, for example, the value of Ψ at the mid-length of a uniformly loaded cantilever having a value of B/L less than 0.6. In such cases, the finite element method also gives values of Ψ that exceed unity; this is because the maximum longitudinal stress in the flange does not occur at the web-flange junction.

additional fictitious point of zero moment may be obtained by assuming the existence of a symmetrical span about the fixed end.[r]

(xi) For the purpose of calculating the bending moments along the length of a statically indeterminant girder, the properties of the unreduced cross-section may be used.[s]

3. <u>Effective breadth ratios for deflexion calculations</u>

(i) For simply supported girders, the breadth of flange that can be taken as effective over the length of the girder should be taken as equal to the value given in Table EB1 for the quarter span with a uniformly distributed loading.[t]

(ii) For other than simply supported girders, clause 3(i) should be applied using the technique described in Clause 2(x).[u]

(r) This recommendation is supported by the results presented in Sub-section 5.4.7. It may be that the code being drafted by the B/116 Subcommittee on composite bridges will include tables of effective breadth ratio values for a number of special cases, such as cantilever girders and two span girders. Such values can readily be obtained from formulae of the type given in Fig.5.7. These formulae were obtained by using the techniques described in Clauses 2(ix) and 2(x) (See Appendix D).

(s) This recommendation is supported by the results presented in Sub-section 5.4.7.

(t) It can be seen from Table 5.7 that the values of ψ for deflexion calculations correspond closely to the values of ψ for stress calculations at the quarter-span when the girders are under a uniformly distributed load. This recommendation is further supported by the results presented in Sub-section 5.4.9.

(u) This recommendation is supported by the results presented in Sub-section 5.4.7.

5.6 CONCLUSIONS

(i) The shear lag phenomenon in steel box girder bridges has been studied by means of the finite element method, the analyses being made using the element Q43 (Chapter 3).

(ii) The concepts of stress effective breadth and deflexion effective breadth (Section 5.2) have been used as a basis for quantifying the influence of shear lag on the behaviour of a girder. From the results of the study it is apparent that:

(a) The effective breadths of a flange are significantly dependent on the plan dimensions of the girder (Table 5.7).

(b) The effective breadths of a flange are dependent on the ratio of stiffener area to plate area in the flange (Fig.5.4).

(c) The effective breadths of a flange are virtually independent of the ratio of flange area to web area, except for the stress effective breadth at a cross-section under a point load (Tables 5.4 and 5.5).

(d) The effective breadths of a flange of a multi-cell box or a multi-box system can be estimated using those of single cell box girders.

(e) For a simply supported girder under a uniformly distributed load, the stress effective breadth of a flange at the mid-span becomes smaller as the load is more nearly concentrated towards the mid-span (Fig.5.6). A movement of the point load away from the mid-span reduces still further the effective breadth of the flange at the loaded cross-section (Table 5.8).

(f) The stress effective breadth of a flange decreases rapidly in the region of a point load or a support (Figs 5.12 and 5.13).

(g) For a simply supported girder under a uniformly distributed load, the stress effective breadth of a flange is practically constant over the length of the girder, except near the supports (Figs 5.9 and 5.10).

(h) For a simply supported girder, the deflexion effective breadth of a flange is practically independent of the position along the span and the type of loading (Figs 5.14 and 5.15).

(i) The effective breadths of a flange of a continuous girder can be conveniently estimated by treating each portion of girder between adjacent points of zero moment as an equivalent simply supported span.

(iii) For the statically indeterminant girders considered in the study, it was found that a good estimate of the longitudinal bending moment distribution could be obtained from the engineering theory of bending using the properties of the unreduced cross-section.

(iv) Design rules have been formulated on the basis of the results of the study. These rules can be used to obtain an estimate of the variation of the stress and deflexion effective breadths along the span of a box girder bridge having any practical plan dimensions, cross-sectional properties, support conditions, and load distribution.

(v) Although the rules can be used to obtain a comprehensive knowledge of the effect of shear lag on the behaviour of a bridge, in general, it should be only necessary to consider this effect for a limited number of conditions. For example, during the preliminary design stage of a bridge, it is likely that the designer would need only consider the effect of shear lag on the longitudinal stresses in the region of internal supports with the bridge under loads that approximate a uniformly distributed load.

CHAPTER 6.

PARAMETRIC STUDY OF SOME ASPECTS OF THE INCOMPLETE INTERACTION PHENOMENON IN COMPOSITE BOX GIRDER BRIDGES

6.1 INTRODUCTION

In a box girder bridge of the type considered in Chapter 4, the concrete slab is likely to be connected to the steel plate by some natural bond. However, this natural bond may not exist throughout the life of the bridge and consequently the mechanical shear connectors should be designed to resist all the interface forces arising from composite action between the concrete slab and the steel plate. Such forces result from both the longitudinal bending of the bridge and the local bending of the top flange.

Since the shear connectors are of finite stiffness, these forces will cause some relative movement between the concrete slab and the steel plate. This movement may cause the bridge to behave somewhat differently from one having complete interaction. However, little is known about the actual effects of this movement; the only published information appears to be that given by Clarke and Morley in a recent paper[32] which was primarily concerned with the local bending behaviour of composite plates.

The work described in this chapter was therefore undertaken with a view to examining some aspects of the longitudinal bending behaviour of composite box girder bridges. The analytical techniques described in Chapter 4 were employed in obtaining the results presented here.

6.2 DETAILS OF GIRDERS USED IN STUDY

The study reported here employed several girders having the cross-sections shown in Fig.6.1 and having decks of breadth to length ratio (B/L) of 0.05 or 0.20. The girders were considered to be simply supported and to have end diaphragms of infinite in-plane stiffness.

Details of the shear connexions in the top flange of the girders are given in Table 6.1. The shear connexion I1 was designed in accordance with CP117: part 2: 1967,[39] to accommodate the longitudinal interface shear forces that would be developed by the maximum point load which could be placed at the mid-span of the girders having a B/L value of 0.05. It was assumed that the shear connexion would be provided by $\frac{3}{4}$ by 4 in. headed studs; the value of the slip modulus for such connectors given in Ref.45 (Fig.24) was used in calculating the slip modulus per unit length of the shear connexion I1. The shear connexions I2 to I4 were assumed to have the same slip modulus as the shear connexion I1, but different proportions of the total number of connectors placed directly over the webs. The shear connexion I5 was arbitrarily assumed to have a 50 per cent greater slip modulus than the shear connexion I4. The shear connexion C was selected to have a slip modulus which, for all practical purposes, ensured complete interaction between the concrete slab and the steel plate. In all cases, the connectors were considered to be evenly spaced along the length of the girders and, in the case of the shear connexions C and I2 to I5, the connectors distributed over the flange were considered to be evenly spaced in the transverse direction.

It should be noted that the girders only approximately represent those occurring in practice, some simplifications having been made for the purpose of the study.

6.3 PRELIMINARY INVESTIGATION

This section describes a preliminary investigation that was carried out in order to determine finite element idealizations that would be suitable for use in studying the longitudinal bending behaviour of composite tee and single cell box girders. Also, the results of the investigation are used to ascertain the existence of any similarities in the behaviour of the two types of girder. For the purpose of the investigation, the girders having the shear connexions C and I4 were analysed for a uniform load over the length of each web and for a point load over each web at the mid-span.

6.3.1 Finite element idealizations

In obtaining the finite element solutions, the girders were idealized as follows:

(i) In the case of the tee girders, the concrete slab and the steel plate were represented by R5 elements (see Section 4.2), while the web plate was represented by line elements.[17]

(ii) In the case of the box girders, the concrete slab and the top steel flange plate were represented by R6 elements (see Section 4.2), while the webs and the bottom flange were represented by Q33 elements (see Section 3.1).

(iii) In both cases, the shear connexion between the concrete slab and the steel plate was represented by linkage elements (see Section 4.2) that allowed slip in the plane of the interface. (It was assumed that uplift forces, which are discussed in Ref.46, would be resisted by the connectors without separation, and would not affect the behaviour of the girders.)

The girders were each analysed using several different mesh schemes. (The line element[17] used in the analysis of the tee girders is based on the assumptions of the elementary theory of bending. For the sake of consistency, the webs of the box girders were also assumed to behave in accordance with this theory, and hence in all the discretizations of the boxes only one element was used over the depth of the webs (see Section 5.3).) It was found that for each girder a subdivision of the flange as shown in Fig.6.2 gave values of the maximum deflexion, longitudinal plate stress component, longitudinal slab stress component, and longitudinal connector force component that were within 8 per cent of those obtained using finer mesh schemes. Accordingly, all the subsequent results given in this chapter were obtained using the mesh division shown in Fig.6.2.

6.3.2 Types of girder cross-section

Some of the results obtained from the analyses referred to in Sub-section 6.3.1 are given in Table 6.2. These results illustrate the markedly similar effect the introduction of a flexible shear connexion has on the longitudinal bending behaviour of composite tee and box girders. In view of this similarity, and in view of the fact that the idealization of a tee-section requires the use of fewer nodes than a box-section, the examples given in the remainder of this chapter have been based on the tee-section only.

6.4 INFLUENCE OF SHEAR CONNECTOR FLEXIBILITY AND DISTRIBUTION ON GIRDER BEHAVIOUR

To investigate the influence of the shear connector flexibility and distribution on the longitudinal bending behaviour of composite girders, the tee girders described in Section 6.2 were analysed for a uniform load over the length of the web and for a point load over the web at the mid-span. Some of the results are presented in this section. In general, the results for the girders with incomplete interaction (shear connexions I1 to I5) have been given as a ratio of the corresponding results for the girders with complete interaction (shear connexion C).

6.4.1 Deflexions

The values of the deflexions at the centre of the various girders are given in Table 6.3. It can be seen that for those girders in which the connectors are concentrated over the web, the connector flexibility does not greatly affect the deflexions. However, as the proportion of the total number of connectors placed directly over the web is decreased, the deflexions of the shorter girders (B/L=0.20) are significantly affected, although those of the longer girders (B/L=0.05) are not. This is because less shear is transmitted across the flange of the shorter girders, as a result of shear lag, and hence less force can be transmitted through the connectors distributed over the flange. Finally, it is interesting to note that the corresponding deflexions of the girders having the shear connexions I4 and I5 are not markedly different.

6.4.2 Stresses

The values of the maximum longitudinal extensional stresses for the concrete slab and the steel plate at the centre of the various girders are given in Tables 6.4 and 6.5. It can be seen that the variation of these stresses with the type of shear connexion shows similar trends to that of the mid-span deflexions (Table 6.3). However, the trends are more marked in the case of the stresses. This is because the loss of interaction between the slab and the plate affects the upper section modulus of a cross-section to a greater extent than the moment of inertia of the cross-section. Further, for the point load cases, shear lag action would particularly reduce the effectiveness of the connectors distributed over the flange in the vicinity of the load, and this local effect would influence the mid-span stresses more than the deflexions.

6.4.3 Effective breadth ratios

The values of the stress effective breadth ratios for the concrete slab and the steel plate at the mid-span of the various girders are given in Tables 6.6 and 6.7. It can be seen that the effective breadth ratios for the girders having the shear connexions C and I1 are almost identical to those given by the design rules proposed in Section 5.5; the slightly higher values obtained in this investigation for the point load case would be at least partly due to the coarser idealizations used in the present analyses. It can also be seen that for the flexible connexions, as the proportion of the total number of connectors placed directly over the web is decreased, the effective breadth ratios for the slab increase whereas those for the plate decrease. These trends are due to horizontal shear being transmitted from the plate to the slab through the connectors distributed over the flange.

6.4.4 Shear connector forces

The values of the forces in the shear connectors directly over the web at the quarter-span and support sections of the various girders are given in Table 6.8. These values suggest that the proportion of the longitudinal shear force taken by the connectors over the web depends primarily on the proportion of the total number of connectors placed directly over the web. It appears to be relatively independent of the type of load, the position along the girder, and the total slip modulus of the connectors for practical values of the total slip modulus. Further, analyses which employed girders identical to those with the shear connexion I4 but having a 4 in. thick concrete slab gave practically the same results as those presented in Table 6.8. It should be recalled also that the tests described in Sub-section 6.3.1 showed that practical variations in the spacing of the connectors distributed over the flange of a girder only slightly affect the proportion of the longitudinal shear force carried by the connectors directly over the web.

The distributions of the connector forces across the flange at the quarter-span and support sections of the various girders are shown in Figs 6.3 to 6.6. The force F in the connectors has been presented in the following non-dimensional form:

$$\gamma = \frac{F\ K_{rs}}{F_{TC}\ K_s}$$

where

K_{rs} is the total slip modulus of the transverse row of connectors at the cross-section being considered

F_{TC} is the total longitudinal shear force that would occur in the row of connectors if all the connectors in the girder were infinitely stiff

K_s is the slip modulus of the connector being considered

It can be seen that, in all cases, γ for the longitudinal forces in the connectors varies almost parabolically from a maximum value A at the web to a value that is generally between 0.05A and 0.10A at the edge of the flange. It should be noted that the curves for the girders having the same proportion of the total number of connectors placed directly over the web are all very similar. The distributions of γ for the transverse forces in the connectors do not exhibit any such regular pattern.

The total longitudinal force occurring in each row of connectors was obtained and compared with the force F_{TC}. Except for the rows in the immediate vicinity of a point load, it was found that in each case the total longitudinal force was within 15 per cent of F_{TC}.

On the basis of the observations made in this sub-section, a formula has been proposed for predicting the distribution of the longitudinal forces in the connectors of a tee girder of practical proportions (see Section 6.5).

6.5 PROPOSALS FOR DESIGN RULES

It is clear from the examples discussed in Section 6.4 that the nearer the shear connectors are to the web of a composite girder, the more efficient they are in resisting the longitudinal shear force that is developed when the girder undergoes deformation. Further, the behaviour of the girders having large B/L values is significantly affected by the distribution of the connectors, whereas that of the girders having small B/L values is not. It therefore seems appropriate that the connectors designed to transmit the longitudinal shear force should be confined to a region bounded by two lines parallel to the web. The distance of each line from the web should reflect the B/L value of the girder, and hence it could be conveniently specified in terms of an effective breadth value for the flange. However, no specific distance will be recommended here since further numerical tests would be necessary before a reliable value could be established.

An estimate of the longitudinal shear force F occurring in a connector on the flange of a composite tee girder, as a result of longitudinal bending of the girder, may be obtained from the following formula:[a]

$$F = \frac{C\, F_{TC}\, K_s\, A}{K_{rs}} \left[0.95 \left(\frac{x}{B}\right)^2 + 0.05 \right]$$

where

- C is a coefficient selected so that the sum of F for the row of connectors at the cross-section being considered is equal to F_{TC}
- F_{TC} is the total longitudinal shear force that would occur in the row of connectors assuming complete interaction
- K_s is the slip modulus of the connector
- K_{rs} is the total slip modulus of the row of connectors
- A is a constant depending on the ratio of the slip modulus of the connector directly over the web at the cross-section to K_{rs}, and should be obtained from Fig.6.7[b]

(a) This formula was obtained by first assuming that the variation of $F\, K_{rs}/F_{TC}\, K_s$ across the girder could be expressed as a parabola having a value of A at the web, a value of 0.05A at the flange edge, and zero slope at the flange edge. The resulting equation was then re-arranged to give an expression for F, and the coefficient C was introduced.

(b) The curve shown in this figure is based on the values given in Table 6.8 for the girders having a B/L value of 0.05 and the shear connexions I1 to I4. To obtain the curve, the connector forces were multiplied by K_{rs}/K_s, K_s being the slip modulus of the connector over the web.

B is the distance between the web centre line and a free edge of the flange

x is the distance from the free edge of the flange to the connector

Curves plotted according to the above formula are shown in Figs 6.3 to 6.6. It is likely that this formula could also be applied to multi-web girders provided that each web and the associated portions of flange are treated separately in a manner similar to that described in Sub-section 5.4.3. However, further studies will have to be carried out in order to confirm the validity of this suggestion.

Appreciable transverse shear forces can sometimes occur in the connectors of a composite girder when it is subjected to longitudinal bending loads (see Sub-section 6.4.4). However, the limited number of examples considered here have not provided sufficient information for the formulation of a design rule which could be used in estimating these forces.

It should be mentioned that in cases where some connectors are placed directly over the webs of a composite girder, and where sufficient connectors are provided to limit the connector forces to within the allowable values specified in CP117: part 2: 1967, it is likely that a specification of the type recommended in the first paragraph of this section would be automatically satisfied.

6.6 CONCLUSIONS

(i) The finite element techniques described in Chapter 4 have been used to study some aspects of the effect of shear connector flexibility on the longitudinal bending behaviour of girders having composite flanges.

(ii) From the results of the study, it is apparent that the overall longitudinal bending behaviour of a composite girder is significantly dependent on the manner in which the shear connectors are distributed across the flange of the girder (Tables 6.3 to 6.7). It appears that the connectors provided to resist the longitudinal shear forces in a girder should be confined to the regions of flange immediately adjacent to each web, and that the width of these regions should reflect the B/L value of the flange. It was not possible, however, to establish a definite relationship from the limited number of cases considered in this chapter.

(iii) It has been shown that when a composite girder is subjected to longitudinal bending and the proportion of the total number of shear connectors placed directly over the webs is decreased, the forces occurring in those connectors remaining over the webs increase significantly (Table 6.8). Nevertheless, appreciable longitudinal and lateral forces can also occur in the connectors distributed over the flange. A simple rule for estimating the magnitude of such longitudinal forces has been presented (Section 6.5).

(iv) It should be emphasized that the number of variables considered in this study has been kept to a minimum in order that a clear understanding of the behaviour of the girders could be obtained. It is intended that further variables will be considered in subsequent studies.

CHAPTER 7.

GENERAL CONCLUSIONS

7.1 SUMMARY OF WORK

The work described herein on the linear static analysis of box girder bridges has involved:

(i) the development of a general purpose finite element computer program ICSAS (see Chapter 2)

(ii) the development of several special purpose elements for the efficient analysis of box girder bridges (see Chapter 3) and for use in the analysis of composite box girder bridges having either complete or incomplete interaction at the concrete-steel interfaces (see Chapter 4); these elements have been incorporated in the program ICSAS

(iii) the use of the program ICSAS in a parametric study of the shear lag phenomenon in steel box girders (see Chapter 5) and of the incomplete interaction phenomenon in composite box girder bridges (see Chapter 6); the results of these studies have been used as a basis for the formulation of design rules.

7.2 CONCLUDING REMARKS

The finite element method has proved to be suitable for the linear static analysis of any box girder bridge, irrespective of its complexity. Therefore, the method provides the basis for a valuable research and design tool.

It should be emphasized, however, that the computer cost involved in the finite element analysis of a box girder bridge is often considerable, even with the availability of special elements such as those presented in Chapter 3. Thus, there is still a need for alternative procedures for assessing the structural behaviour of this type of bridge.

One important application of the finite element method has been its use in 'numerical experiments', the results of which have enabled the development and verification of such alternative procedures. For example, in addition to the two parametric studies reported in Chapters 5 and 6, the program ICSAS has been used recently in studies, commissioned by the Committee of Investigation into the Design and Erection of Steel Box Girder Bridges,[47] that have lead to:

(i) the determination of the types of box girder bridge that are amenable to analysis by the beam on elastic foundation analogy

(ii) the formulation of design rules for estimating the stresses in the diaphragms of steel box girder bridges

The procedures of the finite element method for linear static analysis can be utilised in conjunction with one of several iterative schemes to incorporate the effects of geometrical and material non-linearity. However, the practical application of these techniques to box girder bridges, especially in the case of the complete structure, is generally limited by computer costs. Nevertheless, at the present rate of development in computer technology, cost should not continue to be an obstacle and the finite element method will, presumably, contribute further to the engineer's knowledge on the structural behaviour of box girder bridges.

REFERENCES

1. Massonnet, C. and Gandolfi, A. Sur certains cas exceptionnels dans la theorie des ponts a poutres multiples. Publs int. Ass. Bridge struct. Engng, vol.27, 1967, pp.73-94.

2. Lightfoot, E. and Sawko, F. Grid frameworks resolved by generalized slope deflection. Engineering, Lond., vol.87, 1959, pp.18-20.

3. Vlasov, V.Z. Thin-walled elastic beams. Jerusalem, Israel Program for Scientific Translations, 1961.

4. Wright, R.N., Abdel-Samad, S.R., and Robinson, A.R. BEF analogy for analysis of box girders. J. struct. Div., Proc. Am. Soc. civ. Engrs, vol.94, 1968, pp.1719-43.

5. Richmond, B. Twisting of thin-walled box girders, Proc. Instn civ. Engrs, vol.33, 1966, pp.659-75.

6. Goldberg,J.E. and Leve, H.L. Theory of prismatic folded plate structures. Publs.int. Ass. Bridge struct. Engng, vol.17, 1957, pp.59-86.

7. Scordelis, A.C. Analysis of simply supported box girder bridges. Report No.SESM-66-17, Dept. of Civil Engineering, Univ. of California, Berkeley, 1966.

8. Cheung, Y.K. Folded plate structures by finite strip method. J. struct. Div., Proc. Am. Soc. civ. Engrs, vol.95, 1969, pp.2963-79.

9. Zienkiewicz, O.C. The finite element method in engineering science London, McGraw-Hill, 1971.

10. Desai, C.S. and Abel, J.F. Introduction to the finite element method. New York, Van Nostrand Reinhold company, 1972.

11. Lim, P.T.K. Elastic analysis of bridge structures by the finite element method. Ph.D. thesis, University of London, 1971.

12. Gallagher, R.H. Large-scale computer programs for structural analysis. General Purpose Finite Element Computer Programs. Edited by Marcal, P.V. New York, The American Society of Mechanical Engineers, 1970.

13. Lim, P.T.K. and Moffatt, K.R. ICSAS Plane Stress Subsystem-User's manual. Research report, Engineering Structures Laboratories, Imperial College, 1972.

14. Lim, P.T.K., Kilford, J.T., and Moffatt, K.R. Finite element analysis of curved box girder bridges. Developments in Bridge Design and Construction (Proceedings of the International Conference at University College, Cardiff, 1971); edited by Rockey, K.C., Bannister, J.L., and Evans, H.R. London, Crosby Lockwood, 1972.

15. Lim, P.T.K. and Moffatt, K.R. Finite element analysis of curved slab bridges with special reference to local stresses. Developments in Bridge Design and Construction (Proceedings of the International Conference at University College, Cardiff, 1971); edited by Rockey, K.C., Bannister, J.L., and Evans, H.R. London, Crosby Lockwood, 1972.

16. Osborne-Moss, D.M. Limit states of composite steel-concrete bridges. Ph.d. thesis, University of London, 1971.

17. Gustafson, W.C. and Wright, R.N. Analysis of skewed composite girder bridges. J. struct. Div., Proc. Am. Soc. civ. Engrs., vol.94, 1968, pp.919-41.

18. Williams, D.G. Analysis of a doubly plated grillage under in-plane and normal loading. Ph.d. thesis, University of London, 1969.

19. Lim, P.T.K. and Moffatt, K.R. Finite element analysis of a ship's double bottom. Symposium on Finite Element Techniques, The Institut fur Statik and Dynamik der Luft-und Raumfahrtkonstruktionen, University of Stuttgart, Stuttgart, 1969.

20. El—gaaly, M.A. Analysis of multi-cell box gates for dry docks. J. struct. Div., Proc. Am. Soc. civ. Engrs., vol.91, 1965, pp.171-95.

21. Dowling, P.J., Chatterjee, S., Frieze, P.A., and Moolani, F.M. The experimental and predicted collapse behaviour of rectangular stiffened steel box girders. Proceedings of the International Conference on Steel Box Girder Bridges, Institution of Civil Engineers, London, 1973.

22. Duke, A. Tests and analysis on a perspex model of a tanker. British Ship Research Association report WG/SSD30, 1972.

23. Malewski, P.A.D. A comparison of numerical and experimental analyses of two dimensional elastic pierced shear walls. M.Sc. report, University of London, 1972.

24. Sawko, F. Recent developments in the analysis of steel bridges using electronic computers. Proceedings of the British Constructional Steelwork Association Conference on Steel Bridges. Instn of civ. Engrs, London, 1968.

25. Mehrotra, B.L., Mufti, A.A., and Redwood, R.G. Analysis of three dimensional thin-walled structures. J. struct. Div., Proc. Am. Soc. civ. Engrs, vol.95, 1969, pp.2863-72.

26. Sisodiya, R.G., Cheung, Y.K., and Ghali, A. Finite element analysis of skew, curved box-girder bridge. Publs int. Ass. Bridge Struct. Engng, vol.30-11, 1970, pp.191-99.

27. Sisodiya, R.G., Cheung,Y.K., and Ghali, A. New finite elements with application to box girder bridges. Proc. Instn civ. Engrs, supplement (XV11), 1972, p.207-25.

28. Scordelis, A.C. Analytical solutions for box girder bridges. Developments in Bridge Design and Construction (Proceedings of the International Conference at University College, Cardiff, 1971); edited by Rockey, K.C., Bannister, J.L., and Evans, H.R. London, Crosby Lockwood, 1972.

29. Ngo, D. and Scordelis, A.C. Finite element analysis of reinforced concrete beams. J. Am. Concr. Inst., vol.64, 1967, pp.152-63.

30. Billington, C.J. The theoretical and experimental elastic behaviour of box girder bridges. Ph.d. thesis, University of London, 1973.

31. Teraszkiewicz, J.S., Static and fatigue behaviour of simply supported and continuous composite beams of steel and concrete. Ph.d. thesis, University of London, 1967.

32. Clarke, J.L. and Morley, C.T. Steel-concrete composite plates with flexible shear connectors. Proc. Instn civ. Engrs, vol.53, part 2, 1972, pp.557-68.

33. Morley, C.T. Private communication.

34. Kondo, K., Komatsu, S., and Nakai, H. Theoretical and experimental researches on the effective width of girder bridge with steel plate deck. Trans. Japan Soc. civ. Engrs, vol.86, 1962, pp.1-19.

35. Schade, H.A. The effective breadth of stiffened plating under bending loads. Trans. Soc. nav. Archit. mar. Engrs, vol.59, 1951, pp.403-20.

36. Winter, G. Stress distribution in and equivalent width of flanges of wide, thin-wall steel beams. Tech. Notes natn. advis. Comm. Aeronaut., Wash. Note 784, 1940.

37. Yuille, I.M. Shear lag in stiffened plating. Trans. Instn. nav. Archit., vol.97, 1955, pp.252-86.

38. Abdel-Sayed, G. Effective width of steel deck-plate in bridges. J. struct. Div., Proc. Am. Soc. civ. Engrs, vol.95, 1969, pp.1459-74.

39. British Standards, CP 117: Composite construction in structural steel and concrete. Part 2: Beams for bridges, 1967.

40. German Standards, DIN 1073: Steel road bridges, (Draft). 1969.

41. Morley, L.S.D. Skew plates and structures. Oxford, Pergamon Press, 1963.

42. Sawko, F. and Cope, R.J. The use of finite elements for the analysis of right bridge decks. Proceedings of the International Symposium on The Use of Electronic Digital Computers in Structural Engineering, University of Newcastle, 1966.

43. Oden, J.T. Mechanics of elastic structures. New York, McGraw-Hill, 1967.

44. Committee of inquiry into the basis of design and method of erection of steel box girder bridges. Interim Design Rules, Department of the Environment, 1973.

45. Balakrishnan, S. The behaviour of composite steel and concrete beams with welded stud shear connectors. Ph.d. thesis, University of London, 1963.

46. Chapman, J.C. The behaviour of composite beams in steel and concrete. Struct. Engr., vol.42, 1964, pp.115-25.

47. Flint, A.R. and Horne, M.R. Conclusions of research programme and summary of parametric studies. Proceedings of the International Conference on Steel Box Girder Bridges, Institution of Civil Engineers, London, 1973.

48. Livesley, R.K. Matrix methods of structural analysis. Oxford, Pergamon Press, 1964.

49. Dawe, D.J. Parallelogrammic elements in the solution of rhombic cantilever plate problems. J. Strain Anal., vol.1, 1966, pp.223-30.

APPENDIX A.

DERIVATION OF STIFFNESS MATRIX FOR ELEMENT Q40

The element Q40 has at each of its four nodes the degrees of freedom u, v, $\frac{\partial v}{\partial x}$, and $\frac{\partial u}{\partial x}$, where u and v are translations parallel to the x and y axes, respectively, of the element. The element displacement functions, expressed in terms of the generalized co-ordinates ξ and η (Fig. 3.2), take the form

$$u = \alpha_1 + \alpha_2\xi + \alpha_3\eta + \alpha_4\xi^2 + \alpha_5\xi\eta + \alpha_6\xi^3 + \alpha_7\xi^2\eta + \alpha_8\xi^3\eta$$

$$v = \alpha_9 + \alpha_{10}\xi + \alpha_{11}\eta + \alpha_{12}\xi^2 + \alpha_{13}\xi\eta + \alpha_{14}\xi^3 + \alpha_{15}\xi^2\eta + \alpha_{16}\xi^3\eta$$

where α_1 to α_{16} are arbitrary coefficients.

For a quadrilateral, the x, y co-ordinates are conveniently related to the ξ, η co-ordinates by the following expressions:

$$x = \tfrac{1}{4}\{(1-\xi)(1-\eta)x_i + (1+\xi)(1-\eta)x_j + (1+\xi)(1+\eta)x_k + (1-\xi)(1+\eta)x_l\}$$

$$y = \tfrac{1}{4}\{(1-\xi)(1-\eta)y_i + (1+\xi)(1-\eta)y_j + (1+\xi)(1+\eta)y_k + (1-\xi)(1+\eta)y_l\}$$

Since it is difficult, if not impossible, to express u and v in terms of x and y, the derivation of the stiffness matrix given here has been carried out in terms of the generalized co-ordinates.

The stiffness matrix $[K]$ of the element can be obtained using the standard equation[9]

$$[K] = ([C]^{-1})^t \left(\iint [Q]^t\, [D]\, [Q]\, dxdy\right) [C]^{-1}$$

The following paragraphs indicate procedures by means of which the matrices appearing in the above equation may be evaluated.

The matrix $[C]$ relates the nodal parameter vector $\{\delta\}$ to the coefficient vector $\{\alpha\}$ according to the equation

$$\{\delta\} = [C]\{\alpha\}$$

where

$$\{\delta\} = \begin{Bmatrix} u_i \\ v_i \\ (\frac{\partial v}{\partial x})_i \\ (\frac{\partial u}{\partial x})_i \\ \vdots \\ (\frac{\partial u}{\partial x})_k \end{Bmatrix}$$

The term $\frac{\partial v}{\partial x}$ can be obtained using the chain rule for partial derivatives as follows:

$$\frac{\partial v}{\partial \xi} = \frac{\partial v}{\partial x}\frac{\partial x}{\partial \xi} + \frac{\partial v}{\partial y}\frac{\partial y}{\partial \xi}$$

$$\frac{\partial v}{\partial \eta} = \frac{\partial v}{\partial x}\frac{\partial x}{\partial \eta} + \frac{\partial v}{\partial y}\frac{\partial y}{\partial \eta}$$

from which

$$\frac{\partial v}{\partial x} = \frac{1}{J}\left(\frac{\partial v}{\partial \xi}\frac{\partial y}{\partial \eta} - \frac{\partial v}{\partial \eta}\frac{\partial y}{\partial \xi}\right)$$

where J is the determinant of the Jacobian matrix

$$\begin{bmatrix} \frac{\partial x}{\partial \xi} & \frac{\partial y}{\partial \xi} \\ \frac{\partial x}{\partial \eta} & \frac{\partial y}{\partial \eta} \end{bmatrix}$$

Similarly

$$\frac{\partial u}{\partial x} = \frac{1}{J} \left(\frac{\partial u}{\partial \xi} \frac{\partial y}{\partial \eta} - \frac{\partial u}{\partial \eta} \frac{\partial y}{\partial \xi} \right)$$

By using the above expressions, it is possible to obtain the matrix $[C]$ and hence its inverse, for which a numerical procedure is necessary.

The rigidity matrix $[D]$ relates the stress resultant vector $\{\sigma\}$ to the strain vector $\{\varepsilon\}$ according to the equation

$$\{\sigma\} = [D] \{\varepsilon\}$$

For an orthotropic plate with principal directions of orthotropy coinciding with the x and y axes of the element, this relationship takes the standard form

$$\begin{Bmatrix} \sigma_x h \\ \sigma_y h \\ \tau_{xy} h \end{Bmatrix} = \begin{bmatrix} C_x & C_1 & 0 \\ C_1 & C_y & 0 \\ 0 & 0 & C_{xy} \end{bmatrix} \begin{Bmatrix} \varepsilon_x \\ \varepsilon_y \\ \gamma_{xy} \end{Bmatrix}$$

where

$$C_x = E_x h/(1 - \nu_{xy}\,\nu_{yx})$$

$$C_y = E_y h/(1 - \nu_{xy}\,\nu_{yx})$$

$$C_{xy} = Gh$$

$$C_1 = \nu_{xy}\,E_y h/(1 - \nu_{xy}\,\nu_{yx})$$

In the above expressions E_x and E_y are the elastic moduli, G is the shear modulus, and ν_{xy} and ν_{yx} are the Poisson's ratios of the element, with respect to the x and y axes.

The matrix $[Q]$ relates the strain vector $\{\varepsilon\}$ to the coefficient vector $\{\alpha\}$ according to the equation

$$\{\varepsilon\} = [Q]\{\alpha\}$$

Following the procedure used in obtaining the expressions for $\frac{\partial v}{\partial x}$ and $\frac{\partial u}{\partial x}$, the expressions for the individual strain components are obtained as

$$\varepsilon_x = \frac{\partial u}{\partial x} = \frac{1}{J}\left(\frac{\partial u}{\partial \xi}\frac{\partial y}{\partial \eta} - \frac{\partial u}{\partial \eta}\frac{\partial y}{\partial \xi}\right)$$

$$\varepsilon_y = \frac{\partial v}{\partial y} = -\frac{1}{J}\left(\frac{\partial v}{\partial \xi}\frac{\partial x}{\partial \eta} - \frac{\partial v}{\partial \eta}\frac{\partial x}{\partial \xi}\right)$$

$$\gamma_{xy} = \frac{\partial u}{\partial y} + \frac{\partial v}{\partial x} = -\frac{1}{J}\left(\frac{\partial u}{\partial \xi}\frac{\partial x}{\partial \eta} - \frac{\partial u}{\partial \eta}\frac{\partial x}{\partial \xi} - \frac{\partial v}{\partial \xi}\frac{\partial y}{\partial \eta} + \frac{\partial v}{\partial \eta}\frac{\partial y}{\partial \xi}\right)$$

Hence the matrix $[Q]$ can be obtained.

Before the integration can be carried out, the element of area dxdy must also be expressed in terms of the ξ,η co-ordinates using the expression $dxdy = J\, d\xi d\eta$, and the limits of integration changed to -1 and +1 in both variables (Ref. 9, pp. 142). The actual integration can be simply achieved using the Gaussian quadrature formula (Ref. 9, pp. 146).

For a rectangular or parallelogrammic element, it is only necessary to use four pivotal points in each direction in order to obtain a stiffness matrix identical to that obtained by explicit integration. However, as the shape of the element deviates from that of a parallelogram, more pivotal points are required for the result of the integration to converge. For an element of the most general shape likely to be encountered in a practical mesh, it was found necessary to use six pivotal points in each direction.

Finally, it should be noted that following the evaluation of the nodal parameters, the stress resultant vector $\{\sigma\}$ can be obtained from the expression

$$\{\sigma\} = [D]\ [Q]\ [C]^{-1}\ \{\delta\}$$

APPENDIX B.

DERIVATION OF STIFFNESS MATRICES FOR ELEMENTS T30 AND T40

The elements T30 and T40 were primarily developed for use with the elements Q30 and Q40, respectively, in a mesh scheme of the type shown in Fig. 3.3. For this reason, the formulation of the element stiffness matrices is given here for the limiting case of a right-angled triangle (Fig. B.1). The generalization of the elements to the case of a general triangle can be achieved using a procedure similar to that described in Appendix A.

Since the element T30 is a special case of the element T40, the latter will be considered first. The element T40 has the degrees of freedom u, v, $\frac{\partial v}{\partial x}$, and $\frac{\partial u}{\partial x}$, where u and v are translations parallel to the x and y axes, respectively, of the element. The element displacement functions take the form

$$u = \alpha_1 + \alpha_2 x + \alpha_3 y + \alpha_4 x^2 + \alpha_5 xy + \alpha_6 x^3$$

$$v = \alpha_7 + \alpha_8 x + \alpha_9 y + \alpha_{10} x^2 + \alpha_{11} xy + \alpha_{12} x^3$$

where α_1 to α_{12} are arbitrary coefficients.

The stiffness matrix $[k]$ of the element can be obtained using the standard equation[9]

$$[k] = ([C]^{-1})^t \left(\iint [Q]^t\ [D]\ [Q]\ dx\ dy\right) [C]^{-1}$$

The following paragraphs define the matrices appearing in the above equation.

The matrix $[C]$ relates the nodal parameter vector $\{\delta\}$ to the coefficient vector $\{\alpha\}$ according to the equation

$$\{\delta\} = [C]\,\{\alpha\}$$

which may be inverted and written in the form

$$\begin{Bmatrix} \alpha_1 \\ \alpha_2 \\ \alpha_3 \\ \alpha_4 \\ \alpha_5 \\ \alpha_6 \\ \alpha_7 \\ \alpha_8 \\ \alpha_9 \\ \alpha_{10} \\ \alpha_{11} \\ \alpha_{12} \end{Bmatrix} = \begin{bmatrix} 1 & 0 & 0 & 0 & 0 & 0 & 0 & 0 & 0 & 0 & 0 & 0 \\ 0 & 0 & 0 & 1 & 0 & 0 & 0 & 0 & 0 & 0 & 0 & 0 \\ \frac{-1}{b} & 0 & 0 & 0 & 0 & 0 & 0 & 0 & \frac{1}{b} & 0 & 0 & 0 \\ \frac{-3}{a^2} & 0 & 0 & \frac{-2}{a} & \frac{3}{a^2} & 0 & 0 & \frac{-1}{a} & 0 & 0 & 0 & 0 \\ 0 & 0 & 0 & \frac{-1}{b} & 0 & 0 & 0 & 0 & 0 & 0 & 0 & \frac{1}{b} \\ \frac{2}{a^3} & 0 & 0 & \frac{1}{a^2} & \frac{-2}{a^3} & 0 & 0 & \frac{1}{a^2} & 0 & 0 & 0 & 0 \\ 0 & 1 & 0 & 0 & 0 & 0 & 0 & 0 & 0 & 0 & 0 & 0 \\ 0 & 0 & 1 & 0 & 0 & 0 & 0 & 0 & 0 & 0 & 0 & 0 \\ 0 & \frac{-1}{b} & 0 & 0 & 0 & 0 & 0 & 0 & 0 & \frac{1}{b} & 0 & 0 \\ 0 & \frac{-3}{a^2} & \frac{-2}{a} & 0 & 0 & \frac{3}{a^2} & \frac{-1}{a} & 0 & 0 & 0 & 0 & 0 \\ 0 & 0 & \frac{-1}{b} & 0 & 0 & 0 & 0 & 0 & 0 & 0 & \frac{1}{b} & 0 \\ 0 & \frac{2}{a^3} & \frac{1}{a^2} & 0 & 0 & \frac{-2}{a^3} & \frac{1}{a^2} & 0 & 0 & 0 & 0 & 0 \end{bmatrix} \begin{Bmatrix} u_i \\ v_i \\ (\frac{\partial v}{\partial x})_i \\ (\frac{\partial u}{\partial x})_i \\ u_j \\ v_j \\ (\frac{\partial v}{\partial x})_j \\ (\frac{\partial u}{\partial x})_j \\ u_k \\ v_k \\ (\frac{\partial v}{\partial x})_k \\ (\frac{\partial u}{\partial x})_k \end{Bmatrix} \qquad \text{(a)}$$

The rigidity matrix $[D]$ relates the stress resultant vector $\{\sigma\}$ to the strain vector $\{\varepsilon\}$ according to the equation $\{\sigma\} = [D]\{\varepsilon\}$, the expanded form of which is given in Appendix A.

The matrix $[Q]$ relates the strain vector $\{\varepsilon\}$ to the coefficient vector $\{\alpha\}$ according to the equation

$$\{\varepsilon\} = [Q]\{\alpha\}$$

By virtue of the prescribed displacement functions, this equation takes the form

$$\begin{Bmatrix} \frac{\partial u}{\partial x} \\ \frac{\partial v}{\partial y} \\ \frac{\partial u}{\partial y}+\frac{\partial v}{\partial x} \end{Bmatrix} = \begin{bmatrix} 0 & 1 & 0 & 2x & y & 3x^2 & 0 & 0 & 0 & 0 & 0 & 0 \\ 0 & 0 & 0 & 0 & 0 & 0 & 0 & 0 & 1 & 0 & x & 0 \\ 0 & 0 & 1 & 0 & x & 0 & 0 & 1 & 0 & 2x & y & 3x^2 \end{bmatrix} \begin{Bmatrix} \alpha_1 \\ \cdot \\ \cdot \\ \cdot \\ \alpha_{12} \end{Bmatrix} \quad \text{(b)}$$

The non-zero terms of the symmetric matrix

$$[\bar{k}] = \iint [Q]^t \, [D] \, [Q] \, dx \, dy \quad \text{(c)}$$

are as follows:

$\bar{k}_{2,2} = \frac{1}{2} a \, b \, C_x$ $\bar{k}_{3,3} = \frac{1}{2} a \, b \, C_{xy}$

$\bar{k}_{2,4} = \frac{1}{3} a^2 \, b \, C_x$ $\bar{k}_{4,4} = \frac{1}{3} a^3 \, b \, C_x$

$\bar{k}_{2,5} = \frac{1}{6} a \, b^2 \, C_x$ $\bar{k}_{3,5} = \frac{1}{6} a^2 \, b \, C_{xy}$

$\bar{k}_{4,5} = \frac{1}{12} a^2 \, b^2 \, C_x$ $\bar{k}_{5,5} = \frac{1}{12} (a \, b^3 \, C_x + a^3 \, b \, C_{xy})$

$\bar{k}_{2,6} = \frac{1}{4} a^3 \, b \, C_x$ $\bar{k}_{4,6} = \frac{3}{10} a^4 \, b \, C_x$

$$\bar{k}_{5,6} = \frac{1}{20} a^3 b^2 C_x \qquad \bar{k}_{6,6} = \frac{3}{10} a^5 b C_x$$

$$\bar{k}_{3,8} = \frac{1}{2} a b C_{xy} \qquad \bar{k}_{5,8} = \frac{1}{6} a^2 b C_{xy}$$

$$\bar{k}_{8,8} = \frac{1}{2} a b C_{xy} \qquad \bar{k}_{2,9} = \frac{1}{2} a b C_1$$

$$\bar{k}_{4,9} = \frac{1}{3} a^2 b C_1 \qquad \bar{k}_{5,9} = \frac{1}{6} a b^2 C_1$$

$$\bar{k}_{6,9} = \frac{1}{4} a^3 b C_1 \qquad \bar{k}_{9,9} = \frac{1}{2} a b C_y$$

$$\bar{k}_{3,10} = \frac{1}{3} a^2 b C_{xy} \qquad \bar{k}_{5,10} = \frac{1}{6} a^3 b C_{xy}$$

$$\bar{k}_{8,10} = \frac{1}{3} a^2 b C_{xy} \qquad \bar{k}_{10,10} = \frac{1}{3} a^3 b C_{xy}$$

$$\bar{k}_{2,11} = \frac{1}{6} a^2 b C_1 \qquad \bar{k}_{3,11} = \frac{1}{6} a b^2 C_{xy}$$

$$\bar{k}_{4,11} = \frac{1}{6} a^3 b C_1 \qquad \bar{k}_{5,11} = \frac{1}{24} a^2 b^2 (C_1 + C_{xy})$$

$$\bar{k}_{6,11} = \frac{3}{20} a^4 b C_1 \qquad \bar{k}_{8,11} = \frac{1}{6} a b^2 C_{xy}$$

$$\bar{k}_{9,11} = \frac{1}{6} a^2 b C_y \qquad \bar{k}_{10,11} = \frac{1}{12} a^2 b^2 C_{xy}$$

$$\bar{k}_{11,11} = \frac{1}{12} (a^3 b C_y + a b^3 C_{xy}) \qquad \bar{k}_{3,12} = \frac{1}{4} a^3 b C_{xy}$$

$$\bar{k}_{5,12} = \frac{3}{20} a^4 b C_{xy} \qquad \bar{k}_{8,12} = \frac{1}{4} a^3 b C_{xy}$$

$$\bar{k}_{10,12} = \frac{3}{10} a^4 b C_{xy} \qquad \bar{k}_{11,12} = \frac{1}{20} a^3 b^2 C_{xy}$$

$$\bar{k}_{12,12} = \frac{3}{10} a^5 b C_{xy}$$

Finally, it should be noted that following the evaluation of the nodal parameters, the stress resultant vector $\{\sigma\}$ can be obtained from the expression

$$\{\sigma\} = [D]\ [Q]\ [C]^{-1}\ \{\delta\}$$

The element T30 has three degrees of freedom u, v, and $\frac{\partial v}{\partial x}$ at each node and has displacement functions that take the form

$$u = \alpha_1 + \alpha_2\, x + \alpha_3\, y$$

$$v = \alpha_7 + \alpha_8\, x + \alpha_9\, y + \alpha_{10}\, x^2 + \alpha_{11}\, x\, y + \alpha_{12}\, x^3$$

Hence, the matrices $[Q]$ and $[\bar{k}]$ may be obtained from Eqs (b) and (c) by eliminating the terms corresponding to α_4, α_5, and α_6, while the equation corresponding to Eq. (a) may be written as

$$\begin{Bmatrix} \alpha_1 \\ \alpha_2 \\ \alpha_3 \\ \alpha_7 \\ \alpha_8 \\ \alpha_9 \\ \alpha_{10} \\ \alpha_{11} \\ \alpha_{12} \end{Bmatrix} = \begin{bmatrix} 1 & 0 & 0 & 0 & 0 & 0 & 0 & 0 & 0 \\ -\frac{1}{a} & 0 & 0 & \frac{1}{a} & 0 & 0 & 0 & 0 & 0 \\ -\frac{1}{b} & 0 & 0 & 0 & 0 & 0 & \frac{1}{b} & 0 & 0 \\ 0 & 1 & 0 & 0 & 0 & 0 & 0 & 0 & 0 \\ 0 & 0 & 1 & 0 & 0 & 0 & 0 & 0 & 0 \\ 0 & -\frac{1}{b} & 0 & 0 & 0 & 0 & 0 & \frac{1}{b} & 0 \\ 0 & -\frac{3}{a^2} & -\frac{2}{a} & 0 & \frac{3}{a^2} & -\frac{1}{a} & 0 & 0 & 0 \\ 0 & 0 & -\frac{1}{b} & 0 & 0 & 0 & 0 & 0 & \frac{1}{b} \\ 0 & \frac{2}{a^3} & \frac{1}{a^2} & 0 & -\frac{2}{a^3} & \frac{1}{a^2} & 0 & 0 & 0 \end{bmatrix} \begin{Bmatrix} u_i \\ v_i \\ (\frac{\partial v}{\partial x})_i \\ u_j \\ v_j \\ (\frac{\partial v}{\partial x})_j \\ u_k \\ v_k \\ (\frac{\partial v}{\partial x})_k \end{Bmatrix}$$

APPENDIX C.

DERIVATION OF STIFFNESS MATRICES FOR ELEMENTS R5 AND R6

The formulation of the stiffness matrices for the laminated elements R5 and R6 is described here for the limiting case of a rectangular element (Fig. C.1) for which an explicit form of the matrices may be obtained. The generalization of the elements to the case of a general quadrilateral can be achieved using a procedure similar to that described in Appendix A.

Since the element R5 is a special case of the element R6, the latter will be considered first. The element R6 has the degrees of freedom u, v, w, $\frac{\partial w}{\partial y}$, $-\frac{\partial w}{\partial x}$, and $\frac{\partial v}{\partial x}$, where u, v, and w are translations parallel to the x, y, and z axes, respectively, of the element. The element displacement functions take the form

$$u = \alpha_1 + \alpha_2 x + \alpha_3 y + \alpha_4 xy$$

$$v = \alpha_5 + \alpha_6 x + \alpha_7 y + \alpha_8 x^2 + \alpha_9 xy + \alpha_{10} x^3 + \alpha_{11} x^2 y + \alpha_{12} x^3 y$$

$$w = \alpha_{13} + \alpha_{14} x + \alpha_{15} y + \alpha_{16} x^2 + \alpha_{17} xy + \alpha_{18} y^2 + \alpha_{19} x^3 + \alpha_{20} x^2 y + \alpha_{21} xy^2 + \alpha_{22} y^3 + \alpha_{23} x^3 y + \alpha_{24} xy^3$$

where α_1 to α_{24} are arbitrary coefficients.

The stiffness matrix $[k]$ of the element can be obtained using the standard equation[9]

$$[k] = ([C]^{-1})^t \left(\iint [Q]^t \, [D] \, [Q] \, dx \, dy\right) [C]^{-1}$$

The following paragraphs define the matrices appearing in the above equation.

The matrix $[C]$ relates the nodal parameter vector $\{\delta\}$ to the coefficient vector $\{\alpha\}$ according to the equation

$$\{\delta\} = [C]\{\alpha\}$$

The non-zero terms of the inverse of the matrix $[C]$ are as follows:

$C_{11} = 1.0$	$C_{2,1} = \frac{-1}{a}$	$C_{3,1} = \frac{-1}{b}$	$C_{4,1} = \frac{1}{ab}$
$C_{5,2} = 1.0$	$C_{7,2} = \frac{-1}{b}$	$C_{8,2} = \frac{-3}{a^2}$	$C_{10,2} = \frac{2}{a^3}$
$C_{11,2} = \frac{3}{a^2b}$	$C_{12,2} = \frac{-2}{a^3b}$	$C_{13,3} = 1.0$	$C_{16,3} = \frac{-3}{a^2}$
$C_{17,3} = \frac{-1}{ab}$	$C_{18,3} = \frac{-3}{b^2}$	$C_{19,3} = \frac{2}{a^3}$	$C_{20,3} = \frac{3}{a^2b}$
$C_{21,3} = \frac{3}{ab^2}$	$C_{22,3} = \frac{2}{b^3}$	$C_{23,3} = \frac{-2}{a^3b}$	$C_{24,3} = \frac{-2}{ab^3}$
$C_{15,4} = 1.0$	$C_{17,4} = \frac{-1}{a}$	$C_{18,4} = \frac{-2}{b}$	$C_{21,4} = \frac{2}{ab}$
$C_{22,4} = \frac{1}{b^2}$	$C_{24,4} = \frac{-1}{ab^2}$	$C_{14,5} = -1.0$	$C_{16,5} = \frac{2}{a}$
$C_{17,5} = \frac{1}{b}$	$C_{19,5} = \frac{-1}{a^2}$	$C_{20,5} = \frac{-2}{ab}$	$C_{23,5} = \frac{1}{a^2b}$
$C_{6,6} = 1.0$	$C_{8,6} = \frac{-2}{a}$	$C_{9,6} = \frac{-1}{b}$	$C_{10,6} = \frac{1}{a^2}$
$C_{11,6} = \frac{2}{ab}$	$C_{12,6} = \frac{-1}{a^2b}$	$C_{2,7} = \frac{1}{a}$	$C_{4,7} = \frac{-1}{ab}$
$C_{8,8} = \frac{3}{a^2}$	$C_{10,8} = \frac{-2}{a^3}$	$C_{11,8} = \frac{-3}{a^2b}$	$C_{12,8} = \frac{2}{a^3b}$

$C_{16,9} = \frac{3}{a^2}$ $\quad C_{17,9} = \frac{1}{ab}$ $\quad C_{19,9} = \frac{-2}{a^3}$ $\quad C_{20,9} = \frac{-3}{a^2b}$

$C_{21,9} = \frac{-3}{ab^2}$ $\quad C_{23,9} = \frac{2}{a^3b}$ $\quad C_{24,9} = \frac{2}{ab^3}$ $\quad C_{17,10} = \frac{1}{a}$

$C_{21,10} = \frac{-2}{ab}$ $\quad C_{24,10} = \frac{1}{ab^2}$ $\quad C_{16,11} = \frac{1}{a}$ $\quad C_{19,11} = \frac{-1}{a^2}$

$C_{20,11} = \frac{-1}{ab}$ $\quad C_{23,11} = \frac{1}{a^2b}$ $\quad C_{8,12} = \frac{-1}{a}$ $\quad C_{10,12} = \frac{1}{a^2}$

$C_{11,12} = \frac{1}{ab}$ $\quad C_{12,12} = \frac{-1}{a^2b}$ $\quad C_{4,13} = \frac{1}{ab}$ $\quad C_{11,14} = \frac{3}{a^2b}$

$C_{12,14} = \frac{-2}{a^3b}$ $\quad C_{17,15} = \frac{-1}{ab}$ $\quad C_{20,15} = \frac{3}{a^2b}$ $\quad C_{21,15} = \frac{3}{ab^2}$

$C_{23,15} = \frac{-2}{a^3b}$ $\quad C_{24,15} = \frac{-2}{ab^3}$ $\quad C_{21,16} = \frac{-1}{ab}$ $\quad C_{24,16} = \frac{1}{ab^2}$

$C_{20,17} = \frac{1}{ab}$ $\quad C_{23,17} = \frac{-1}{a^2b}$ $\quad C_{11,18} = \frac{-1}{ab}$ $\quad C_{12,18} = \frac{1}{a^2b}$

$C_{3,19} = \frac{1}{b}$ $\quad C_{4,19} = \frac{-1}{ab}$ $\quad C_{7,20} = \frac{1}{b}$ $\quad C_{11,20} = \frac{-3}{a^2b}$

$C_{12,20} = \frac{2}{a^3b}$ $\quad C_{17,21} = \frac{1}{ab}$ $\quad C_{18,21} = \frac{3}{b^2}$ $\quad C_{20,21} = \frac{-3}{a^2b}$

$C_{21,21} = \frac{-3}{ab^2}$ $\quad C_{22,21} = \frac{-2}{b^3}$ $\quad C_{23,21} = \frac{2}{a^3b}$ $\quad C_{24,21} = \frac{2}{ab^3}$

$C_{18,22} = \frac{-1}{b}$ $\quad C_{21,22} = \frac{1}{ab}$ $\quad C_{22,22} = \frac{1}{b^2}$ $\quad C_{24,22} = \frac{-1}{ab^2}$

$C_{17,23} = \frac{-1}{b}$ $\quad C_{20,23} = \frac{2}{ab}$ $\quad C_{23,23} = \frac{-1}{a^2b}$ $\quad C_{9,24} = \frac{1}{b}$

$C_{11,24} = \frac{-2}{ab}$ $\quad C_{12,24} = \frac{1}{a^2b}$

The rigidity matrix $[D]$ relates the vector of stress resultants and couples $\{\sigma\}$ to the vector of strains and curvatures at the reference surface $\{\varepsilon\}$ according to the equation $\{\sigma\} = [D]\{\varepsilon\}$, the expanded form of which has been derived in Chapter 4.

The matrix $[Q]$ relates the vector $\{\varepsilon\}$ to the coefficient vector $\{\alpha\}$ according to the equation

$$\{\varepsilon\} = [Q]\{\alpha\}$$

By virtue of the prescribed displacement functions, this equation takes the form

$$\begin{Bmatrix} \frac{\partial u}{\partial x} \\ \frac{\partial v}{\partial y} \\ \frac{\partial u}{\partial y} + \frac{\partial v}{\partial x} \\ -\frac{\partial^2 w}{\partial x^2} \\ -\frac{\partial^2 w}{\partial y^2} \\ -2\frac{\partial^2 w}{\partial x \partial y} \end{Bmatrix} = \begin{bmatrix} Q_{11} & 0 \\ 0 & Q_{22} \end{bmatrix} \begin{Bmatrix} \alpha_1 \\ \cdot \\ \cdot \\ \cdot \\ \cdot \\ \alpha_{24} \end{Bmatrix} \qquad \text{(a)}$$

where

$$[Q_{11}] = \begin{bmatrix} 0 & 1 & 0 & y & 0 & 0 & 0 & 0 & 0 & 0 & 0 & 0 \\ 0 & 0 & 0 & 0 & 0 & 0 & 1 & 0 & x & 0 & x^2 & x^3 \\ 0 & 0 & 1 & x & 0 & 1 & 0 & 2x & y & 3x^2 & 2xy & 3x^2y \end{bmatrix}$$

and

$$\left[Q_{22}\right] = \begin{bmatrix} 0 & 0 & 0 & -2 & 0 & 0 & -6x & -2y & 0 & 0 & -6xy & 0 \\ 0 & 0 & 0 & 0 & 0 & -2 & 0 & 0 & -2x & -6y & 0 & -6xy \\ 0 & 0 & 0 & 0 & -2 & 0 & 0 & -4x & -4y & 0 & -6x^2 & -6y^2 \end{bmatrix}$$

The non-zero terms of the symmetric matrix

$$[\,\bar{k}\,] = \iint [Q]^t \,[D]\, [Q]\, dx\, dy \tag{b}$$

are as follows:

$\bar{k}_{2,2} = R_{11}\, a\, b$

$\bar{k}_{3,3} = R_{33}\, a\, b$

$\bar{k}_{2,4} = \frac{1}{2} R_{11}\, a\, b^2$

$\bar{k}_{3,4} = \frac{1}{2} R_{33}\, a^2\, b$

$\bar{k}_{4,4} = \frac{1}{3} (R_{11}\, a\, b^3 + R_{33}\, a^3\, b)$

$\bar{k}_{3,6} = R_{33}\, a\, b$

$\bar{k}_{4,6} = \frac{1}{2} R_{33}\, a^2\, b$

$\bar{k}_{6,6} = R_{33}\, a\, b$

$\bar{k}_{2,7} = R_{12}\, a\, b$

$\bar{k}_{4,7} = \frac{1}{2} R_{12}\, a\, b^2$

$\bar{k}_{7,7} = R_{22}\, a\, b$

$\bar{k}_{3,8} = R_{33}\, a^2\, b$

$\bar{k}_{4,8} = \frac{2}{3} R_{33}\, a^3\, b$

$\bar{k}_{6,8} = R_{33}\, a^2\, b$

$\bar{k}_{8,8} = \frac{4}{3} R_{33}\, a^3\, b$

$\bar{k}_{2,9} = \frac{1}{2} R_{12}\, a^2\, b$

$\bar{k}_{3,9} = \frac{1}{2} R_{33}\, a\, b^2$

$\bar{k}_{4,9} = \frac{1}{4}\, a^2\, b^2\, (R_{12} + R_{33})$

$\bar{k}_{6,9} = \frac{1}{2} R_{33}\, a\, b^2$

$\bar{k}_{7,9} = \frac{1}{2} R_{22}\, a^2\, b$

$\bar{k}_{8,9} = \frac{1}{2} R_{33}\, a^2\, b^2$

$\bar{k}_{9,9} = \frac{1}{3} (R_{22}\, a^3\, b + R_{33}\, a\, b^3)$

$$\bar{k}_{3,10} = R_{33}\, a^3\, b \qquad \bar{k}_{4,10} = \frac{3}{4} R_{33}\, a^4\, b$$

$$\bar{k}_{6,10} = R_{33}\, a^3\, b \qquad \bar{k}_{8,10} = \frac{3}{2} R_{33}\, a^4\, b$$

$$\bar{k}_{9,10} = \frac{1}{2} R_{33}\, a^3\, b^2 \qquad \bar{k}_{10,10} = \frac{9}{5} R_{33}\, a^5\, b$$

$$\bar{k}_{2,11} = \frac{1}{3} R_{12}\, a^3\, b \qquad \bar{k}_{3,11} = \frac{1}{2} R_{33}\, a^2\, b^2$$

$$\bar{k}_{4,11} = \frac{1}{6} a^3\, b^2\, (R_{12} + 2\, R_{33}) \qquad \bar{k}_{6,11} = \frac{1}{2} R_{33}\, a^2\, b^2$$

$$\bar{k}_{7,11} = \frac{1}{3} R_{22}\, a^3\, b \qquad \bar{k}_{8,11} = \frac{2}{3} R_{33}\, a^3\, b^2$$

$$\bar{k}_{9,11} = \frac{1}{4} R_{22}\, a^4\, b + \frac{1}{3} R_{33}\, a^2\, b^3 \qquad \bar{k}_{10,11} = \frac{3}{4} R_{33}\, a^4\, b^2$$

$$\bar{k}_{11,11} = \frac{1}{5} R_{22}\, a^5\, b + \frac{4}{9} R_{33}\, a^3\, b^3 \qquad \bar{k}_{2,12} = \frac{1}{4} R_{12}\, a^4\, b$$

$$\bar{k}_{3,12} = \frac{1}{2} R_{33}\, a^3\, b^2 \qquad \bar{k}_{4,12} = \frac{1}{8} a^4\, b^2\, (R_{12} + 3\, R_{33})$$

$$\bar{k}_{6,12} = \frac{1}{2} R_{33}\, a^3\, b^2 \qquad \bar{k}_{7,12} = \frac{1}{4} R_{22}\, a^4\, b$$

$$\bar{k}_{8,12} = \frac{3}{4} R_{33}\, a^4\, b^2 \qquad \bar{k}_{9,12} = \frac{1}{5} R_{22}\, a^5\, b + \frac{1}{3} R_{33}\, a^3\, b^3$$

$$\bar{k}_{10,12} = \frac{9}{10} R_{33}\, a^5\, b^2 \qquad \bar{k}_{11,12} = \frac{1}{6} R_{22}\, a^6\, b + \frac{1}{2} R_{33}\, a^4\, b^3$$

$$\bar{k}_{12,12} = \frac{1}{7} R_{22}\, a^7\, b + \frac{3}{5} a^5\, b^3 \qquad \bar{k}_{2,16} = -\, 2\, T_{11}\, a\, b$$

$$\bar{k}_{4,16} = -\, T_{11}\, a\, b^2 \qquad \bar{k}_{7,16} = -\, 2\, T_{21}\, a\, b$$

$$\bar{k}_{9,16} = -\, T_{21}\, a^2\, b \qquad \bar{k}_{11,16} = -\, \frac{2}{3} T_{21}\, a^3\, b$$

$$\bar{k}_{12,16} = -\, \frac{1}{2} T_{21}\, a^4\, b \qquad \bar{k}_{16,16} = 4\, S_{11}\, a\, b$$

$\bar{k}_{3,17} = -2\ T_{33}\ a\ b$ $\bar{k}_{4,17} = -\ T_{33}\ a^2\ b$

$\bar{k}_{6,17} = -2\ T_{33}\ a\ b$ $\bar{k}_{8,17} = -2\ T_{33}\ a^2\ b$

$\bar{k}_{9,17} = -\ T_{33}\ a\ b^2$ $\bar{k}_{10,17} = -2\ T_{33}\ a^3\ b$

$\bar{k}_{11,17} = -\ T_{33}\ a^2\ b^2$ $\bar{k}_{12,17} = -\ T_{33}\ a^3\ b^2$

$\bar{k}_{17,17} = 4\ S_{33}\ a\ b$ $\bar{k}_{2,18} = -2\ T_{12}\ a\ b$

$\bar{k}_{4,18} = -\ T_{12}\ a\ b^2$ $\bar{k}_{7,18} = -2\ T_{22}\ a\ b$

$\bar{k}_{9,18} = -\ T_{22}\ a^2\ b$ $\bar{k}_{11,18} = -\frac{2}{3}\ T_{22}\ a^3\ b$

$\bar{k}_{12,18} = -\frac{1}{2}\ T_{22}\ a^4\ b$ $\bar{k}_{16,18} = 4\ S_{12}\ a\ b$

$\bar{k}_{18,18} = 4\ S_{22}\ a\ b$ $\bar{k}_{2,19} = -3\ T_{11}\ a^2\ b$

$\bar{k}_{4,19} = -\frac{3}{2}\ T_{11}\ a^2\ b^2$ $\bar{k}_{7,19} = -3\ T_{21}\ a^2\ b$

$\bar{k}_{9,19} = -2\ T_{21}\ a^3\ b$ $\bar{k}_{11,19} = -\frac{3}{2}\ T_{21}\ a^4\ b$

$\bar{k}_{12,19} = -\frac{6}{5}\ T_{21}\ a^5\ b$ $\bar{k}_{16,19} = 6\ S_{11}\ a^2\ b$

$\bar{k}_{18,19} = 6\ S_{12}\ a^2\ b$ $\bar{k}_{19,19} = 12\ S_{11}\ a^3\ b$

$\bar{k}_{2,20} = -\ T_{11}\ a\ b^2$ $\bar{k}_{3,20} = -2\ T_{33}\ a^2\ b$

$\bar{k}_{4,20} = -\frac{2}{3}\ (T_{11}\ a\ b^3 + 2\ T_{33}\ a^3\ b)$ $\bar{k}_{6,20} = -2\ T_{33}\ a^2\ b$

$\bar{k}_{7,20} = -\ T_{21}\ a\ b^2$ $\bar{k}_{8,20} = -\frac{8}{3}\ T_{33}\ a^3\ b$

$$\bar{k}_{9,20} = -a^2 b^2 (\tfrac{1}{2} T_{21} + T_{33}) \qquad \bar{k}_{10,20} = -3 T_{33} a^4 b$$

$$\bar{k}_{11,20} = -\tfrac{1}{3} a^3 b^2 (T_{21} + 4 T_{33}) \qquad \bar{k}_{12,20} = -\tfrac{1}{4} a^4 b^2 (T_{21} + 6 T_{33})$$

$$\bar{k}_{16,20} = 2 S_{11} a b^2 \qquad \bar{k}_{17,20} = 4 S_{33} a^2 b$$

$$\bar{k}_{18,20} = 2 S_{12} a b^2 \qquad \bar{k}_{19,20} = 3 S_{11} a^2 b^2$$

$$\bar{k}_{20,20} = \tfrac{4}{3} S_{11} a b^3 + \tfrac{16}{3} S_{33} a^3 b \qquad \bar{k}_{2,21} = -T_{12} a^2 b$$

$$\bar{k}_{3,21} = -2 T_{33} a b^2 \qquad \bar{k}_{4,21} = -a^2 b^2 (\tfrac{1}{2} T_{12} + T_{33})$$

$$\bar{k}_{6,21} = -2 T_{33} a b^2 \qquad \bar{k}_{7,21} = -T_{22} a^2 b$$

$$\bar{k}_{8,21} = -2 T_{33} a^2 b^2 \qquad \bar{k}_{9,21} = -\tfrac{2}{3} T_{22} a^3 b - \tfrac{4}{3} T_{33} a b^3$$

$$\bar{k}_{10,21} = -2 T_{33} a^3 b^2 \qquad \bar{k}_{11,21} = -\tfrac{1}{2} T_{22} a^4 b - \tfrac{4}{3} T_{33} a^2 b^3$$

$$\bar{k}_{12,21} = -\tfrac{2}{5} T_{22} a^5 b - \tfrac{4}{3} T_{33} a^3 b^3 \qquad \bar{k}_{16,21} = 2 S_{12} a^2 b$$

$$\bar{k}_{17,21} = 4 S_{33} a b^2 \qquad \bar{k}_{18,21} = 2 S_{22} a^2 b$$

$$\bar{k}_{19,21} = 4 S_{12} a^3 b \qquad \bar{k}_{20,21} = a^2 b^2 (S_{12} + 4 S_{33})$$

$$\bar{k}_{21,21} = \tfrac{4}{3} S_{22} a^3 b + \tfrac{16}{3} S_{33} a b^3 \qquad \bar{k}_{2,22} = -3 T_{12} a b^2$$

$$\bar{k}_{4,22} = 2 T_{12} a b^3 \qquad \bar{k}_{7,22} = -3 T_{22} a b^2$$

$$\bar{k}_{9,22} = -\tfrac{3}{2} T_{22} a^2 b^2 \qquad \bar{k}_{11,22} = -T_{22} a^3 b^2$$

$$\bar{k}_{12,22} = -\tfrac{3}{4} T_{22} a^4 b^2 \qquad \bar{k}_{16,22} = 6 S_{12} a b^2$$

$\bar{k}_{18,22} = 6\ S_{22}\ a\ b^2$

$\bar{k}_{19,22} = 9\ S_{12}\ a^2\ b^2$

$\bar{k}_{20,22} = 4\ S_{12}\ a\ b^3$

$\bar{k}_{21,22} = 3\ S_{22}\ a^2\ b^2$

$\bar{k}_{22,22} = 12\ S_{22}\ a\ b^3$

$\bar{k}_{2,23} = -\frac{3}{2}\ T_{11}\ a^2\ b^2$

$\bar{k}_{3,23} = -2\ T_{33}\ a^3\ b$

$\bar{k}_{4,23} = -T_{11}\ a^2\ b^3 - \frac{3}{2}\ T_{33}\ a^4\ b$

$\bar{k}_{6,23} = -2\ T_{33}\ a^3\ b$

$\bar{k}_{7,23} = -\frac{3}{2}\ T_{21}\ a^2\ b^2$

$\bar{k}_{8,23} = -3\ T_{33}\ a^4\ b$

$\bar{k}_{9,23} = -a^3\ b^2\ (T_{21} + T_{33})$

$\bar{k}_{10,23} = -\frac{18}{5}\ T_{33}\ a^5\ b$

$\bar{k}_{11,23} = -\frac{3}{4}\ a^4\ b^2\ (T_{21} + 2\ T_{33})$

$\bar{k}_{12,23} = -\frac{3}{5}\ a^5\ b^2\ (T_{21} + 3\ T_{33})$

$\bar{k}_{16,23} = 3\ S_{11}\ a^2\ b^2$

$\bar{k}_{17,23} = 4\ S_{33}\ a^3\ b$

$\bar{k}_{18,23} = 3\ S_{12}\ a^2\ b^2$

$\bar{k}_{19,23} = 6\ S_{11}\ a^3\ b^2$

$\bar{k}_{20,23} = 2\ S_{11}\ a^2\ b^3 + 6\ S_{33}\ a^4\ b$

$\bar{k}_{21,23} = 2\ a^3\ b^2\ (S_{12} + 2\ S_{33})$

$\bar{k}_{22,23} = 6\ S_{12}\ a^2\ b^3$

$\bar{k}_{23,23} = 4\ S_{11}\ a^3\ b^3 + \frac{36}{5}\ a^5\ b$

$\bar{k}_{2,24} = -\frac{3}{2}\ T_{12}\ a^2\ b^2$

$\bar{k}_{3,24} = -2\ T_{33}\ a\ b^3$

$\bar{k}_{4,24} = -a^2\ b^3\ (T_{12} + T_{33})$

$\bar{k}_{6,24} = -2\ T_{33}\ a\ b^3$

$\bar{k}_{7,24} = -\frac{3}{2}\ T_{22}\ a^2\ b^2$

$\bar{k}_{8,24} = -2\ T_{33}\ a^2\ b^3$

$\bar{k}_{9,24} = -T_{22}\ a^3\ b^2 - \frac{3}{2}\ T_{33}\ a\ b^4$

$\bar{k}_{10,24} = -2\ T_{33}\ a^3\ b^3$

$\bar{k}_{11,24} = -\frac{3}{4}\ T_{22}\ a^4\ b^2 - \frac{3}{2}\ T_{33}\ a^2\ b^4$

$\bar{k}_{12,24} = -\frac{3}{5} T_{22}\ a^5\ b^2 - \frac{3}{2} T_{33}\ a^3\ b^4$ $\quad \bar{k}_{16,24} = 3\ S_{12}\ a^2\ b^2$

$\bar{k}_{17,24} = 4\ S_{33}\ a\ b^3$ $\quad \bar{k}_{18,24} = 3\ S_{22}\ a^2\ b^2$

$\bar{k}_{19,24} = 6\ S_{12}\ a^3\ b^2$ $\quad \bar{k}_{20,24} = 2\ a^2\ b^3\ (S_{12} + 2\ S_{33})$

$\bar{k}_{21,24} = 2\ S_{22}\ a^3\ b^2 + 6\ S_{33}\ a\ b^4$ $\quad \bar{k}_{22,24} = 6\ S_{22}\ a^2\ b^3$

$\bar{k}_{23,24} = 4\ a^3\ b^3\ (S_{12} + S_{33})$ $\quad \bar{k}_{24,24} = 4\ S_{22}\ a^3\ b^3 + \frac{36}{5} S_{33}\ a\ b^5$

Finally, the stress matrix for the k th lamina can be obtained from the expression

$$[S] = \begin{bmatrix} s & 0 \\ 0 & s \end{bmatrix}^k [Q] \left[C^{-1}\right]$$

where $[s]^k$ is the square matrix appearing in Eq. 4.3.

The element R5 has the degrees of freedom u, v, w, $\frac{\partial w}{\partial y}$, and $-\frac{\partial w}{\partial x}$ at each node and has displacement functions that take the form

$$u = \alpha_1 + \alpha_2 x + \alpha_3 y + \alpha_4 xy$$

$$v = \alpha_5 + \alpha_6 x + \alpha_7 y + \alpha_9 xy$$

$$w = \alpha_{13} + \alpha_{14}x + \alpha_{15}y + \alpha_{16}x^2 + \alpha_{17}xy + \alpha_{18}y^2 + \alpha_{19}x^3 + \alpha_{20}x^2y + \alpha_{21}xy^2 + \alpha_{22}y^3 + \alpha_{23}x^3y + \alpha_{24}xy^3$$

Hence, the matrices $[Q]$ and $[\bar{k}]$ may be obtained from Eqs (a) and (b) by eliminating the terms corresponding to α_8, α_{10}, α_{11}, and α_{12}, while the non-zero terms appearing in the inverse of the matrix $[C]$ are as follows:

$C_{1,1} = 1.0$	$C_{2,1} = \frac{-1}{a}$	$C_{3,1} = \frac{-1}{b}$	$C_{4,1} = \frac{1}{ab}$
$C_{5,2} = 1.0$	$C_{6,2} = \frac{-1}{a}$	$C_{7,2} = \frac{-1}{b}$	$C_{8,2} = \frac{1}{ab}$
$C_{9,3} = 1.0$	$C_{12,3} = \frac{-3}{a^2}$	$C_{13,3} = \frac{-1}{ab}$	$C_{14,3} = \frac{-3}{b^2}$
$C_{15,3} = \frac{2}{a^3}$	$C_{16,3} = \frac{3}{a^2 b}$	$C_{17,3} = \frac{3}{ab^2}$	$C_{18,3} = \frac{2}{b^3}$
$C_{19,3} = \frac{-2}{a^3 b}$	$C_{20,3} = \frac{-2}{ab^3}$	$C_{11,4} = 1.0$	$C_{13,4} = \frac{-1}{a}$
$C_{14,4} = \frac{-2}{b}$	$C_{17,4} = \frac{2}{ab}$	$C_{18,4} = \frac{1}{b^2}$	$C_{20,4} = \frac{-1}{ab^2}$
$C_{10,5} = -1.0$	$C_{12,5} = \frac{2}{a}$	$C_{13,5} = \frac{1}{b}$	$C_{15,5} = \frac{-1}{a^2}$
$C_{16,5} = \frac{-2}{ab}$	$C_{19,5} = \frac{1}{a^2 b}$	$C_{2,6} = \frac{1}{a}$	$C_{4,6} = \frac{-1}{ab}$
$C_{6,7} = \frac{1}{a}$	$C_{8,7} = \frac{-1}{ab}$	$C_{12,8} = \frac{3}{a^2}$	$C_{13,8} = \frac{1}{ab}$
$C_{15,8} = \frac{-2}{a^3}$	$C_{16,8} = \frac{-3}{a^2 b}$	$C_{17,8} = \frac{-3}{ab^2}$	$C_{19,8} = \frac{2}{a^3 b}$
$C_{20,8} = \frac{2}{ab^3}$	$C_{13,9} = \frac{1}{a}$	$C_{17,9} = \frac{-2}{ab}$	$C_{20,9} = \frac{1}{ab^2}$
$C_{12,10} = \frac{1}{a}$	$C_{15,10} = \frac{-1}{a^2}$	$C_{16,10} = \frac{-1}{ab}$	$C_{19,10} = \frac{1}{a^2 b}$
$C_{4,11} = \frac{1}{ab}$	$C_{8,12} = \frac{1}{ab}$	$C_{13,13} = \frac{-1}{ab}$	$C_{16,13} = \frac{3}{a^2 b}$
$C_{17,13} = \frac{3}{ab^2}$	$C_{19,13} = \frac{-2}{a^3 b}$	$C_{20,13} = \frac{-2}{ab^3}$	$C_{17,14} = \frac{-1}{ab}$

$C_{20,14} = \frac{1}{ab^2}$ $\quad C_{16,15} = \frac{1}{ab}$ $\quad C_{19,15} = \frac{-1}{a^2b}$ $\quad C_{3,16} = \frac{1}{b}$

$C_{4,16} = \frac{-1}{ab}$ $\quad C_{7,17} = \frac{1}{b}$ $\quad C_{8,17} = \frac{-1}{ab}$ $\quad C_{13,18} = \frac{1}{ab}$

$C_{14,18} = \frac{3}{b^2}$ $\quad C_{16,18} = \frac{-3}{a^2b}$ $\quad C_{17,18} = \frac{-3}{ab^2}$ $\quad C_{18,18} = \frac{-2}{b^3}$

$C_{19,18} = \frac{2}{a^3b}$ $\quad C_{20,18} = \frac{2}{ab^3}$ $\quad C_{14,19} = \frac{-1}{b}$ $\quad C_{17,19} = \frac{1}{ab}$

$C_{18,19} = \frac{1}{b^2}$ $\quad C_{20,19} = \frac{-1}{ab^2}$ $\quad C_{13,20} = \frac{-1}{b}$ $\quad C_{16,20} = \frac{2}{ab}$

$C_{19,20} = \frac{-1}{a^2b}$

APPENDIX D.

DERIVATION OF FORMULAE FOR ESTIMATING EFFECTIVE FLANGE BREADTHS OF PROPPED CANTILEVER

In this appendix it is shown how values of stress effective breadth ratios for a propped cantilever may be estimated from those for simply supported girders (Table 5.7). The techniques illustrated by these examples could be used to estimate effective breadth ratios for girders having any support condition.

D.1 PROPPED CANTILEVER UNDER UNIFORM LOAD

Consider a propped cantilever subjected to the action of a uniform load along its length (Fig. D.1(a)).

D.1.1 Effective breadth ratio at mid-span

The portion BE of the propped cantilever between the point of contraflexure and the pinned support may be considered as a simply supported girder (Fig. D.1(b)). The effective breadth ratio at the point midway between B and E, Ψ_D, could thus be found from

$$\Psi_D = \Psi_{D'}$$

where $\Psi_{D'}$ is the effective breadth ratio at D'.
However, the values of stress effective breadth ratios over the central half span of a uniformly loaded simply supported girder are practically constant (see Figs 5.9 and 5.10), and therefore it can be assumed that the effective breadth ratio at the mid-span of the propped cantilever, Ψ_C, is given by

$$\Psi_C = \Psi_{D'}$$

D.1.2 Effective breadth ratio at clamped support

It can be seen from Figs D.1(c) and (d) that the bending moment at the position of the clamped support, M_A, could be considered equal to the sum of the moments at A" and A''' ($M_{A''}$, $M_{A'''}$). Therefore it follows from the rule for superposition of effective breadth ratios (Appendix E) that

$$\frac{M_A}{\Psi_A} = \frac{M_{A''}}{\Psi_{A''}} + \frac{M_{A'''}}{\Psi_{A'''}}$$

where Ψ_A, $\Psi_{A''}$, and $\Psi_{A'''}$ are the effective breadth ratios at A, A", and A''' respectively. Writing the bending moments in the above equation in terms of the applied load and solving for the effective breadth ratio at the clamped support of the propped cantilever, Ψ_A, gives

$$\Psi_A = \frac{1}{\dfrac{5}{4\Psi_{A''}} - \dfrac{1}{4\Psi_{A'''}}}$$

D.2 PROPPED CANTILEVER UNDER POINT LOAD

Consider a propped cantilever subjected to the action of a point load at its mid-span (Fig. D.2(a)).

D.2.1 Effective breadth ratio at mid-span

The portion BD of the propped cantilever between the point of contraflexure and the pinned support may be considered as a simply supported girder (Fig. D.2(b)). Therefore the effective breadth ratio at the mid-span of the propped cantilever, Ψ_C, is given by

$$\Psi_C = \Psi_{C'}$$

where $\Psi_{C'}$ is the effective breadth ratio at C' and can be found using Eq. 1 in Fig. 5.7.

D.2.2 Effective breadth ratio at clamped support

It can be seen from Figs D.2(c) and (d) that the bending moment at the position of the clamped support, M_A, could be considered equal to the bending moment at A" ($M_{A''}$). Therefore the effective breadth ratio at the clamped support of the propped cantilever, Ψ_A, is given by

$$\Psi_A = \Psi_{A''}$$

where $\Psi_{A''}$ is the effective breadth ratio at A".

APPENDIX E.

DERIVATION OF FORMULA FOR ESTIMATING EFFECTIVE FLANGE BREADTHS OF BOX GIRDER BRIDGES SUBJECTED TO COMBINED LOAD SYSTEMS

In this appendix an expression is derived for the stress effective breadth ratio associated with a combination of load systems in terms of the effective breadth ratios associated with each load system.

Consider σ_{W1}, σ_{W2},....,σ_{Wn} to be longitudinal stress components in a web, at the level of the mid-plane of the flange plate, due to n load systems acting independently. Assuming that linear elastic theory applies, the longitudinal stress component σ_W that would exist at the point being considered when the loads act simultaneously is given by

$$\sigma_W = \sigma_{W1} + \sigma_{W2} + \cdots + \sigma_{Wn} \qquad (a)$$

From the definition of stress effective breadth (Section 5.2), Eq. (a) can be written in the form

$$\frac{\int_0^B \sigma_x \, dy}{\Psi B} = \frac{\int_0^B \sigma_{x1} \, dy}{\Psi_1 B} + \frac{\int_0^B \sigma_{x2} \, dy}{\Psi_2 B} + \cdots + \frac{\int_0^B \sigma_{xn} \, dy}{\Psi_n B} \qquad (b)$$

where, for the section being considered, σ_x is the longitudinal extensional stress component at a point y within the breadth B of the flange, when the load systems act simultaneously; σ_{x1}, σ_{x2},....,σ_{xn} are the longitudinal extensional stress components at the same point y, when each load system acts independently; Ψ is the effective breadth ratio associated with the combined load system; and Ψ_1, Ψ_2,....,Ψ_n are the effective breadth ratios associated with each load system.

Eq. (b) can be rearranged to give

$$\Psi = \frac{\int_0^B \sigma_x \, dy}{\dfrac{\int_0^B \sigma_{x1} \, dy}{\Psi_1} + \dfrac{\int_0^B \sigma_{x2} \, dy}{\Psi_2} + \dots + \dfrac{\int_0^B \Psi_{xn} \, dy}{\Psi_n}} \tag{c}$$

which can then be written in the form

$$\Psi = \frac{KM}{\dfrac{K_1M_1}{\Psi_1} + \dfrac{K_2M_2}{\Psi_2} + \dots + \dfrac{K_nM_n}{\Psi_n}} \tag{d}$$

where, for the section being considered, M is the longitudinal bending moment due to the load systems acting simultaneously; M_1, M_2,....,M_n are the longitudinal bending moments due to each load system acting independently; and K, K_1, K_2,....,K_n are constants determined by the geometry of the section and the distribution of longitudinal stress across the flange.

If it is assumed that the contribution of the stresses in the webs to the internal moment at the section can be neglected, and if the position of the neutral axis at the section is the same for each load system, Eq. (d) can be reduced to

$$\Psi = \frac{M}{\dfrac{M_1}{\Psi_1} + \dfrac{M_2}{\Psi_2} + \dots + \dfrac{M_n}{\Psi_n}} \tag{e}$$

For practical box girder bridges, the error involved in using Eq. (e) should be generally small. To demonstrate the magnitude of the error that can be involved, the box girder bridges described in Subsection 5.4.3 were subjected to a combination of a uniform load over the length of each web and a point load over each web at the mid-span. The two types of load were selected to give equal bending moments at the mid-span. In each case, the effective breadth value obtained from Eq. (e) in conjunction with the values given in Table 5.6, and the value obtained from the finite element analysis for the combined load system, differed by less than 3.0 per cent.

Table 2.1. Relationship between structural type and element type

		TYPES OF ELEMENT																															
		Beam			Eccentric beam		Symmetrical beam				Linkage				Triangular				Rectangular				Eccentric rectangular		Parallelogrammic				Quadrilateral				Tetrahedra
TYPES OF STRUCTURE		u	uv θ_z	w $\theta_x\theta_y$	uw $\theta_x\theta$	uvw $\theta_x\theta_y\theta_z$	uw	uw θ_y	uw $\theta_y\varepsilon_x$	v $\theta_x\theta_z$	uv	uv θ_z	uvw	w $\theta_x\theta_y$	uv	uv θ_z	uv $\theta_z\varepsilon_x$	w $\theta_x\theta_y$	uv	uv θ_z	uv $\theta_z\varepsilon_x$	w $\theta_x\theta_y$	uvw $\theta_x\theta_y$	uvw $\theta_x\theta_y\theta_z$	uv	uv θ_z	uv $\theta_z\varepsilon_x$	w $\theta_x\theta_y$	uv	uv θ_z	uv $\theta_z\varepsilon_x$	w $\theta_x\theta_y$	uvw
Plane truss	UV	⊞									⊞																						
Plane frame	UVθ_z		⊞									⊞																					
Space truss	UVW	⊞											⊞																				
Plane grillage	W$\theta_x\theta_Y$			⊞										⊞																			
Space frame	UVW$\theta_x\theta_Y\theta_z$		≡	‖		⊞						≡		‖																			
Plane stress	UV	⊞									⊞				⊞				⊞						⊞				⊞				
Plane stress	UVθ_z		⊞									⊞				⊞				⊞						⊞				⊞			
Plane stress	UV$\theta_z\varepsilon_x$																⊞				⊞						⊞				⊞		
Plane strain	UV	⊞									⊞				⊞				⊞						⊞				⊞				
Space membrane	UVW	⊞											⊞		⊞				⊞						⊞				⊞				
Plated grillage	UVW						⊞						⊞		⊞				⊞						⊞				⊞				
Plate	W$\theta_x\theta_Y$			⊞										⊞				⊞				⊞						⊞				⊞	
Ribbed plate	UVW$\theta_x\theta_Y$				⊞						≡			‖	≡			‖	≡			‖	⊞		≡			‖	≡			‖	
Multicellular box	UVW$\theta_x\theta_Y\theta_z$						≡	≡		‖		≡		‖	≡	≡		‖	≡	≡		‖		⊞	≡	≡		‖	≡	≡		‖	
Multicellular box	UVW$\theta_x\theta_Y\theta_z\varepsilon_x$								≡	‖							≡	‖			≡	‖					≡	‖			≡	‖	
Shell	UVW$\theta_x\theta_Y\theta_z$		≡	‖		⊞						≡		‖	≡	≡		‖	≡	≡		‖		⊞	≡	≡		‖	≡	≡		‖	
Shell	UVW$\theta_x\theta_Y\theta_z\varepsilon_x$																≡	‖			≡	‖					≡	‖			≡	‖	
Solid	UVW	⊞											⊞		⊞				⊞						⊞				⊞				⊞
REFERENCES		(48)*	(48)	(48)	(17)		$(\frac{11}{20})$	(11)	(11)	(11)	[4·2]†	[4·2]	[4·2]	[4·2]	(9)	[3·2]	[3·2]	(9)	(9)	(14)	[3·2]	(9)	[4·2]	[4·2]	(9)	(14)	[3·2]	(49)	(9)	(14)	[3·2]	(15)	(9)

≡ Denotes an element the stiffness matrix of which must be used with that of an element of the same type and indicated by the symbol below

‖ Denotes an element the stiffness matrix of which must be used with that of an element of the same type and indicated by the symbol above

⊞ Denotes an element the stiffness matrix of which may be used independently

* Numerals in parentheses refer to corresponding items in list of references

† Numerals in brackets refer to corresponding sections of thesis

Table 3.1. Straight single cell box girder.
Effect of mesh size on displacements and stresses at mid-span for girder under bending and distortional components of eccentric point load at mid-span

(a) Girder simply supported

Mesh	$\frac{w_B^{FE} - w_B^{ETB}}{w_B^{ETB}} \times 100$			$\frac{\sigma_B^{FE} - \sigma_B^{ETB}}{\sigma_B^{ETB}} \times 100$			$\frac{\sigma_{DW}^{FE} - \sigma_{DW}^{BEF}}{\sigma_B^{ETB}} \times 100$			$\frac{\sigma_{DB}^{FE} - \sigma_{DB}^{BEF}}{\sigma_B^{ETB}} \times 100$		
	R23	Q33	Q43	R23	Q33	Q43	R23	Q33	Q43	R23	Q33	Q43
2x1x1	-86·9	-25·4	-1·4	-93·2	-48·6	+0·2	-22·5	-22·2	-21·7	-16·9	-13·1	-13·0
4x1x1	-62·6	-7·2	-1·2	-70·8	-22·7	+0·7	-21·9	-19·8	-11·2	-13·5	-5·1	+4·3
8x1x1	-29·9	-2·6	-1·1	-36·1	-9·8	+1·6	-18·6	-15·5	-4·3	-6·3	-0·4	+4·2
16x1x1	-10·3	-1·4	-1·1	-12·4	-3·4	+2·2	-12·9	-10·5	-2·4	-0·8	+1·4	+2·8
32x1x1	-3·5	-1·1	-1·1	-2·7	-0·2	+2·5	-7·7	-6·6	-1·9	+1·7	+2·3	+2·7
64x1x1	-1·6	-1·1	-1·1	+0·7	+1·4	+2·6	-4·5	-4·2	-1·8	+3·0	+3·1	+3·2

(b) Girder fixed ended

Mesh	$\frac{w_B^{FE} - w_B^{ETB}}{w_B^{ETB}} \times 100$			$\frac{\sigma_B^{FE} - \sigma_B^{ETB}}{\rho_B^{ETB}} \times 100$			$\frac{\sigma_{DW}^{FE} - \sigma_{DW}^{BEF}}{\sigma_B^{ETB}} \times 100$			$\frac{\sigma_{DB}^{FE} - \sigma_{DB}^{BEF}}{\sigma_B^{ETB}} \times 100$		
	R23	Q33	Q43	R23	Q33	Q43	R23	Q33	Q43	R23	Q33	Q43
2x1x1	-86·9	-89·1	-4·9	-100·0	-100·0	+1·0	-46·1	-46·1	-41·2	-48·0	-50·5	-27·0
4x1x1	-62·7	-24·3	-3·2	-80·7	-48·8	-1·4	-43·7	-42·5	-22·7	-27·4	-19·7	+7·2
8x1x1	-30·1	-7·5	-2·2	-45·4	-22·9	-0·1	-37·3	-31·1	-8·6	-12·5	-1·0	+8·3
16x1x1	-10·4	-3·0	-1·7	-18·4	-10·0	+1·2	-25·9	-21·1	-4·9	-1·7	+2·8	+5·6
32x1x1	-3·7	-1·7	-1·4	-6·0	-3·6	+1·8	-15·3	-13·2	-3·9	+3·5	+4·7	+5·4
64x1x1	-1·8	-1·4	-1·3	-1·1	-0·4	+2·0	-9·0	-8·3	-3·5	+6·0	+6·2	+6·5

Note: w_B^{ETB} includes a shear correction

Table 3.2. Effect of element aspect ratio on displacements at mid-span of simply supported box girders (cross-sections as in Fig. 3.4.) with girders under point load over each web at mid-span

Length of girder	Aspect ratio of elements	$\frac{w_B^{FE} - w_B^{ETB}}{w_B^{ETB}} \times 100$		
		R 23	Q 33	Q 43
4 D	0·5	-3·5	-3·1	-2·1
8 D	1·0	-10·2	-2·7	-1·4
16 D	2·0	-29·9	-2·6	-1·1
32 D	4·0	-62·6	-2·6	-1·1
64 D	8·0	-87·0	-2·6	-1·0

Notes:

1. w_B^{ETB} includes a shear correction
2. The girders were analysed using an 8 x 1 x 1 mesh

Table 3.3. Skewed single cell box girder. Comparison of maximum displacements at free end of girder for different mesh types with girder under point load over each web at free end

Total number of nodes used in idealization	Displacement in terms of $(P/ED) \times 10^3$			
	Mesh type 1		Mesh type 2	
	Q33	Q43	T33, Q33	T43, Q43
12	59·7	64·4	54·5	65·0
20	63·5	65·1	64·1	65·6
36	65·0	65·5	65·7	66·0

Table 4.1. Square composite plate model.
Comparison between theoretical and experimental values of slip for model under central patch load

Method	Relative movement of concrete with respect to steel (in x 10^3)																	
	Slip in x direction at gauge no.									Slip in y direction at gauge no.								
	1	2	3	4	5	6	7	8	9	1	2	3	4	5	6	7	8	9
Finite element solution	0	0	0	0·79	0·53	0·15	0·85	0·28	0·54	0·67	1·38	1·25	0·79	1·18	1·25	0·85	0·97	0·54
Fourier series solution	0	0	0	0·83	0·56	0·20	0·89	0·35	0·65	0·65	1·35	1·49	0·83	1·20	1·38	0·89	1·08	0·65
Experiment	0	0	0·16	1·73	0·90	0·43	1·53	0·87	1·22	2·64	2·28	1·65	1·85	1·93	1·33	1·10	0·95	0·51

Table 5.1. Centre line dimensions, wall thicknesses and stiffener details of cross-sections shown in Fig. 5.2

Cross-section numbers	B (feet)	D (feet)	t_f (inches)	t_w (inches)	Details of Stiffeners
1	6	6	$\frac{1}{2}$	$\frac{1}{2}$	-
2	6	6	1	1	-
3	6	12	1	$\frac{1}{2}$	-
4	6	6	1	$\frac{1}{2}$	-
5	6	6	1	$\frac{1}{4}$	-
6	6	3	1	$\frac{1}{2}$	-
7	6	6	2	$\frac{1}{2}$	-
8	6	6	$\frac{1}{2}$	$\frac{1}{2}$	$4\frac{1}{2}$ in × 1 in flats @ 9 in c/c
9	6	6	$\frac{1}{2}$	1	$4\frac{1}{2}$ in × 1 in flats @ 9 in c/c
10	6	6	$\frac{1}{2}$	$\frac{1}{4}$	$4\frac{1}{2}$ in × 1 in flats @ 9 in c/c
11	6	6	$\frac{1}{2}$	$\frac{1}{2}$	$4\frac{1}{2}$ in × $\frac{1}{2}$ in flats @ 9 in c/c
12	6	6	$\frac{1}{2}$	$\frac{1}{2}$	$4\frac{1}{2}$ in × 1 in flats @ 9 in c/c
13	6	6	$\frac{1}{2}$	$\frac{1}{2}$	$4\frac{1}{2}$ in × 1 in flats @ 9 in c/c
14	6	6	$\frac{1}{2}$	2	$4\frac{1}{2}$ in × 1 in flats @ 9 in c/c
15	6	24	$\frac{1}{2}$	$\frac{1}{2}$	$4\frac{1}{2}$ in × 1 in flats @ 9 in c/c
16	6	6	$\frac{1}{2}$	$\frac{1}{2}$	$4\frac{1}{2}$ in × 1 in flats @ 9 in c/c

Table 5.2. Effect of properties of web material on effective breadth ratios at mid-span for simply supported box girders (cross-section 8)

(1) Uniform load over length of each web

$\frac{D}{L} = \frac{B}{L}$	Stress effective breadth ratios		Deflexion effective breadth ratios	
	(a)	(b)	(a)	(b)
0·05	0·97	0·97	0·93	0·93
0·20	0·67	0·67	0·62	0·66
0·40	0·35	0·35	0·33	0·57

(2) Point load over each web at mid-span

$\frac{D}{L} = \frac{B}{L}$	Stress effective breadth ratios		Deflexion effective breadth ratios	
	(a)	(b)	(a)	(b)
0·05	0·75	0·75	0·92	0·92
0·20	0·40	0·38	0·60	0·65
0·40	0·23	0·20	0·32	0·55

Note: The web material was assumed to be isotropic ($E = 30 \times 10^6$ lbf/in^2 $\nu = 0{\cdot}3$) except in the case of column (b) for which the extensional properties were assumed to have the following values:

$E_x = 30 \times 10^6$ lbf/in^2 $\quad E_y = 0$ lbf/in^2 $\quad G = \infty$ lbf/in^2 $\quad \nu_{xy} = 0$

where the directions x and y refer to the longitudinal and transverse directions of the web respectively.

Table 5.3. Comparison of stress effective breadth ratios at mid-span for simply supported box girders (cross-sections 1 and 8) obtained using various methods

(1) Uniform load over length of each web

α	$\frac{B}{L}$	Effective breadth ratios according to		
		Finite element	Kondo et al	Schade
0·0	0·05	0·98	0·98	0·98
	0·10	0·95	0·93	0·94
	0·20	0·81	0·77	0·82
	0·40	0·50	0·48	0·49
1·0	0·05	0·97	0·96	Solution not applicable
	0·10	0·89	0·87	
	0·20	0·67	0·64	
	0·40	0·35	0·36	

(2) Point load over each web at mid-span

α	$\frac{B}{L}$	Effective breadth ratios according to		
		Finite element	Kondo et al	Schade
0·0	0·05	0·83	0·83	0·89
	0·10	0·71	0·71	0·75
	0·20	0·53	0·55	0·56
	0·40	0·33	0·37	0·34
1·0	0·05	0·75	0·78	Solution not applicable
	0·10	0·59	0·63	
	0·20	0·40	0·46	
	0·40	0·23	0·29	

Table 5.4. Effect of varying flange to web areas on stress effective breadth ratios for simply supported box girders (cross-sections 1 to 10) with point load over each web at mid-span

α	$\frac{B}{L}$	Effective breadth ratios at mid-span for β =			Effective breadth ratios at quarter-span for β =		
		2·0	4·0	8·0	2·0	4·0	8·0
0·0	0·05	0·83	0·80	0·77	1·00	1·00	1·00
	0·20	0·53	0·49	0·46	0·97	0·98	0·99
	0·40	0·33	0·30	0·28	0·61	0·63	0·65
1·0	0·05	0·78	0·75	0·72	1·00	1·00	1·00
	0·20	0·44	0·40	0·37	0·81	0·84	0·86
	0·40	0·24	0·23	0·21	0·42	0·44	0·46

Table 5.5. Effect of varying flange to web areas on stress effective breadth ratios at mid-span for simply supported twin box girder bridges (cross-sections 13 to 15) with point load over each web at mid-span

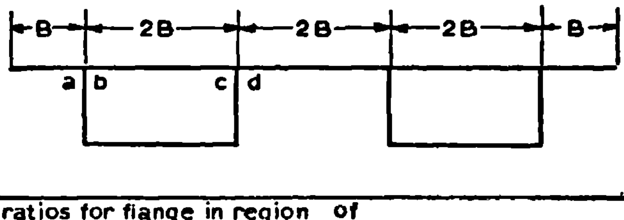

$\frac{B}{L}$	Effective breadth ratios for flange in region of							
	a with β =		b with β =		c with β =		d with β =	
	2·0	8·0	2·0	8·0	2·0	8·0	2·0	8·0
0·05	0·77	0·67	0·80	0·71	0·80	0·71	0·80	0·70
0·20	0·40	0·34	0·45	0·38	0·45	0·38	0·45	0·38
0·40	0·21	0·18	0·25	0·22	0·25	0·22	0·25	0·22

Table 5.6. Stress effective breadth ratios at mid-span for simply supported box girder bridges of various cross-sectional shapes

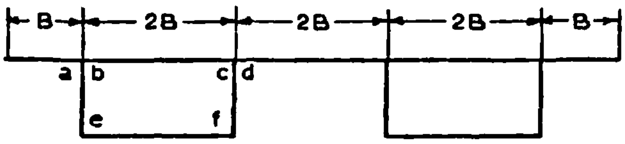

Cross-section no. 13

(1) Uniform load over length of each web

B/L	Effective breadth ratios for flange in region of					
	a	b	c	d	e	f
0·05	0·94	0·96	0·96	0·96	0·97	0·97
0·20	0·62	0·70	0·70	0·69	0·67	0·67
0·40	0·30	0·37	0·37	0·36	0·35	0·35

(2) Point load over each web at mid-span

B/L	Effective breadth ratios for flange in region of					
	a	b	c	d	e	f
0·05	0·67	0·71	0·71	0·70	0·74	0·74
0·20	0·34	0·38	0·38	0·38	0·40	0·40
0·40	0·18	0·22	0·22	0·22	0·23	0·23

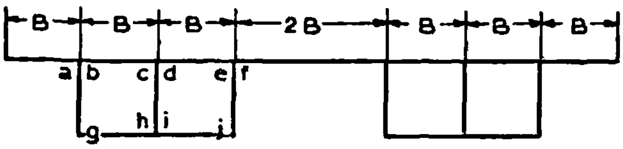

Cross-section no. 16

(1) Uniform load over length of each web

B/L	Effective breadth ratios for flange in region of									
	a	b	c	d	e	f	g	h	i	j
0·05	0·92	0·98	0·99	0·99	0·98	0·97	0·98	0·99	0·99	0·98
0·20	0·57	0·89	0·92	0·92	0·89	0·66	0·89	0·94	0·94	0·89
0·40	0·28	0·67	0·70	0·70	0·66	0·34	0·67	0·72	0·72	0·67

(2) Point load over each web at mid-span

B/L	Effective breadth ratios for flange in region of									
	a	b	c	d	e	f	g	h	i	j
0·05	0·72	0·83	0·87	0·88	0·83	0·75	0·86	0·93	0·93	0·86
0·20	0·33	0·58	0·62	0·62	0·58	0·39	0·59	0·65	0·65	0·59
0·40	0·19	0·39	0·41	0·41	0·39	0·22	0·40	0·44	0·44	0·40

Table 5.7 Effective breadth ratios of simply supported box girders (cross-sections 4 and 8)

(1) Uniform load over length of each web

α	B/L	Stress effective breadth ratios		Deflexion effective breadth ratios	
		1/2 span	1/4 span	1/2 span	1/4 span
0·0	0	1·00	1·00	1·00	1·00
	0·05	0·98	0·98	0·98	0·98
	0·10	0·95	0·93	0·94	0·94
	0·20	0·81	0·77	0·79	0·79
	0·30	0·65	0·60	0·63	0·62
	0·40	0·50	0·46	0·48	0·47
	0·50	0·38	0·36	0·38	0·37
	0·60	0·29	0·28	0·31	0·30
	0·80	0·20	0·19	0·21	0·20
	1·00	0·16	0·15	0·17	0·16
1·0	0	1·00	1·00	1·00	1·00
	0·05	0·97	0·96	0·93	0·92
	0·10	0·89	0·86	0·84	0·84
	0·20	0·67	0·62	0·62	0·62
	0·30	0·48	0·44	0·45	0·44
	0·40	0·35	0·32	0·33	0·33
	0·50	0·27	0·25	0·26	0·25
	0·60	0·22	0·20	0·21	0·20
	0·80	0·16	0·15	0·16	0·16
	1·00	0·12	0·11	0·12	0·12

(2) Point load over each web at mid-span

α	B/L	Stress effective breadth ratios		Deflexion effective breadth ratios	
		1/2 span	1/4 span	1/2 span	1/4 span
0·0	0	1·00	1·00	1·00	1·00
	0·05	0·80	1·00	0·98	0·98
	0·10	0·67	1·00	0·93	0·94
	0·20	0·49	0·98	0·77	0·80
	0·30	0·38	0·82	0·61	0·63
	0·40	0·30	0·63	0·47	0·49
	0·50	0·24	0·47	0·37	0·38
	0·60	0·19	0·36	0·30	0·31
	0·80	0·14	0·23	0·21	0·22
	1·00	0·12	0·19	0·16	0·17
1·0	0	1·00	1·00	1·00	1·00
	0·05	0·75	1·00	0·92	0·93
	0·10	0·59	0·99	0·83	0·85
	0·20	0·40	0·84	0·60	0·63
	0·30	0·30	0·61	0·43	0·45
	0·40	0·23	0·44	0·32	0·33
	0·50	0·18	0·33	0·25	0·26
	0·60	0·14	0·26	0·21	0·22
	0·80	0·10	0·18	0·16	0·17
	1·00	0·08	0·14	0·12	0·13

Table 5.8. Stress effective breadth ratios at point of application of load for simply supported box girders (cross-section 4 and 8) under point loads at various positions

α	$\frac{B}{L}$	Effective breadth ratios at			
		1/8 span	1/4 span	3/8 span	1/2 span
0·0	0·05	0·62* (0·62)†	0·73 (0·72)	0·77 (0·77)	0·80 (0·80)
	0·20	0·28 (0·30)	0·40 (0·40)	0·47 (0·46)	0·49 (0·49)
	0·40		0·23 (0·23)	0·28 (0·27)	0·30 (0·30)
1·0	0·05	0·55 (0·55)	0·69 (0·67)	0·73 (0·73)	0·75 (0·75)
	0·20	0·22 (0·25)	0·33 (0·33)	0·38 (0·38)	0·40 (0·40)
	0·40		0·18 (0·18)	0·21 (0·20)	0·23 (0·23)

* Value given by finite element analysis

† Value given by formula no.1. in Fig. 5.7.

Table 5.9. Stress effective breadth ratios for fixed ended box girder bridges with curtailed middle web (cross-section 12 over end quarter spans)

(1) Uniform load over length of each outer web

B*/L	Effective breadth ratios at mid-span			Effective breadth ratios at supports		
	no curtailed web	curtailed web no diaphragm	curtailed web and diaphragm	no curtailed web	curtailed web no diaphragm	curtailed web and diaphragm
0·05	0·91	0·91	0·92	0·50 (0·68)†	0·50	0·59
0·20	0·40	0·40	0·41	0·17 (0·32)	0·20	0·28

(2) Point load over each web at mid-span

B*/L	Effective breadth ratios at mid-span			Effective breadth ratios at supports		
	no curtailed web	curtailed web no diaphragm	curtailed web and diaphragm	no curtailed web	curtailed web no diaphragm	curtailed web and diaphragm
0·05	0·59	0·59	0·60	0·59 (0·75)	0·59	0·69
0·20	0·23	0·23	0·24	0·22 (0·40)	0·24	0·36

* B taken as half the distance between web centre lines at the mid-span

† Values for 0·5 B/L

Table 6.1. Details of shear connexions between concrete slab and steel plate of girders having cross-sections shown in Fig. 6.1

Shear connexion	k $\left(\frac{\text{lbf/in}}{\text{in}}\right)$	Ratio of slip modulus of connectors over web to total slip modulus of connectors
C	$1{\cdot}00 \times 10^{14}$	$\frac{1}{12}$
I1	$1{\cdot}12 \times 10^{6}$	1
I2	$1{\cdot}12 \times 10^{6}$	$\frac{2}{3}$
I3	$1{\cdot}12 \times 10^{6}$	$\frac{1}{3}$
I4	$1{\cdot}12 \times 10^{6}$	$\frac{1}{12}$
I5	$1{\cdot}68 \times 10^{6}$	$\frac{1}{12}$

Table 6.2. Effect of shear connector flexibility on maximum deflexions and maximum longitudinal plate stresses, slab stresses, and connector forces of simply supported tee and box girders

(1) Uniform load over length of each web

$\frac{B}{L}$	w_{I4}/w_C		σ^c_{I4}/σ^c_C		σ^s_{I4}/σ^s_C		F_{I4}/F_C	
	Tee girder	Box girder	Tee girder	Box girder	Tee girder	Box girder	Tee girder	Box girder
0·05	1·01	1·01	0·98	0·97	1·04	1·05	0·25	0·25
0·20	1·10	1·09	0·87	0·86	1·26	1·28	0·23	0·24

(2) Point load over each web at mid-span

$\frac{B}{L}$	w_{I4}/w_C		σ^c_{I4}/σ^c_C		σ^s_{I4}/σ^s_C		F_{I4}/F_C	
	Tee girder	Box girder	Tee girder	Box girder	Tee girder	Box girder	Tee girder	Box girder
0·05	1·01	1·01	0·93	0·92	1·13	1·15	0·25	0·25
0·20	1·11	1·10	0·79	0·77	1·40	1·43	0·25	0·25

Table 6.3. Effect of shear connector flexibility and distribution on deflexions at centre of simply supported tee girders

(1) Uniform load over length of web

$\frac{B}{L}$	w_I/w_C for shear connexion:				
	I1	I2	I3	I4	I5
0·05	1·00	1·00	1·01	1·01	1·01
0·20	1·02	1·03	1·05	1·10	1·08

(2) Point load over web at mid-span

$\frac{B}{L}$	w_I/w_C for shear connexion:				
	I1	I2	I3	I4	I5
0·05	1·00	1·00	1·01	1·01	1·01
0·20	1·02	1·03	1·05	1·11	1·09

Table 6.4. Effect of shear connector flexibility and distribution on longitudinal stresses in mid-plane of concrete slab at centre of simply supported tee girders

(1) Uniform load over length of web

$\frac{B}{L}$	σ_I/σ_C for shear connexion:				
	I1	I2	I3	I4	I5
0·05	1·00	0·99	0·99	0·98	0·98
0·20	0·96	0·95	0·93	0·87	0·89

(2) Point load over web at mid-span

$\frac{B}{L}$	σ_I/σ_C for shear connexion:				
	I1	I2	I3	I4	I5
0·05	0·98	0·97	0·96	0·93	0·94
0·20	0·92	0·90	0·86	0·79	0·82

Table 6.5. Effect of shear connector flexibility and distribution on longitudinal stresses in mid-plane of steel plate at centre of simply supported tee girders

(1) Uniform load over length of web

$\frac{B}{L}$	σ_I/σ_C for shear connexion:				
	I1	I2	I3	I4	I5
0·05	1·01	1·02	1·03	1·04	1·03
0·20	1·07	1·08	1·13	1·26	1·22

(2) Point load over web at mid-span

$\frac{B}{L}$	σ_I/σ_C for shear connexion:				
	I1	I2	I3	I4	I5
0·05	1·07	1·08	1·10	1·13	1·11
0·20	1·14	1·16	1·23	1·40	1·35

Table 6.6. Effect of shear connector flexibility and distribution on stress effective breadth ratios for concrete slab at mid-span of simply supported tee girders

(1) Uniform load over length of web

$\frac{B}{L}$	ψ for shear connexion:					
	C	I1	I2	I3	I4	I5
0·05	0·98	0·98	0·98	0·98	0·99	0·99
0·20	0·81	0·81	0·84	0·86	0·90	0·89

(2) Point load over web at mid-span

$\frac{B}{L}$	ψ for shear connexion:					
	C	I1	I2	I3	I4	I5
0·05	0·85	0·85	0·86	0·87	0·89	0·88
0·20	0·53	0·53	0·54	0·56	0·59	0·59

Note: In determining the values of ψ given in this table, the value of the stress in the middle plane of the concrete slab above the web of the girders was used as the base stress (see Section 5.2).

Table 6.7. Effect of shear connector flexibility and distribution on stress effective breadth ratios for steel plate at mid-span of simply supported tee girders

(1) Uniform load over web at mid-span

$\frac{B}{L}$	ψ for shear connexion:					
	C	I1	I2	I3	I4	I5
0·05	0·98	0·97	0·96	0·96	0·96	0·96
0·20	0·80	0·79	0·76	0·72	0·67	0·68

(2) Point load over web at mid-span

$\frac{B}{L}$	ψ for shear connexion:					
	C	I1	I2	I3	I4	I5
0·05	0·83	0·82	0·81	0·81	0·80	0·80
0·20	0·52	0·51	0·48	0·46	0·44	0·44

Table 6.8. Effect of shear connector flexibility and distribution on forces in shear connectors over web at quarter-span and support sections of simply supported tee girders

(1) Uniform load over length of web

$\frac{B}{L}$	F/F_{TC} for shear connexion:									
	I 1		I 2		I 3		I 4		I 5	
	quarter-span	support	quarter-span	support	quarter-span	support	quarter-span	support	quarter-span	support
0·05	1·00	1·00	0·86	0·86	0·61	0·61	0·25	0·25	0·29	0·29
0·20	1·00	1·00	0·85	0·83	0·60	0·56	0·24	0·23	0·29	0·27

(2) Point load over web at mid-span

$\frac{B}{L}$	F/F_{TC} for shear connexion:									
	I 1		I 2		I 3		I 4		I 5	
	quarter-span	support	quarter-span	support	quarter-span	support	quarter-span	support	quarter-span	support
0·05	1·00	1·00	0·86	0·86	0·61	0·61	0·25	0·25	0·29	0·29
0·20	1·00	1·00	0·85	0·85	0·58	0·60	0·24	0·25	0·27	0·29

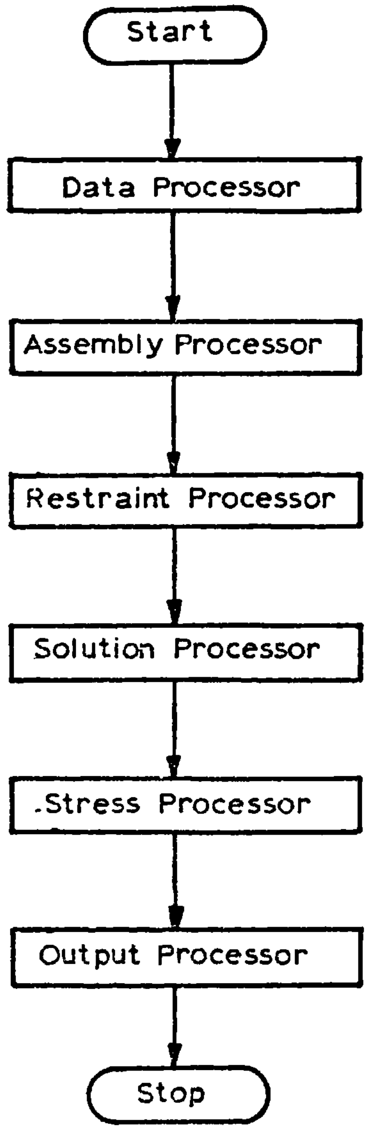

Fig. 2.1. Simplified flow diagram for an analysis by ICSAS.

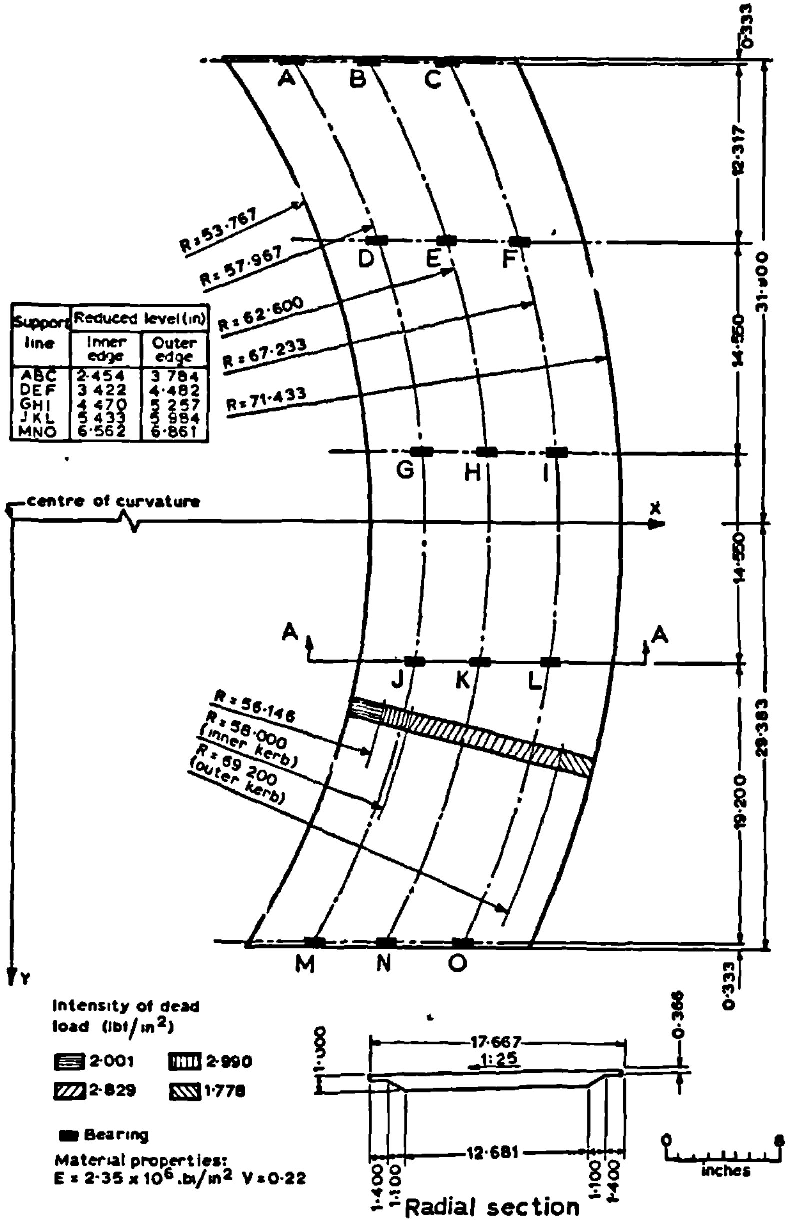

Support line	Reduced level (in)	
	Inner edge	Outer edge
ABC	2·454	3·784
DEF	3·422	4·482
GHI	4·470	5·257
JKL	5·433	5·984
MNO	6·562	6·861

Fig. 2.2. Curved slab bridge model.
Details of model and loading

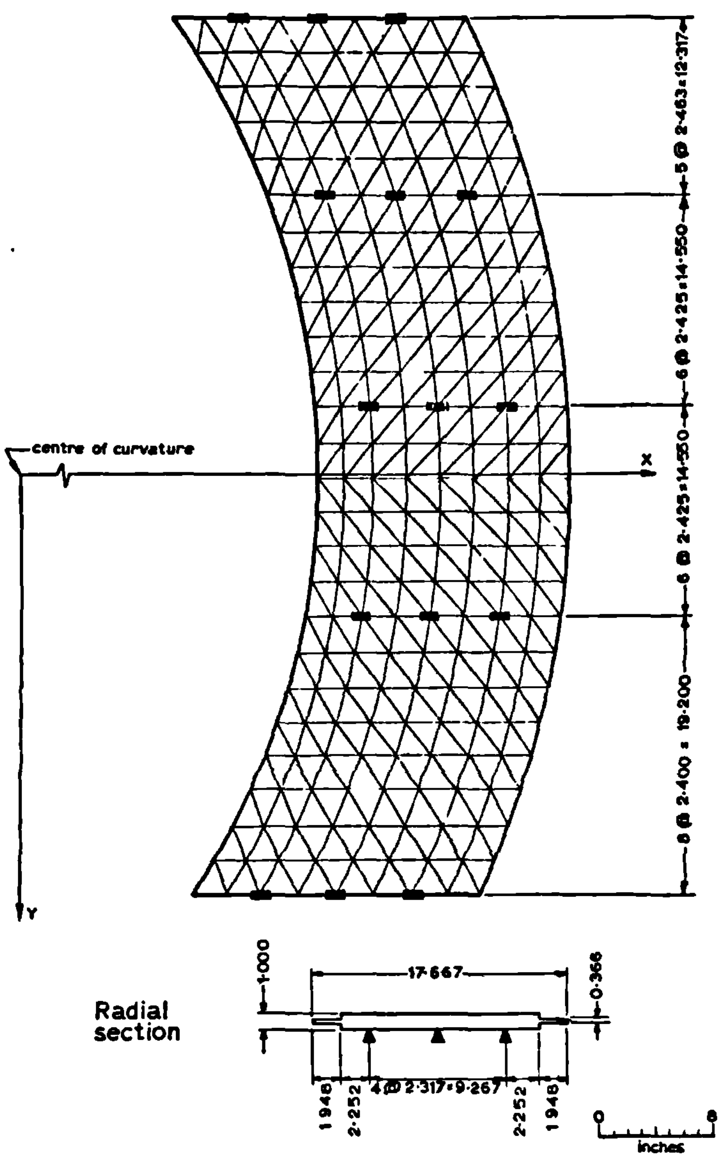

Fig. 2.3. Curved slab bridge model.
Finite element idealization

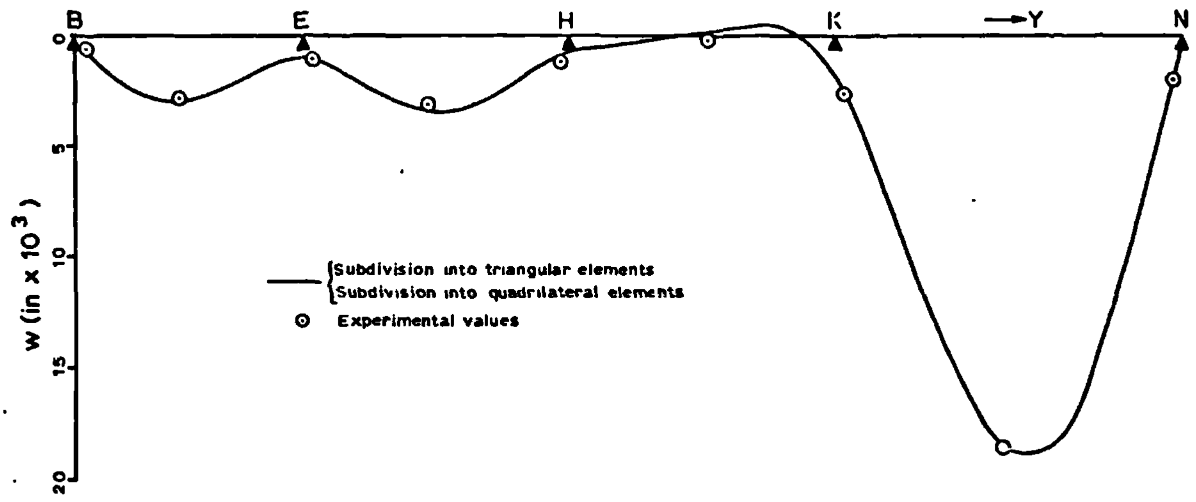

Fig. 2.4. Curved slab bridge model.
Central longitudinal deflexion profile
for model under dead load

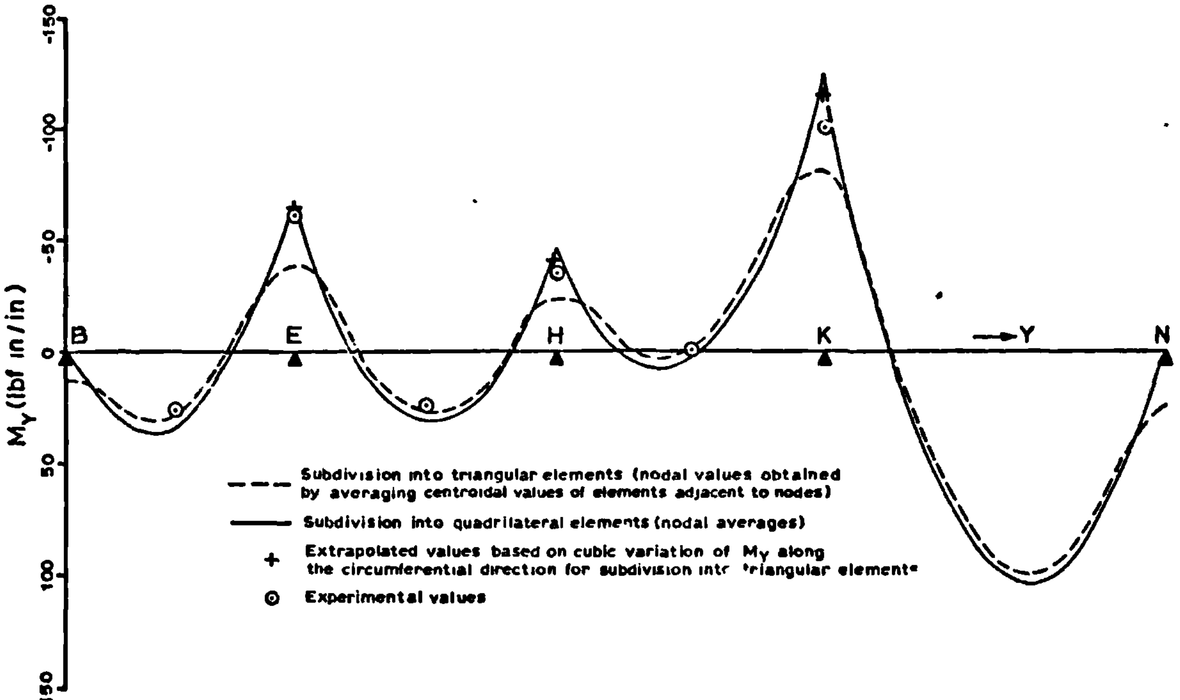

Fig. 2.5. Curved slab bridge model.
Distribution of longitudinal bending moments
along centre line for model under dead load

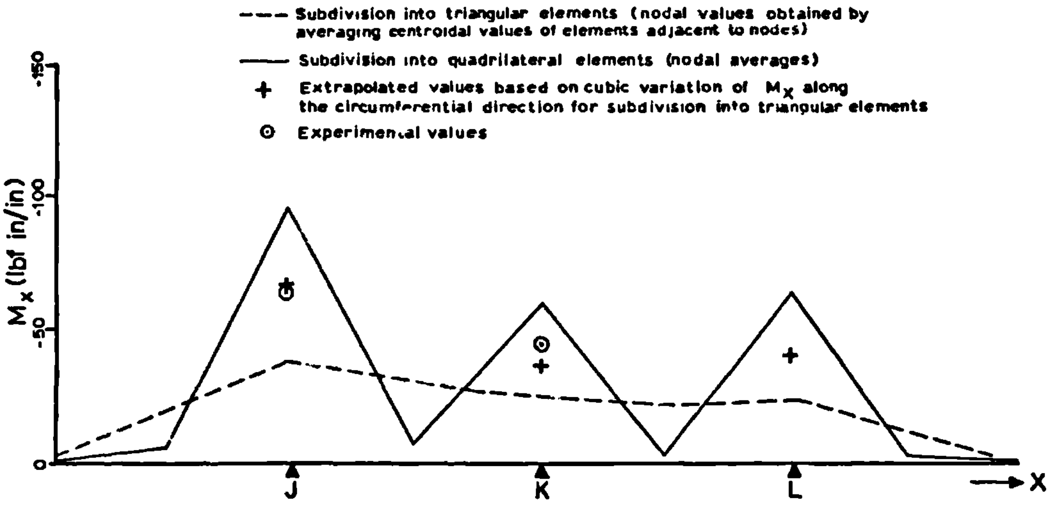

Fig. 2.6. Curved slab bridge model.
Distribution of transverse bending moments across section AA for model under dead load

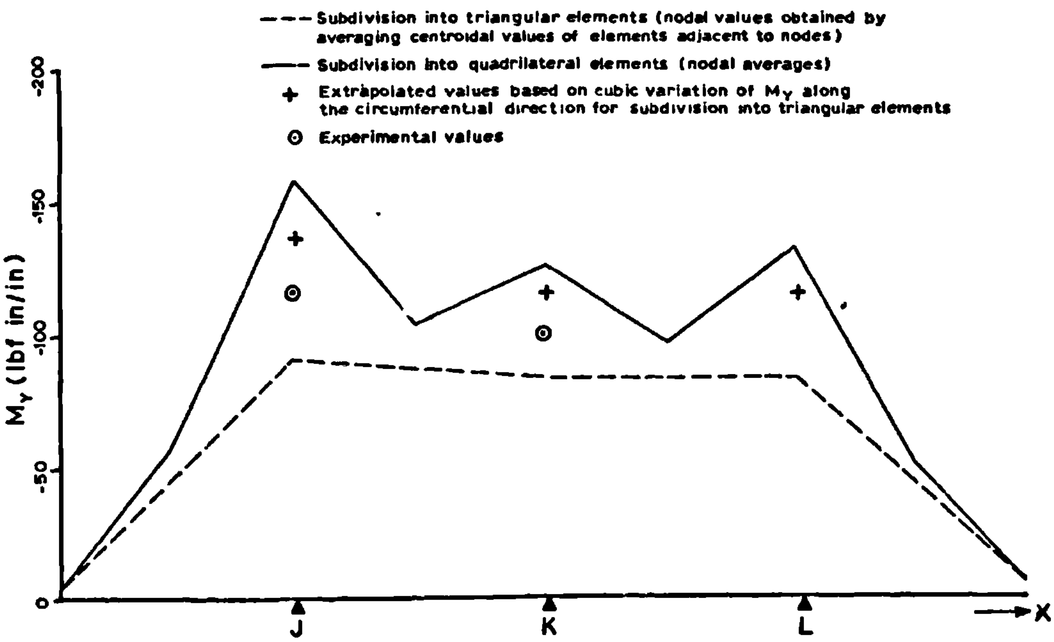

Fig. 2.7. Curved slab bridge model.
Distribution of longitudinal bending moments across section AA for model under dead load

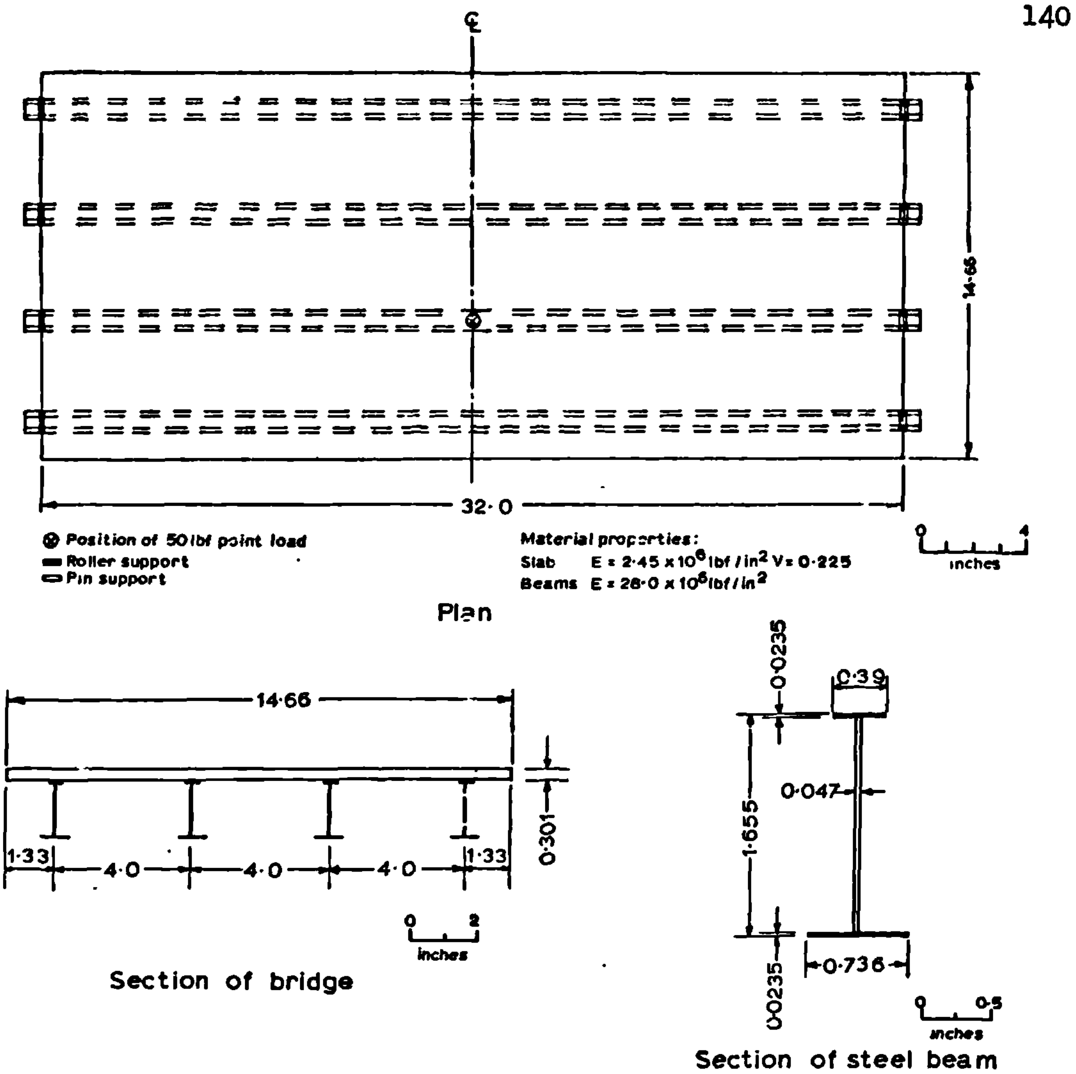

Fig. 2.8. Straight composite beam and slab bridge model.
Details of model and loading

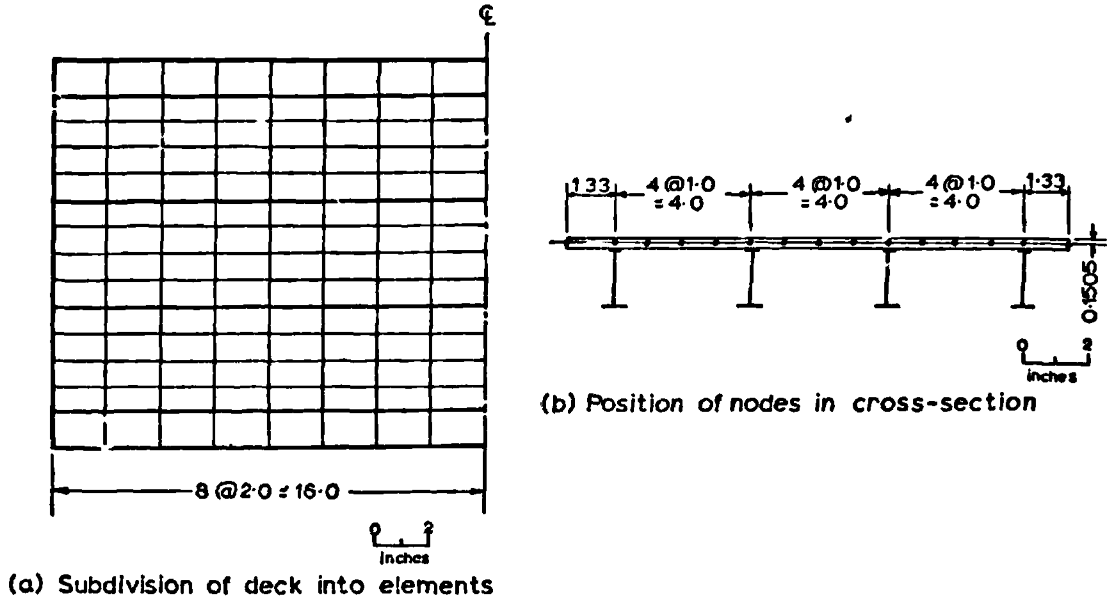

Fig 2.9. Straight composite beam and slab bridge model
Finite element idealization

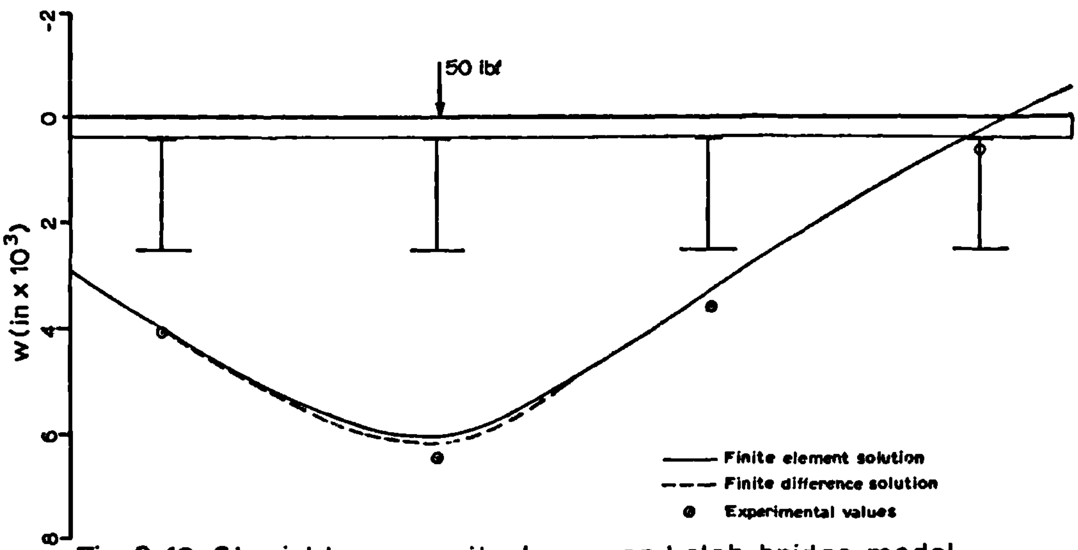

Fig. 2.10. Straight composite beam and slab bridge model. Transverse deflexion profile at mid-span for model under eccentric point load at mid-span

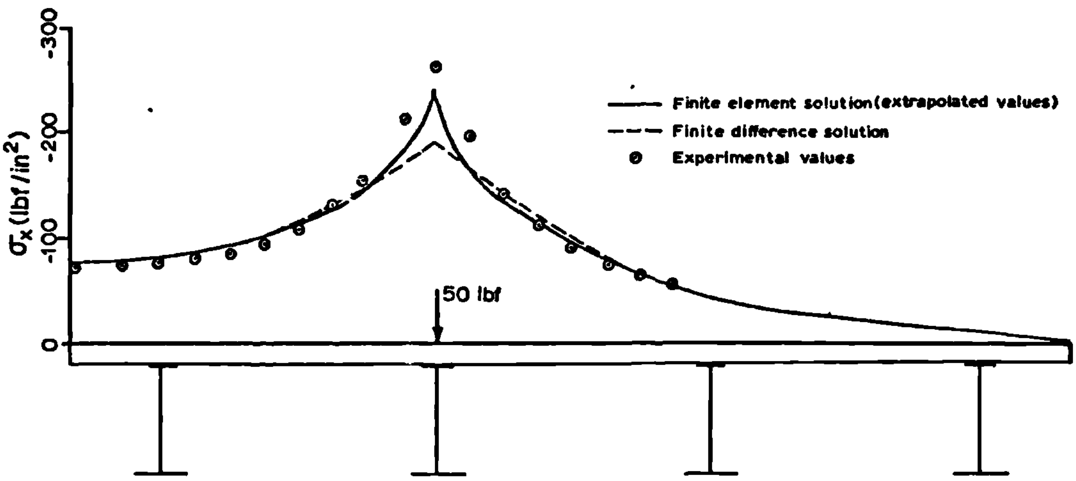

Fig. 2.11. Straight composite beam and slab bridge model. Distribution of longitudinal stresses in top surface of slab at mid-span for model under eccentric point load at mid-span

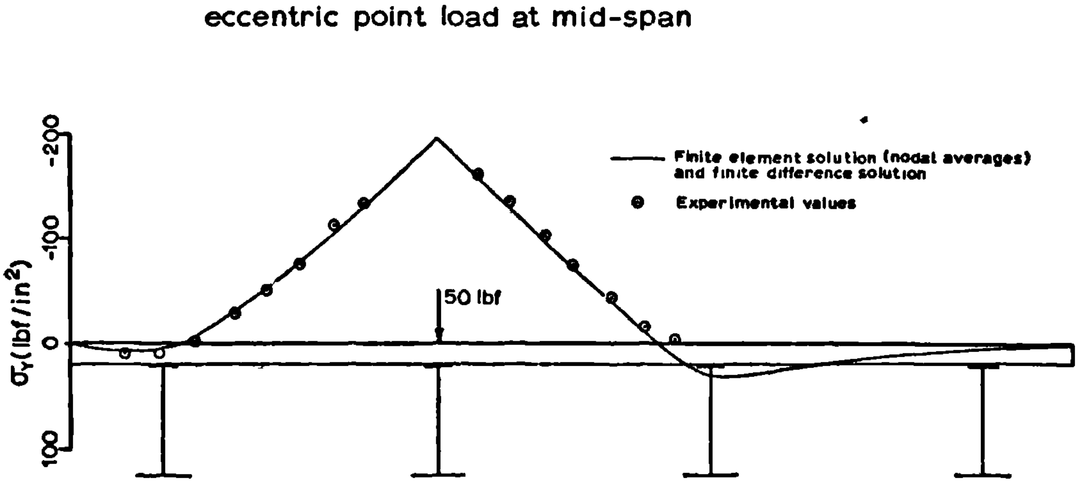

Fig. 2.12. Straight composite beam and slab bridge model. Distribution of transverse stresses in top surface of slab at mid-span for model under eccentric point load at mid-span

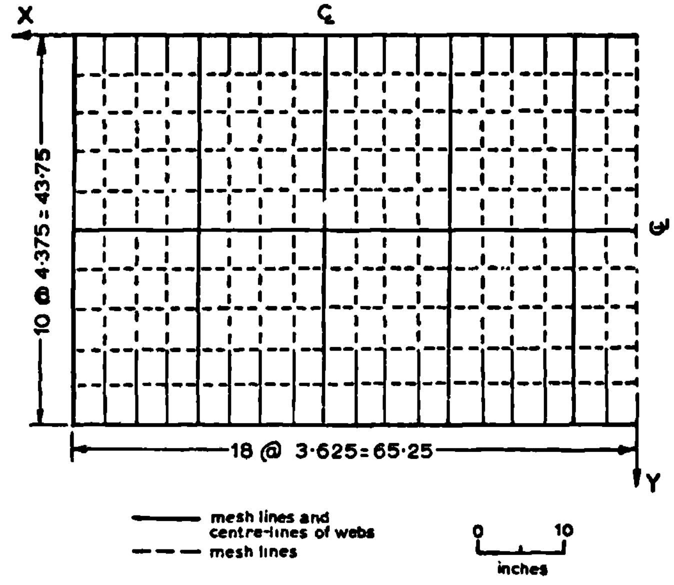

Fig. 2.13. Ship's double-bottom model. Finite element mesh

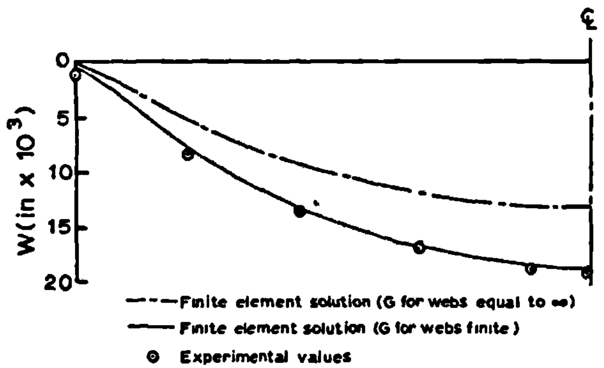

Fig. 2.14. Ship's double-bottom model. Longitudinal deflexion profile along centre girder for model under uniform load of 1 lbf/in^2

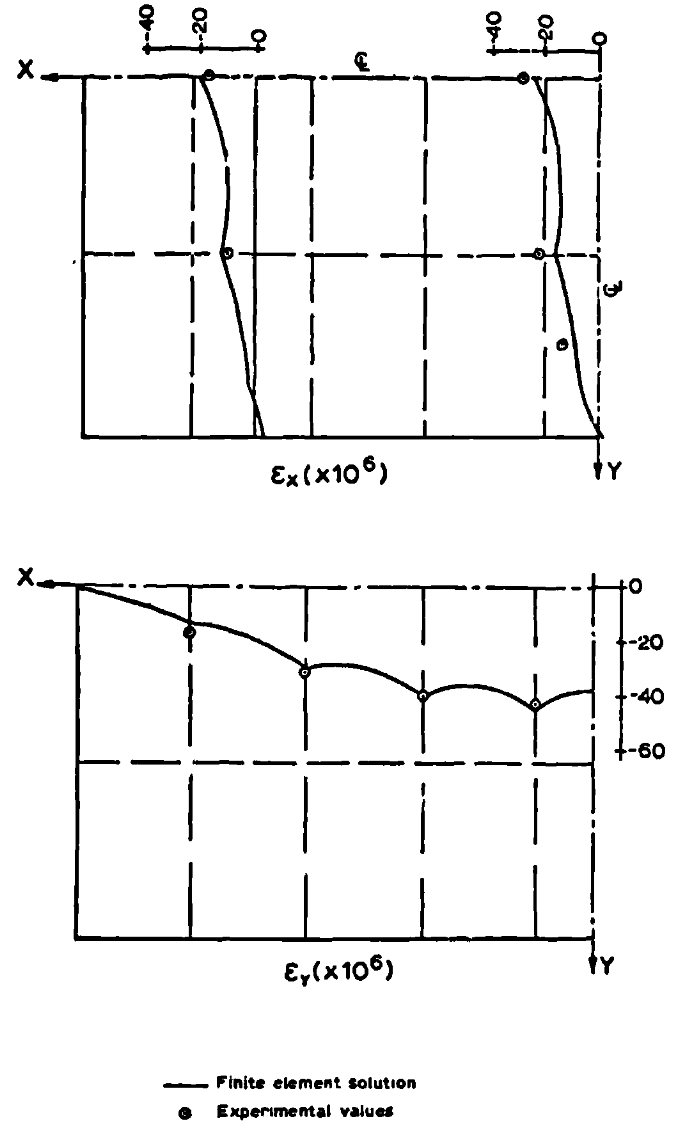

Fig. 2.15. Ship's double-bottom model. Distribution of inner surface strains for model under uniform load of 1 lbf/in^2

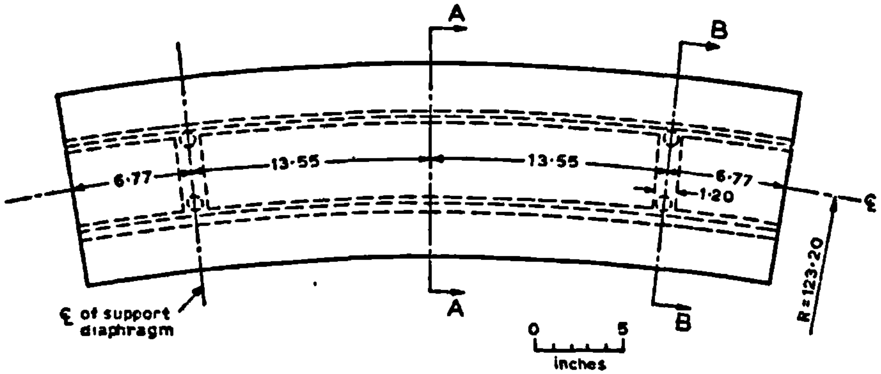

Plan

Material properties:
$E = 2{\cdot}75 \times 10^6\,lbf/in^2$ $V = 0{\cdot}23$

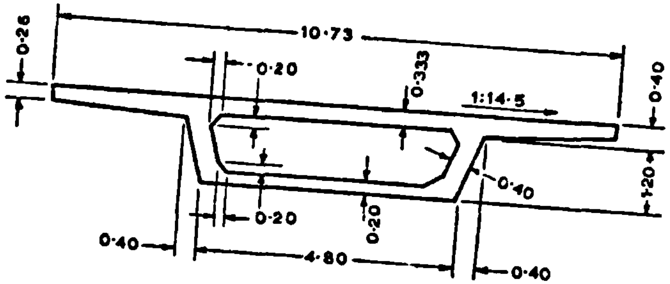

Section AA

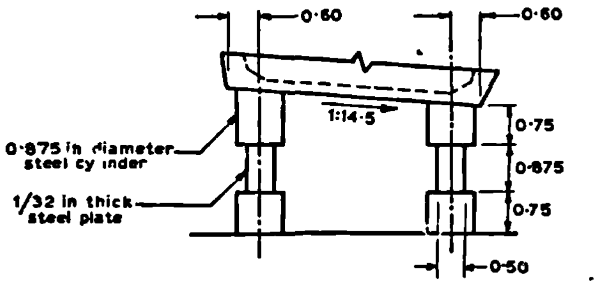

Section BB showing general arrangement of support system

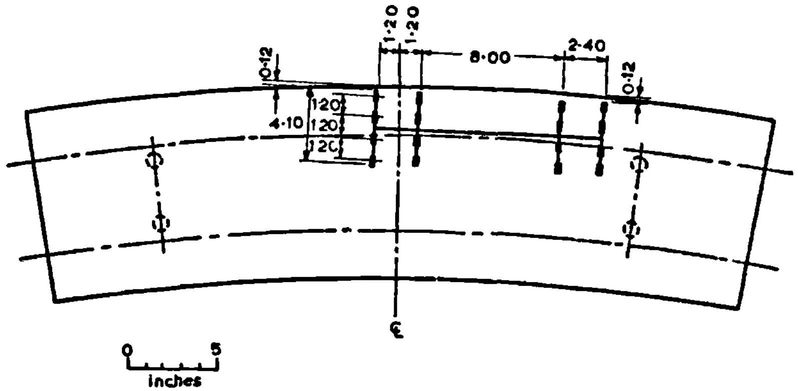

Position of 100lbf Type HB loading

Fig. 2.16. Curved single cell box girder bridge model. Details of model and loading

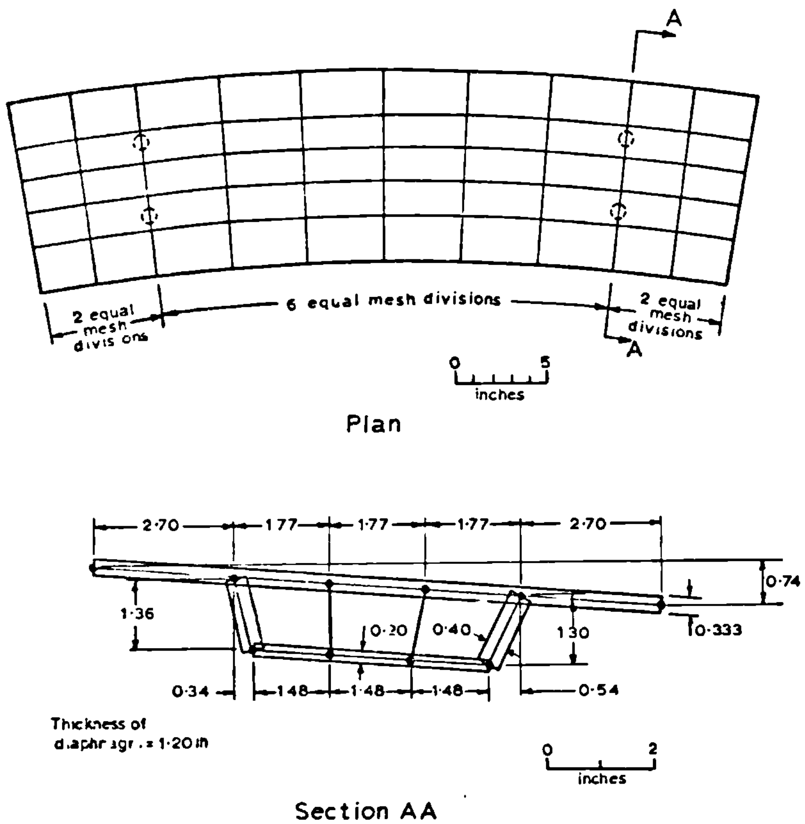

Fig. 2.17. Curved single cell box girder bridge model. Finite element idealization

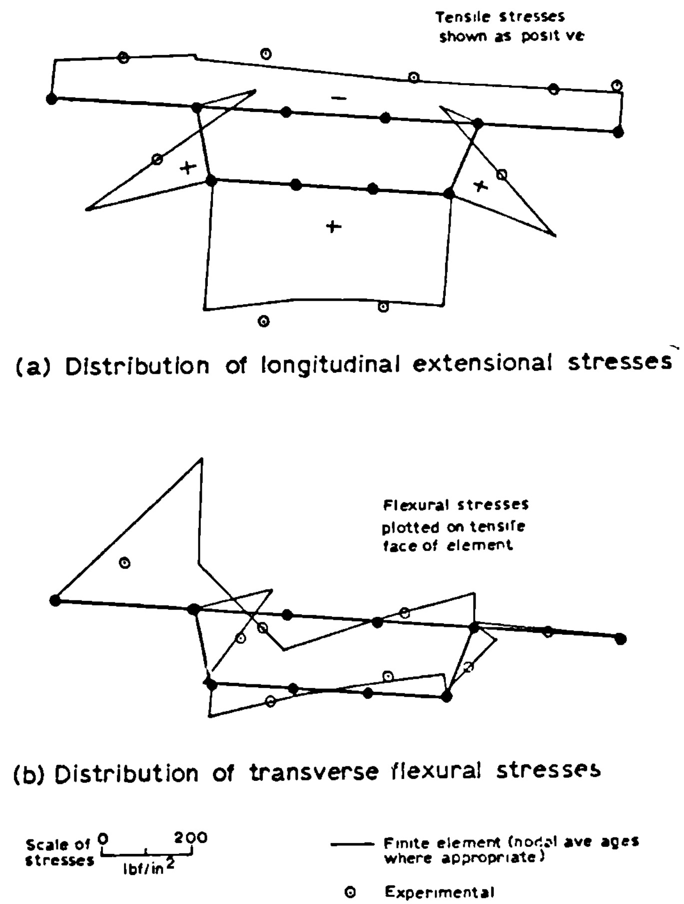

Fig. 2.18. Curved single cell box girder bridge model. Distribution of stresses at centre cross-section for model under Type HB loading

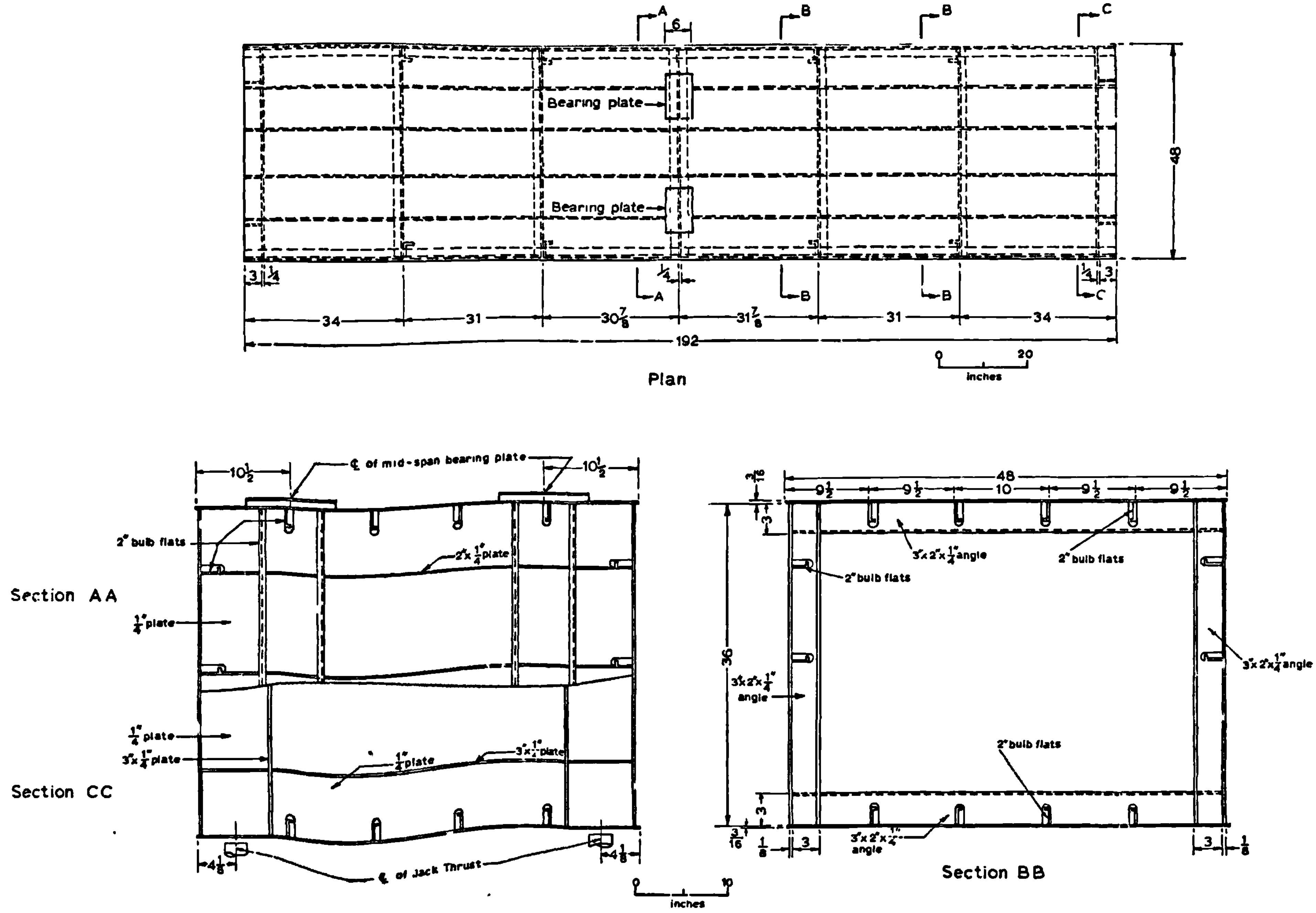

Fig. 2.19. Single cell box girder model.
Details of model

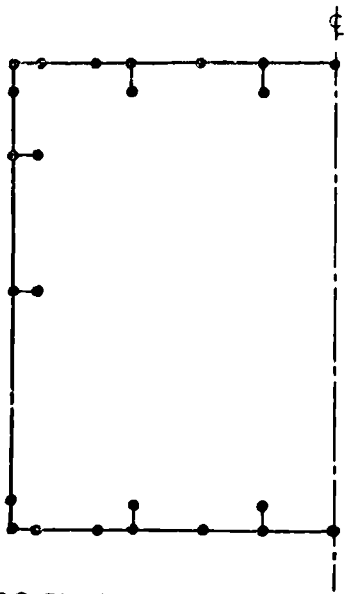

Fig. 2.20. Single cell box-girder model.
Typical cross-sectional arrangement of nodes

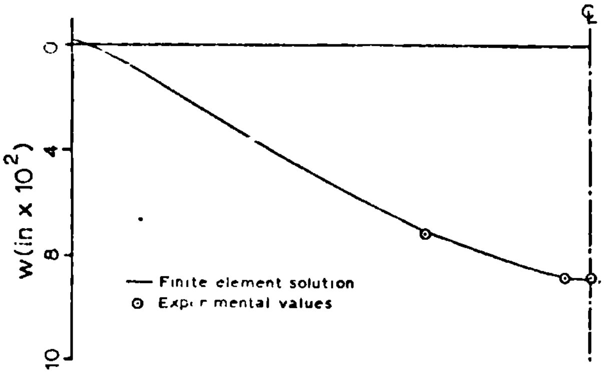

Fig. 2.21. Single cell box girder model. Longitudinal deflexion profile along web-flange junction for model under symmetrical point loads at mid-span

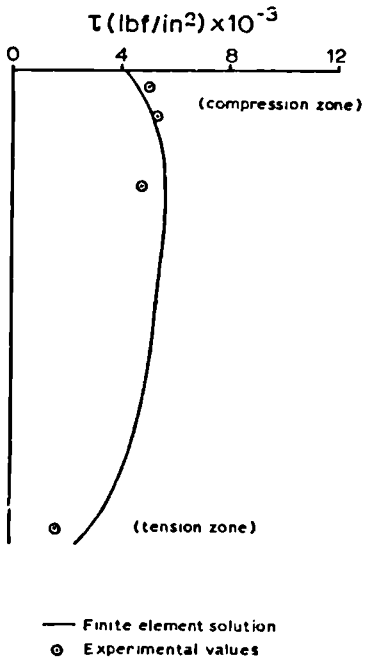

Fig. 2.22. Single cell box-girder model. Distribution of mid-plane shear stresses over depth of web at cross-section $5\frac{1}{6}$ in from mid-span for model under symmetrical point loads at mid-span

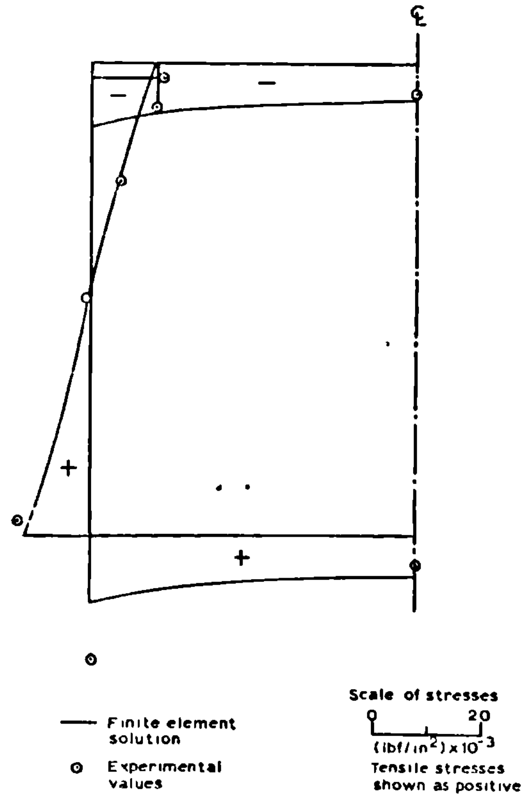

Fig. 2.23. Single cell box-girder model. Distribution of longitudinal extensional stresses at cross-section $5\frac{1}{6}$ in from mid-span for model under symmetrical point loads at mid-span

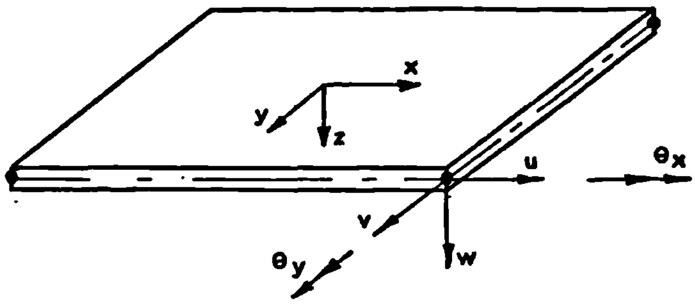

Fig. 3.1. Basic rectangular shell element

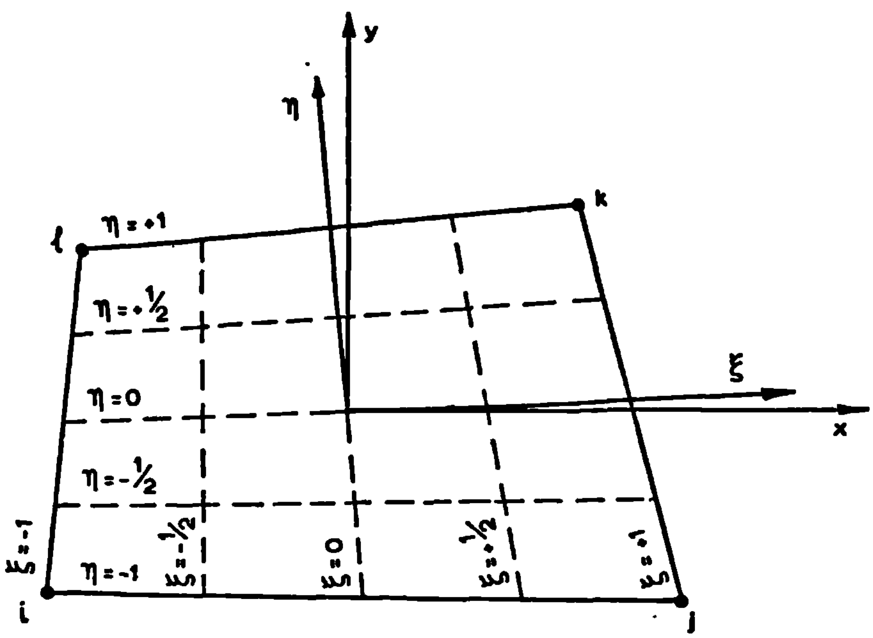

Fig. 3.2. Quadrilateral element and generalized co-ordinate system

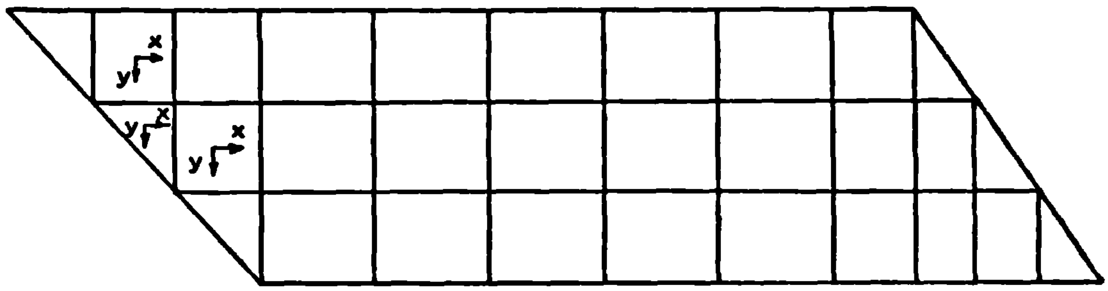

Fig. 3.3. Discretization of a skewed region using triangular and rectangular elements

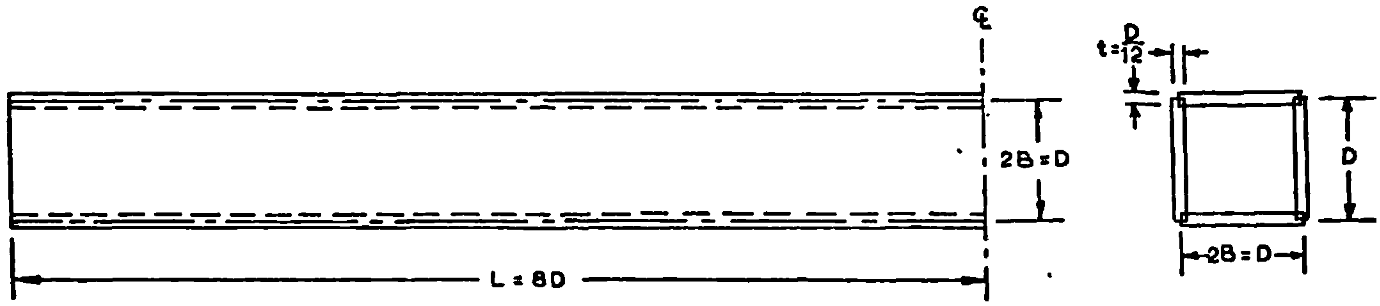

(a) Dimensions of girder

(b) Loading on girder at mid-span

Fig. 3.4. Straight single cell box girder.
Details of girder ($\nu = 0{\cdot}2$) and loading

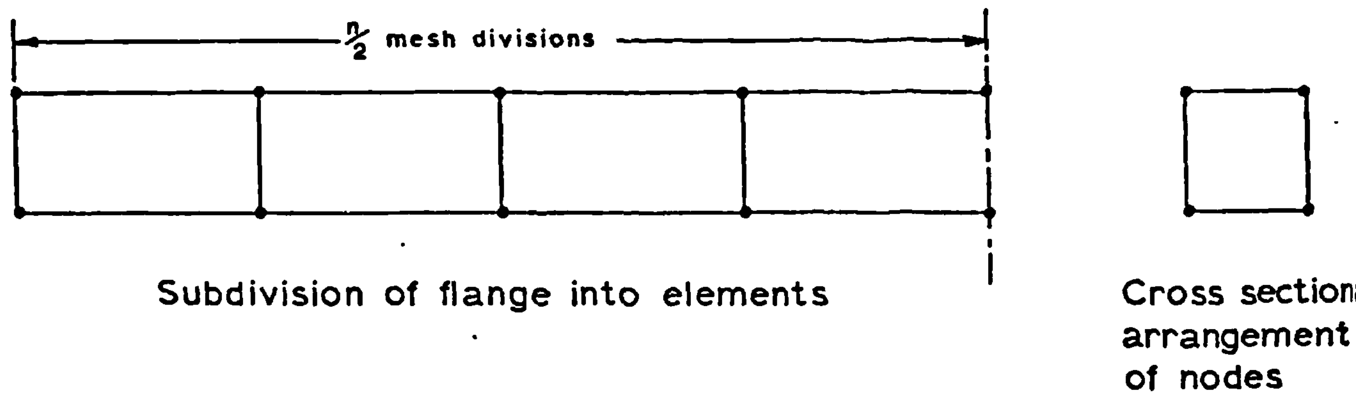

Fig. 3.5. Straight single cell box girder.
Finite element idealization

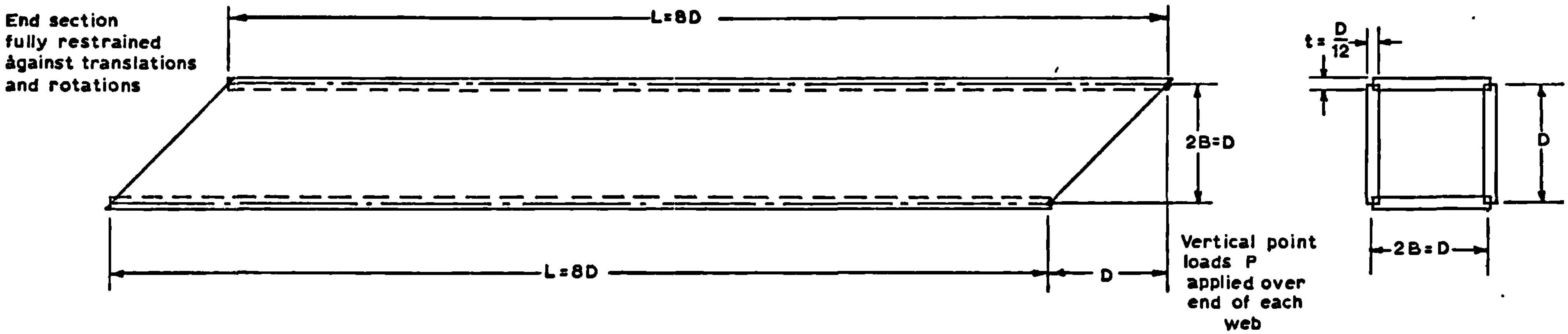

Fig. 3.6. Skewed single cell box girder.
Details of girder ($V = 0{\cdot}2$) and loading

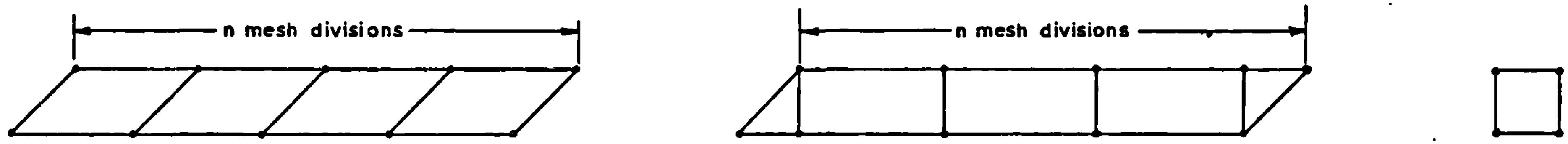

Subdivision of flange into parallelogramic elements (mesh type 1)

Subdivision of flange into rectangular and triangular elements (mesh type 2)

Cross-sectional arrangement of nodes

Fig. 3.7. Skewed single cell box girder.
Finite element idealizations

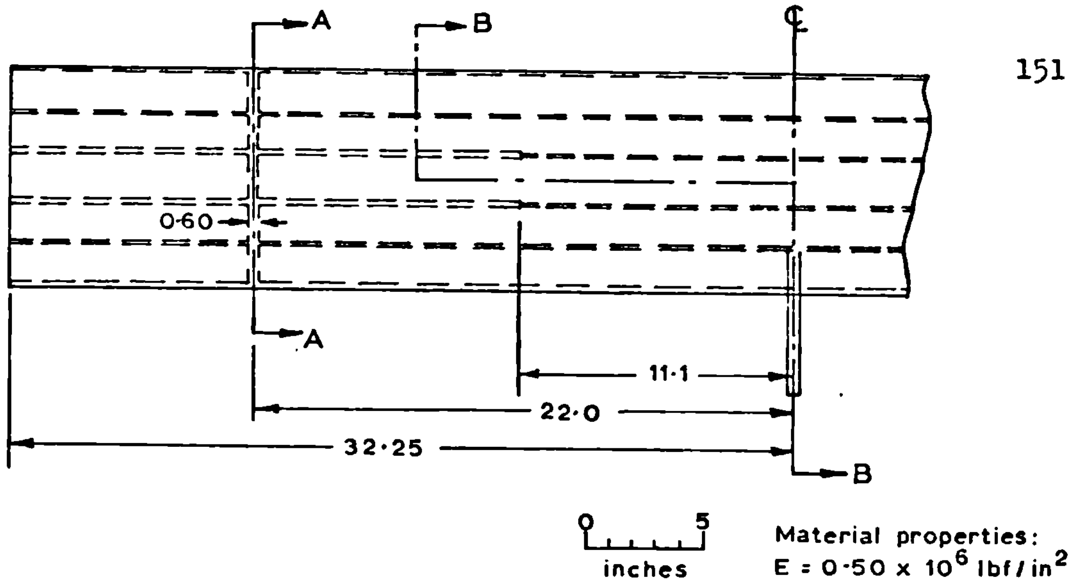

Plan

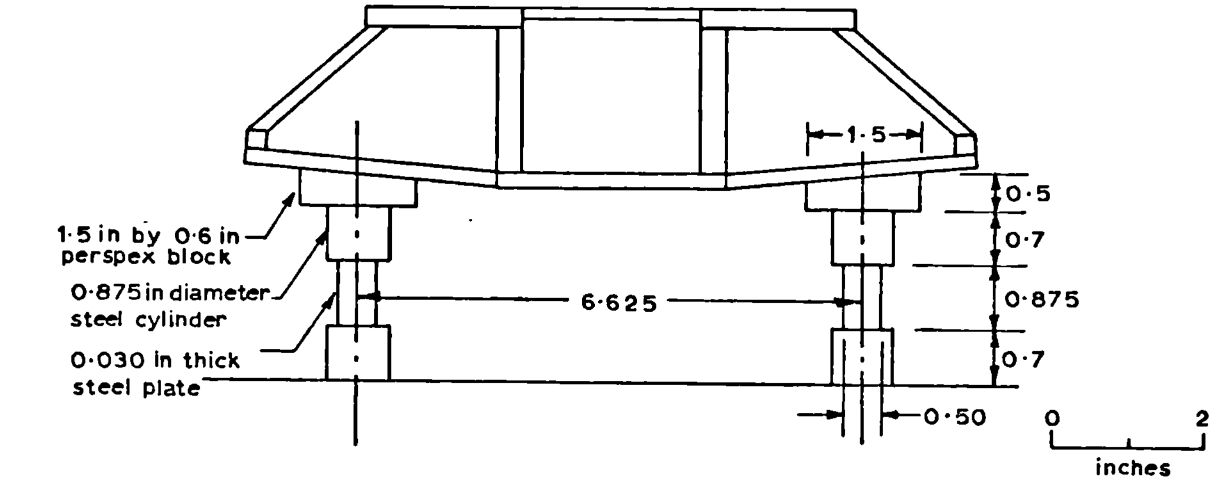

Section AA showing general arrangement of support system

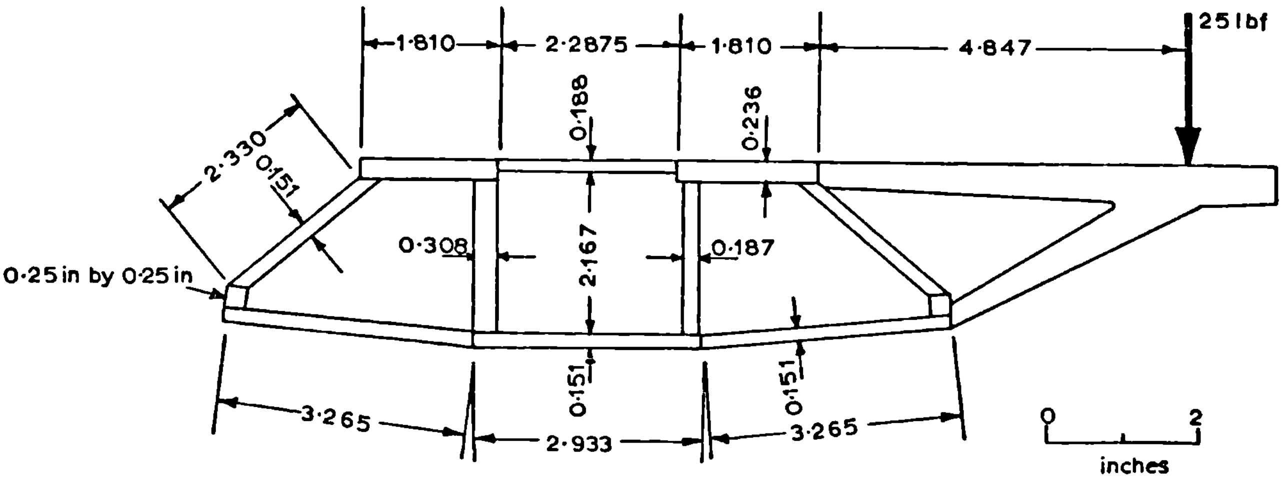

Section BB

Fig. 3.8. Straight three cell box girder bridge model. Details of model and loading

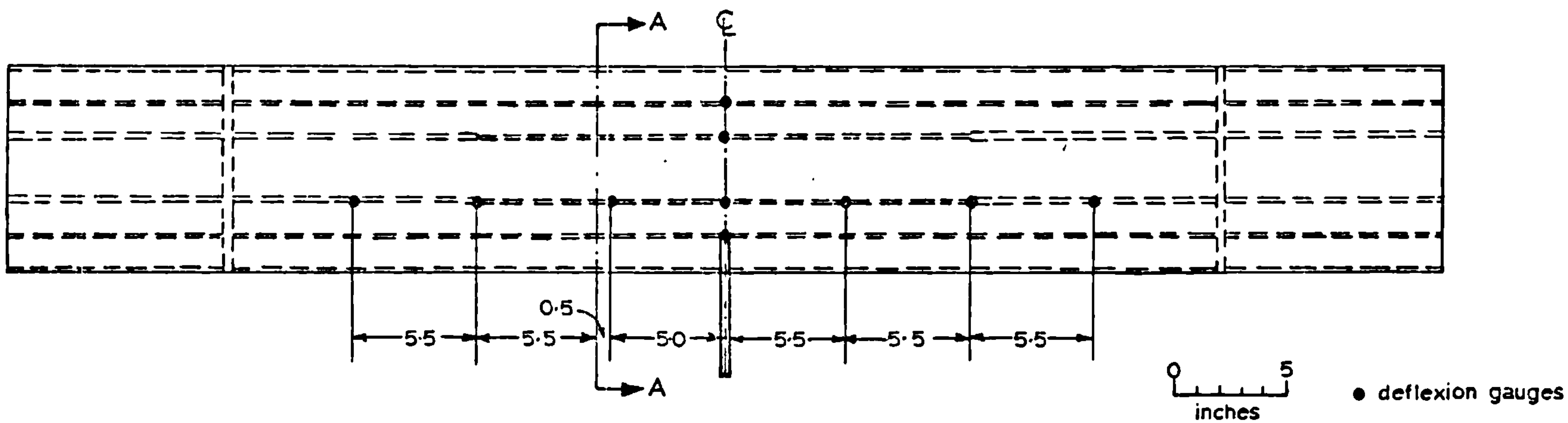

(a) Plan showing position of deflexion gauges

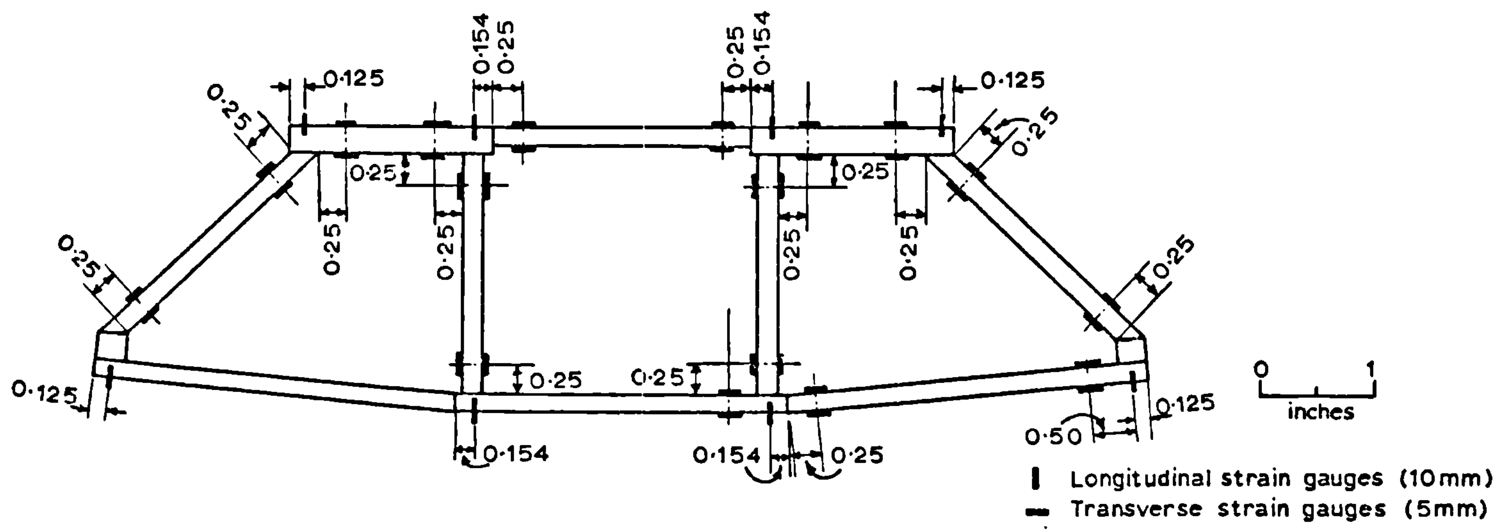

(b) Section AA showing position of strain gauges

Fig. 3.9. Straight three cell box girder bridge model.
Instrumentation of model

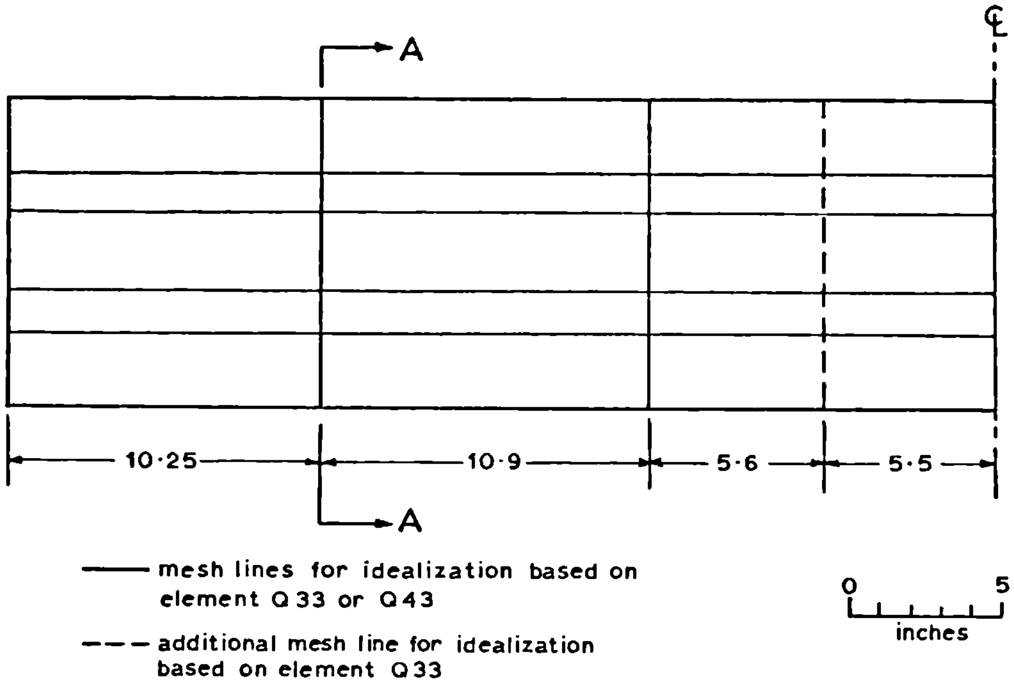

Plan

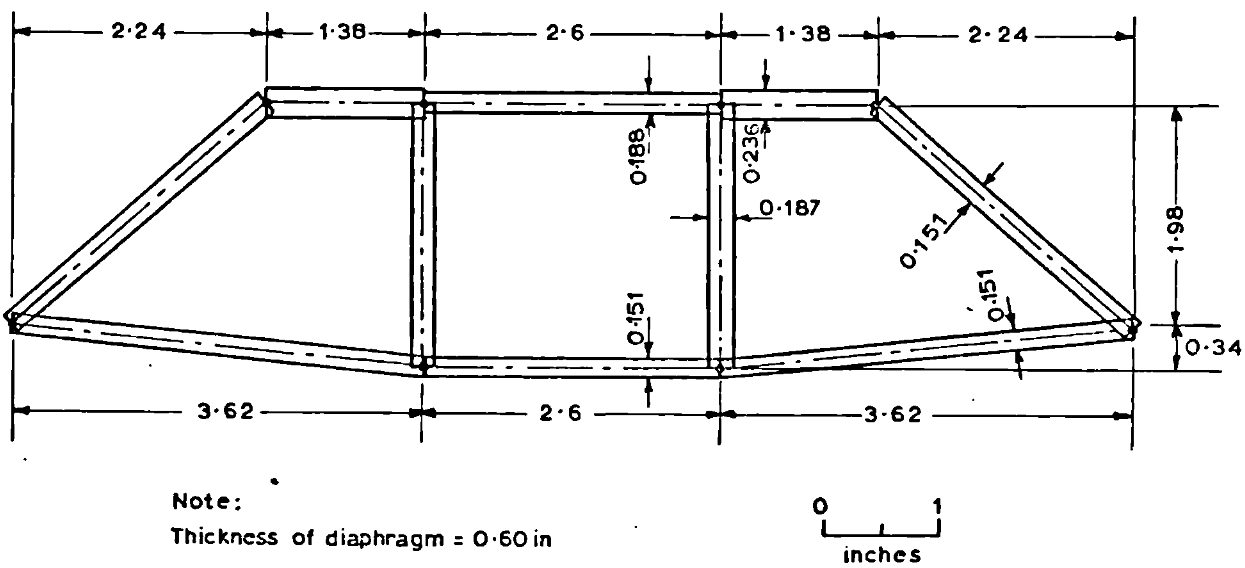

Section AA

Fig. 3.10. Straight three cell box girder bridge model. Finite element idealizations

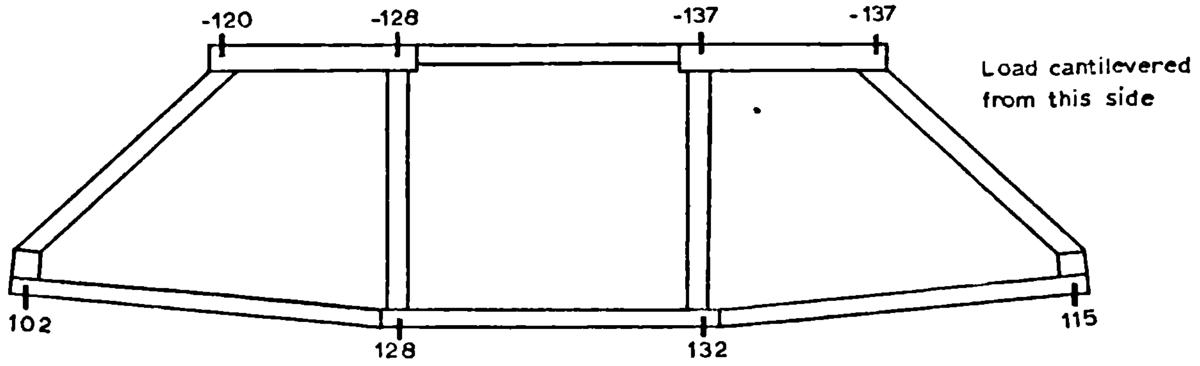

(a) Longitudinal strains (x 10^6)

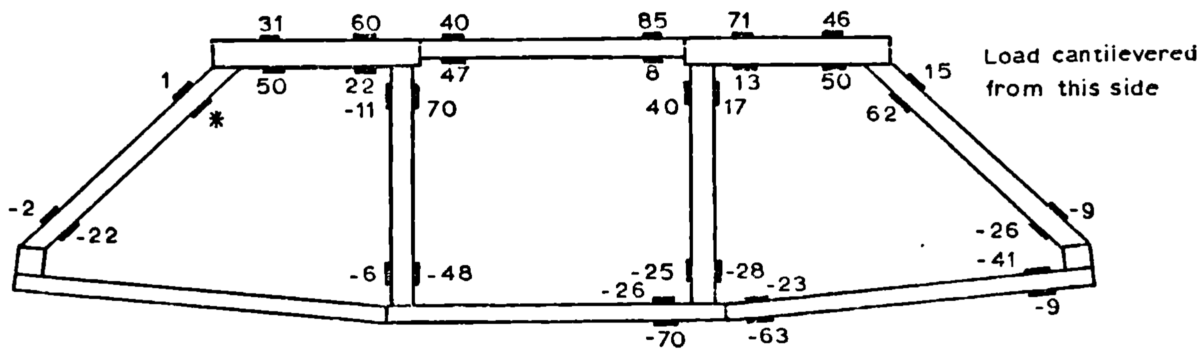

(b) Transverse strains (x 10^6)

* Bad reading

Fig. 3.11. Straight three cell box girder bridge model. Experimental values of strain for model under eccentric point load at mid-span

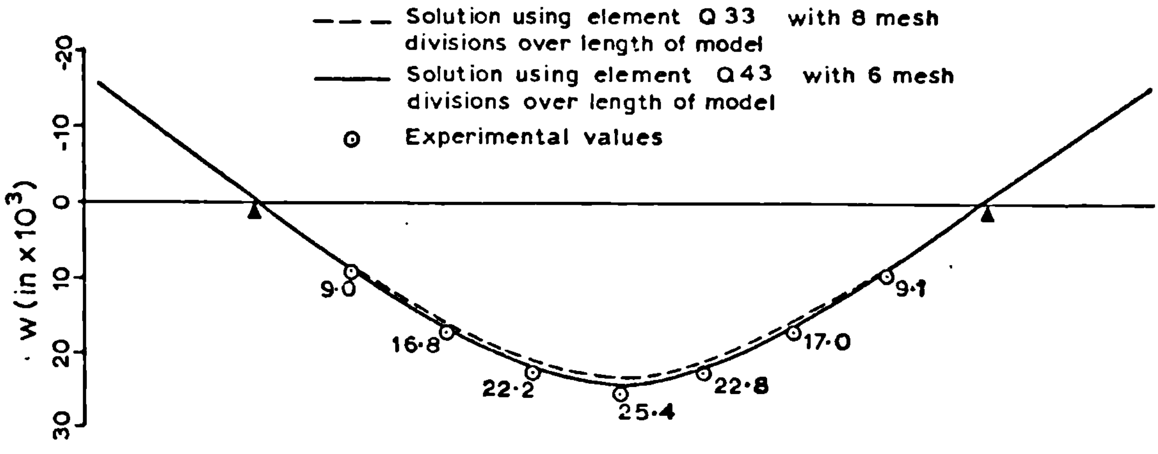

Fig: 3.12. Straight three cell box girder bridge model. Longitudinal deflexion profile along top of vertical web nearer load for model under eccentric point load at mid-span

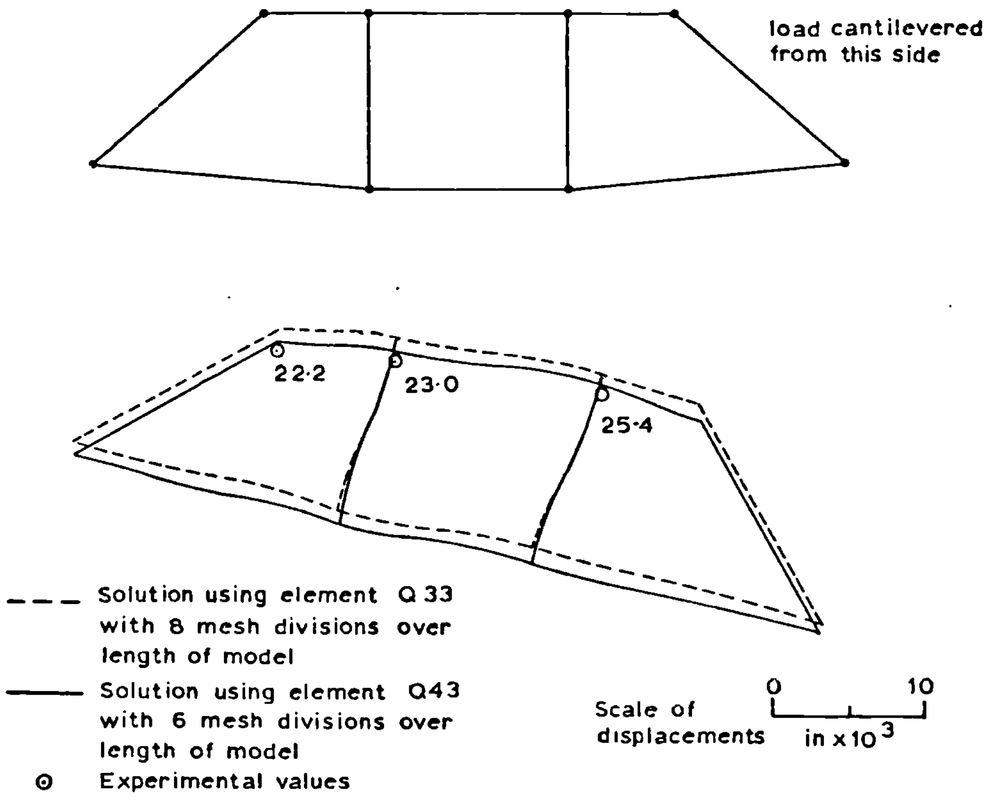

Fig. 3.13. Straight three cell box girder bridge model. Displacements at centre cross-section for model under eccentric point load at mid-span

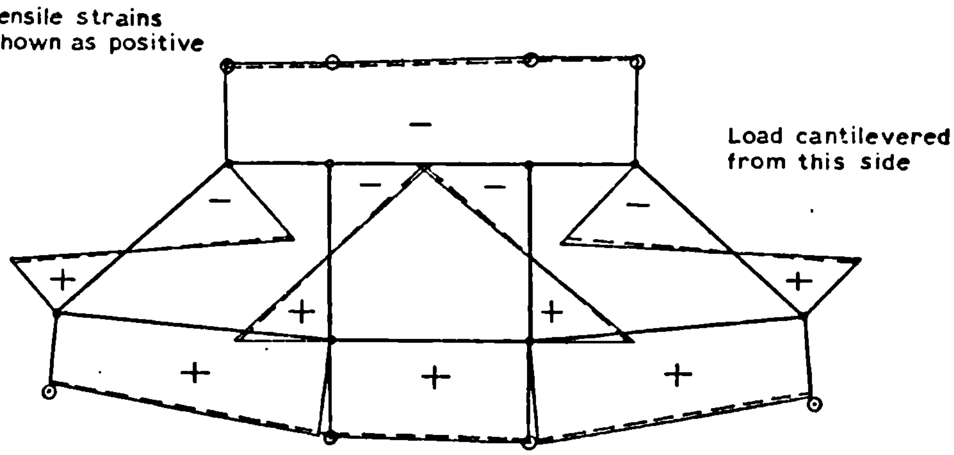

(a) Distribution of longitudinal outer surface strains

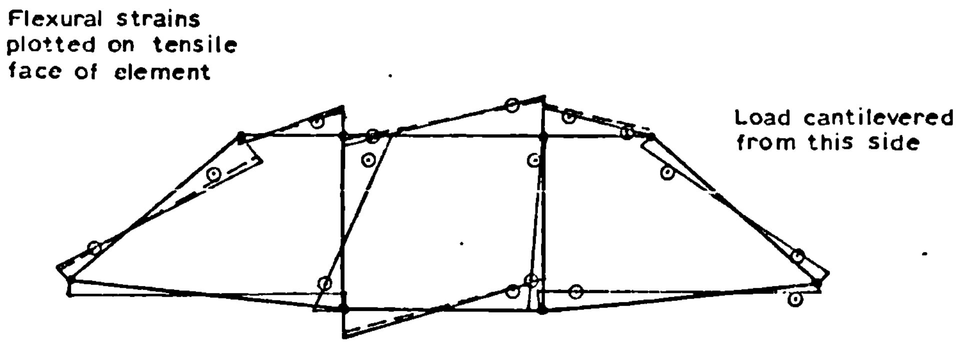

(b) Distribution of transverse flexural strains

— — — Solution using element Q33 with 8 mesh divisions over length of model

——— Solution using element Q43 with 6 mesh divisions over length of model

⊙ Experimental values

0 200
Strain x 10^6

Fig. 3.14. Straight three cell box girder bridge model. Distribution of strains at section 5·5in from mid-span for model under eccentric point load at mid-span

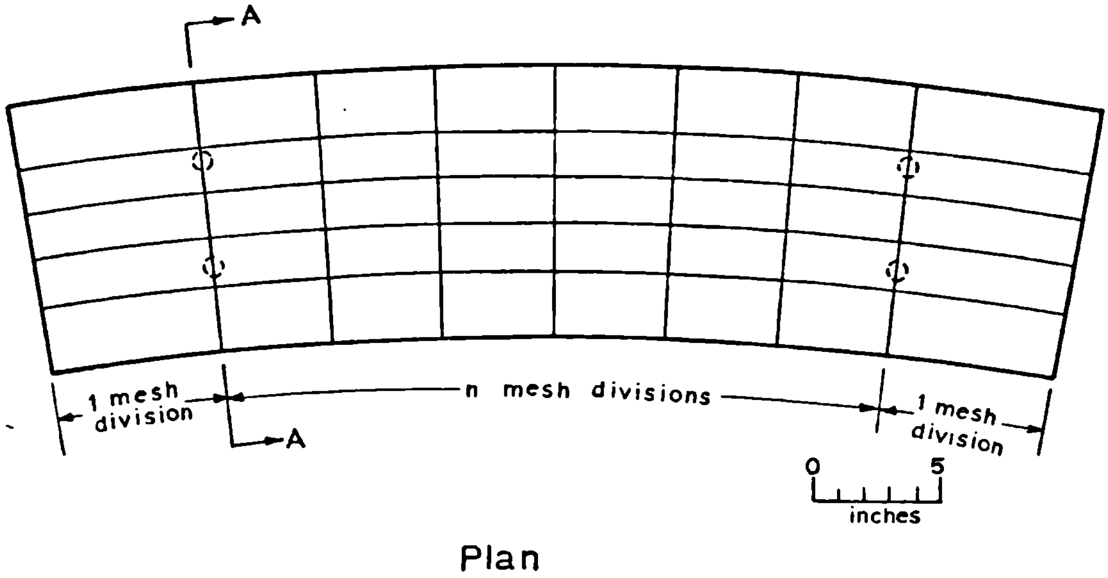

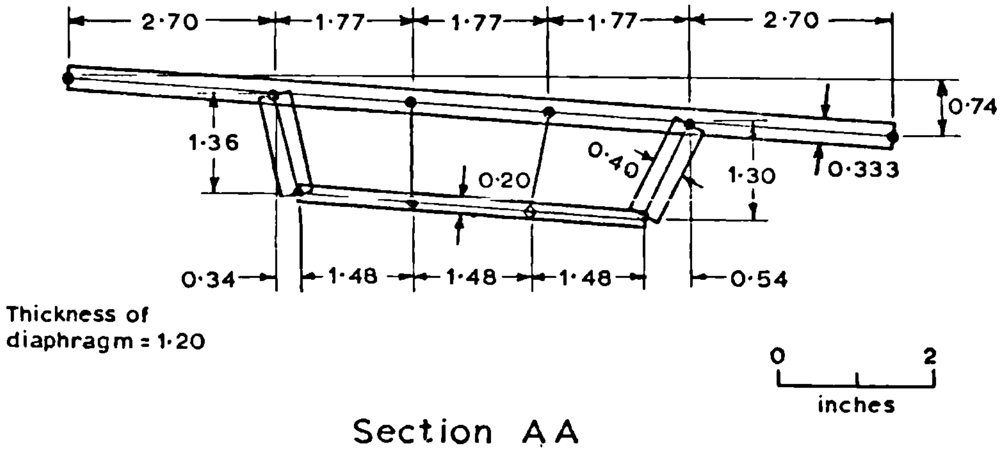

Fig. 3.15. Curved single cell box girder bridge model. Finite element idealization (n x 3 x 1 mesh)

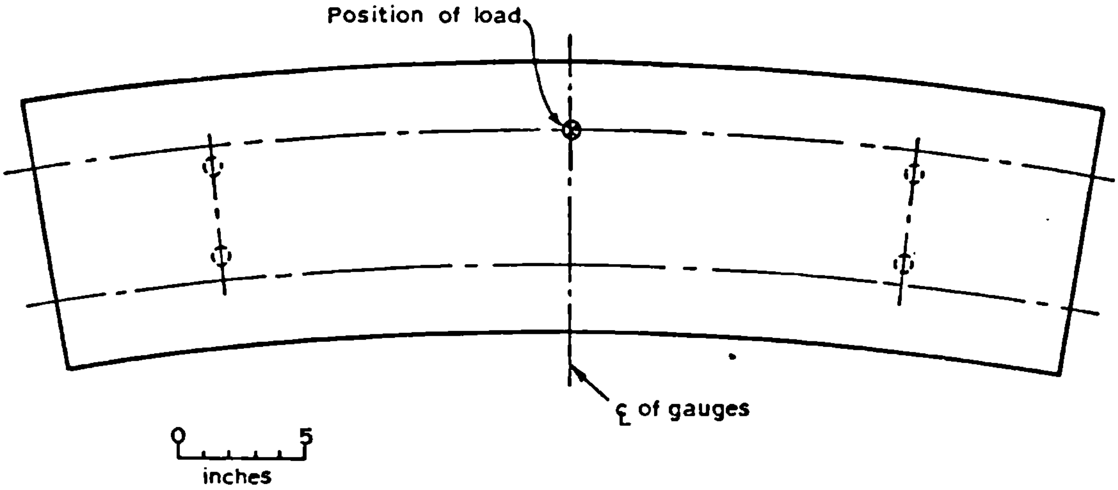

(a) Position of 100 lbf point load

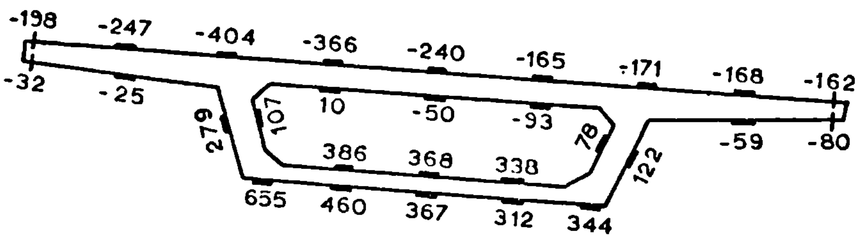

(b) Longitudinal stresses (lbf/in^2)

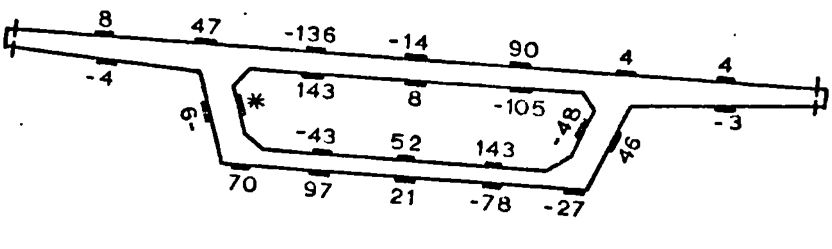

(c) Transverse stresses (lbf/in^2)

* Bad reading

Fig. 3.16. Curved single cell box girder bridge model. Experimental values of stress at centre section for model under eccentric point load at mid-span

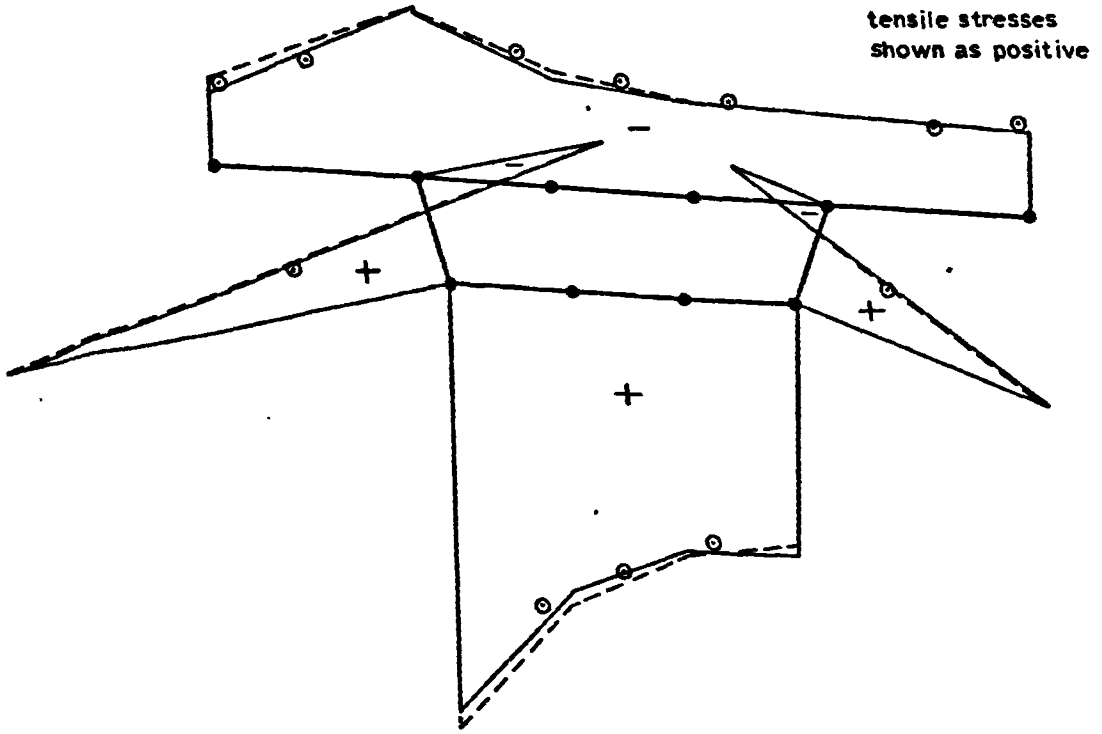

(a) Distribution of longitudinal extensional stresses

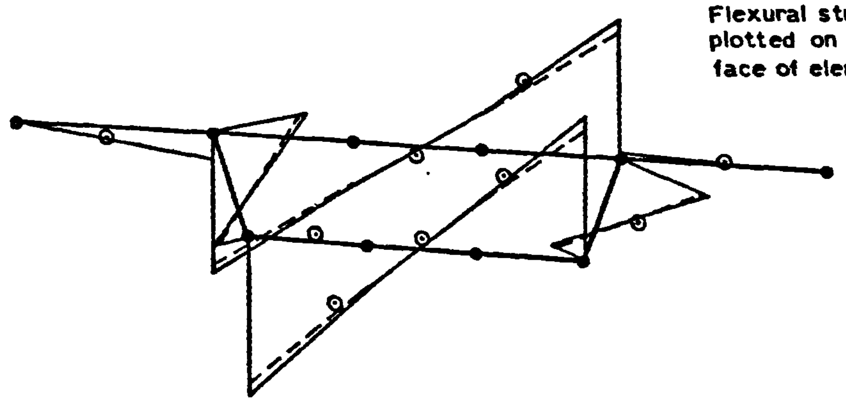

(b) Distribution of transverse flexural stresses

— — — Solution using element Q33 with 8 mesh divisions over length of model (For (a) values at mid-points of longitudinal sides of elements were extrapolated, and averaged where appropriate. For (b) nodal values were averaged where appropriate.)

——— Solution using element Q43 with 6 mesh divisions over length of model (nodal values were averaged where appropriate)

⊙ Experimental values

Scale of stresses 0 — 200 lbf/in^2

Fig. 3.17. Curved single cell box girder bridge model. Distribution of stresses at centre cross-section for model under eccentric point load at mid-span

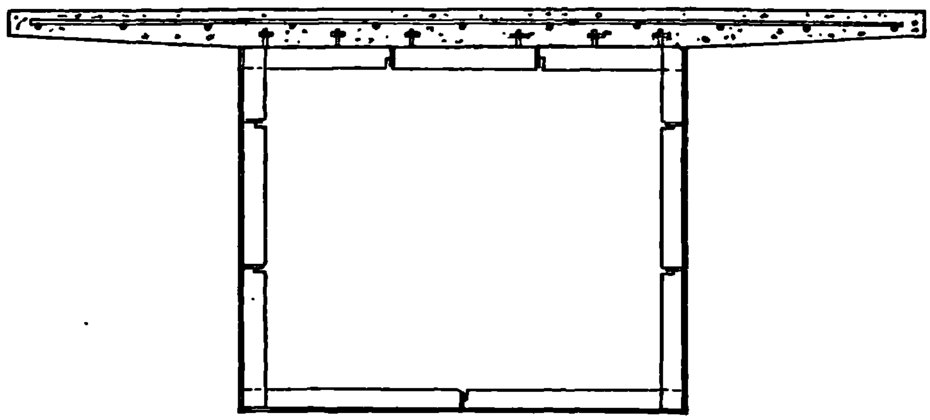

Fig. 4.1. Cross-section of typical composite box girder bridge

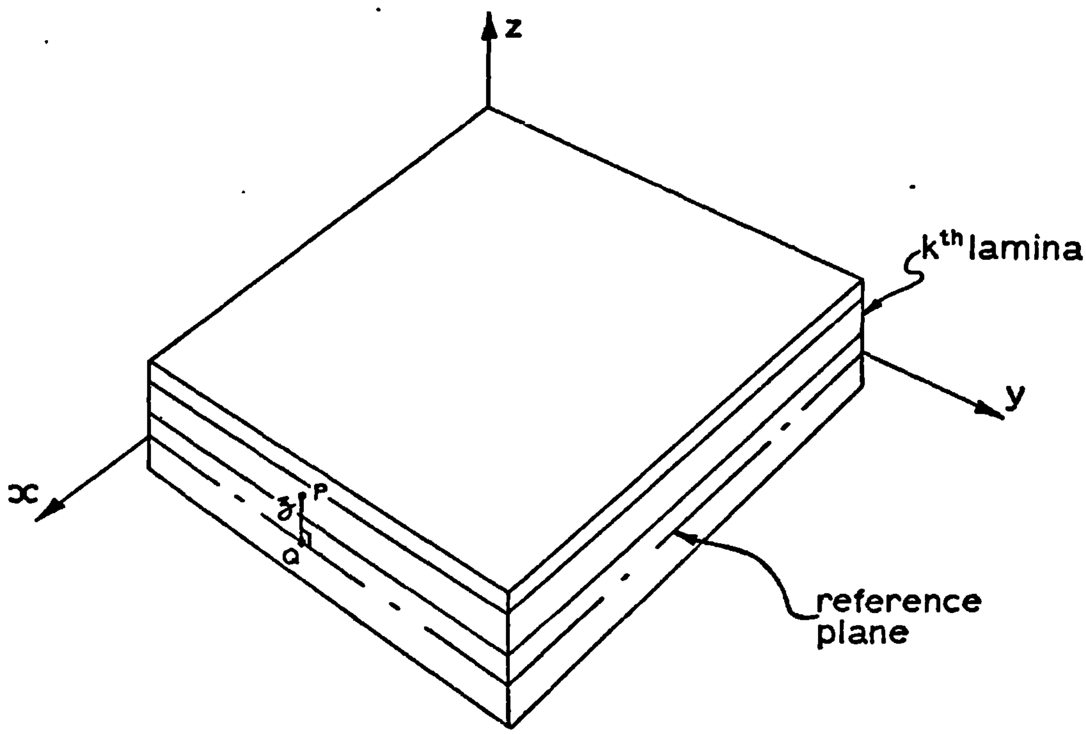

Fig. 4.2. Laminated shell element

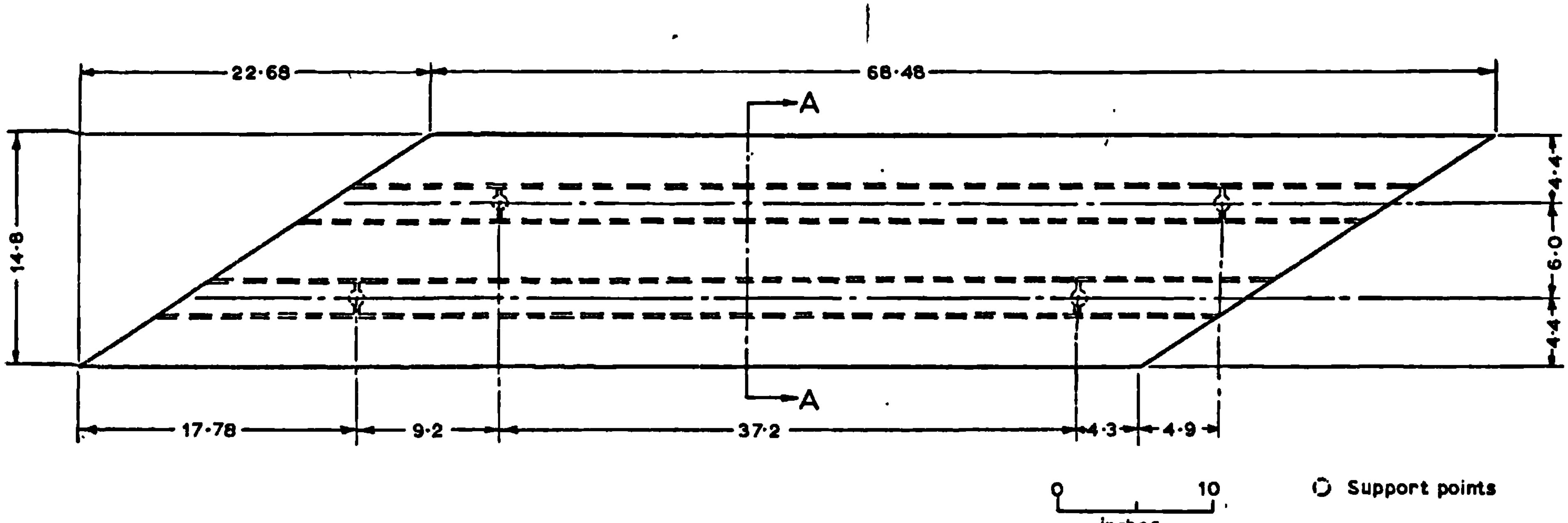

Plan

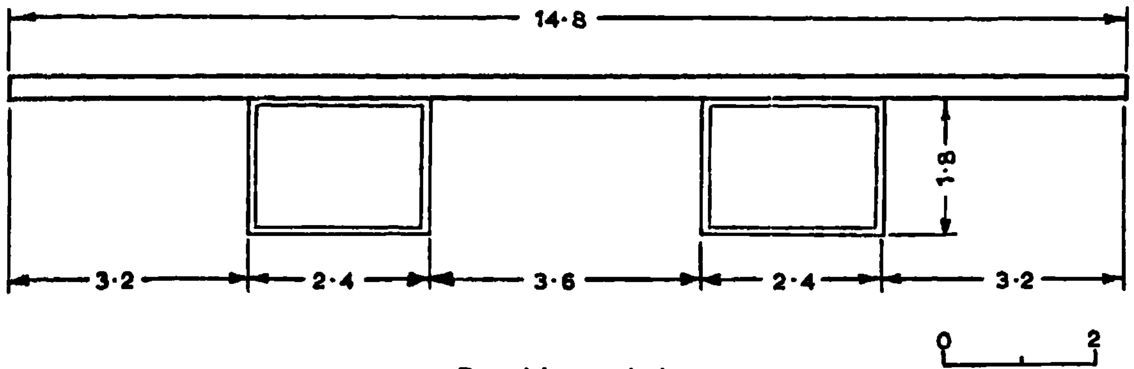

Section AA

Component details:

Slab	$E = 2{\cdot}38 \times 10^6$ lbf/in^2	$V = 0{\cdot}23$	$t = 0{\cdot}30$ in
Boxes	$E = 28{\cdot}0 \times 10^6$ lbf/in^2	$V = 0{\cdot}30$	$t = 0{\cdot}025$ in
Diaphragms	$E = 2{\cdot}38 \times 10^6$ lbf/in^2	$V = 0{\cdot}23$	$t = 0{\cdot}16$ in
Supports	$K = 140{\cdot}0 \times 10^3$ lbf/in		

Fig. 4.3. Skewed composite twin cell box girder bridge model.
Details of model

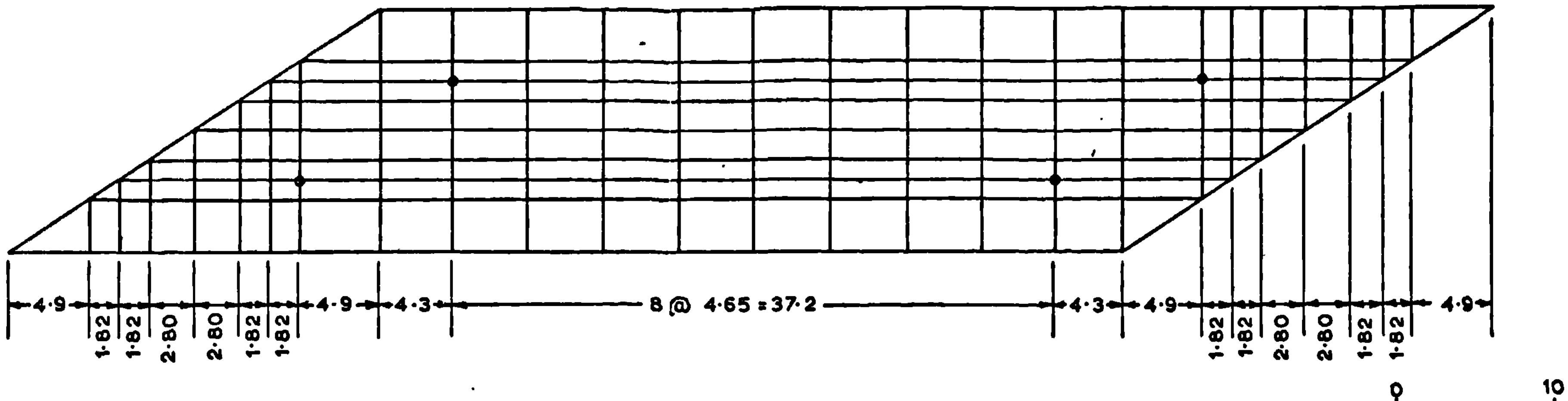

(a) Subdivision of top slab into elements

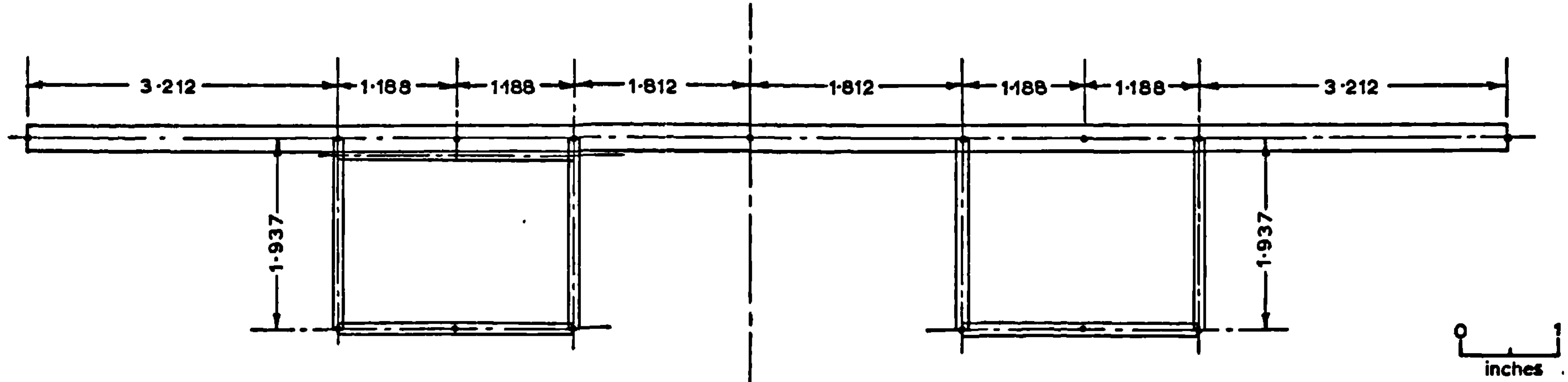

(b) Cross section of bridge showing subdivision into laminated and homogeneous elements

℄

(c) Cross section of bridge showing subdivision into homogeneous elements

Fig. 4.4. Skewed composite twin cell box girder bridge model. Finite element idealizations

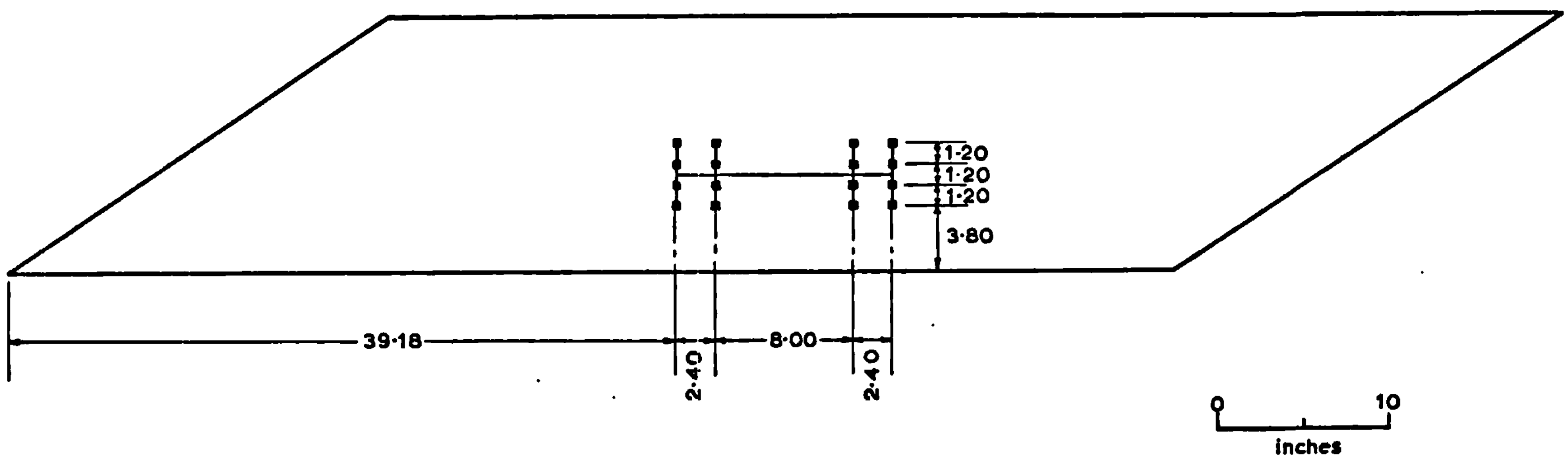

Fig. 4.5. Skewed composite twin cell box girder bridge model.
Position of Type HB loading (total applied load = 448·5 lbf)

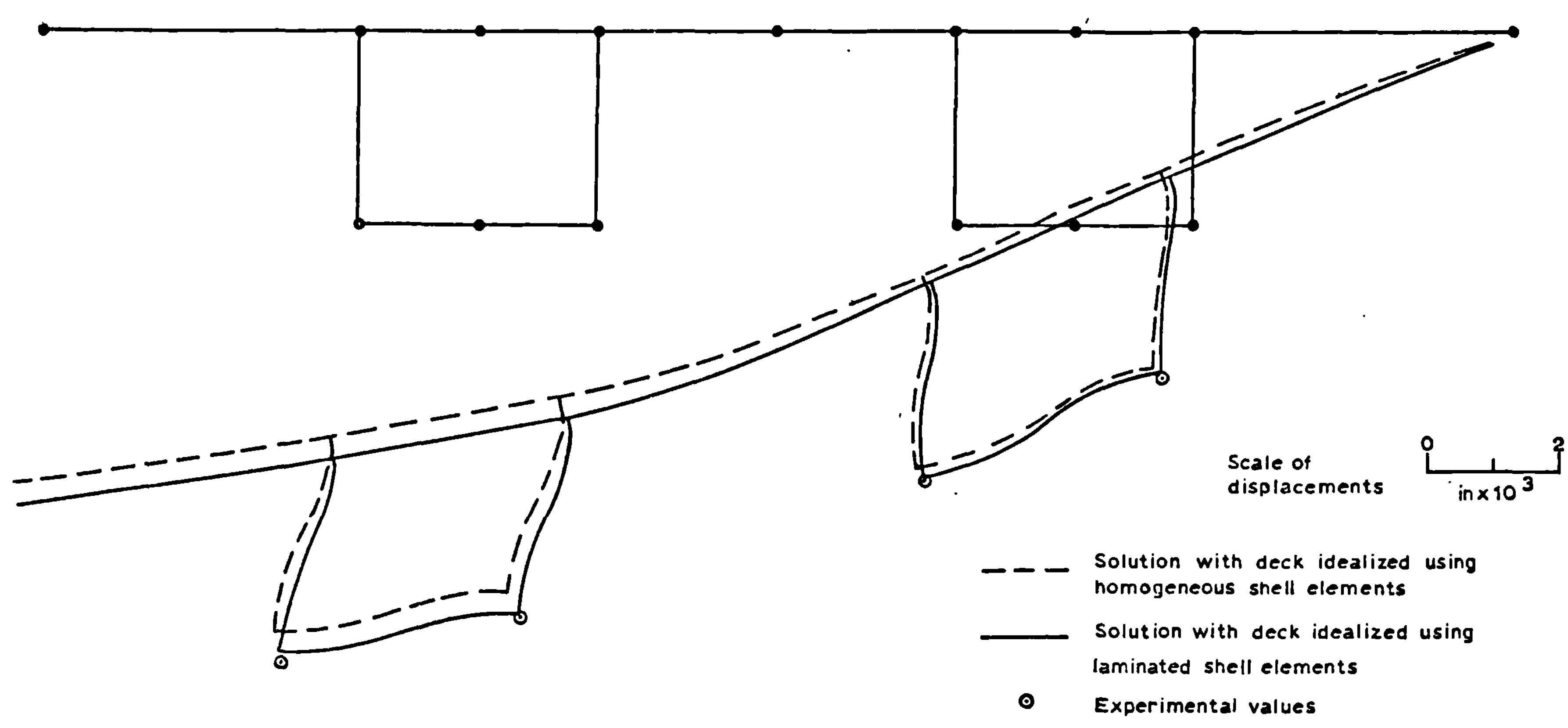

Fig. 4.6. Skewed composite twin cell box girder bridge model. Displacements at centre cross-section for model under Type HB loading

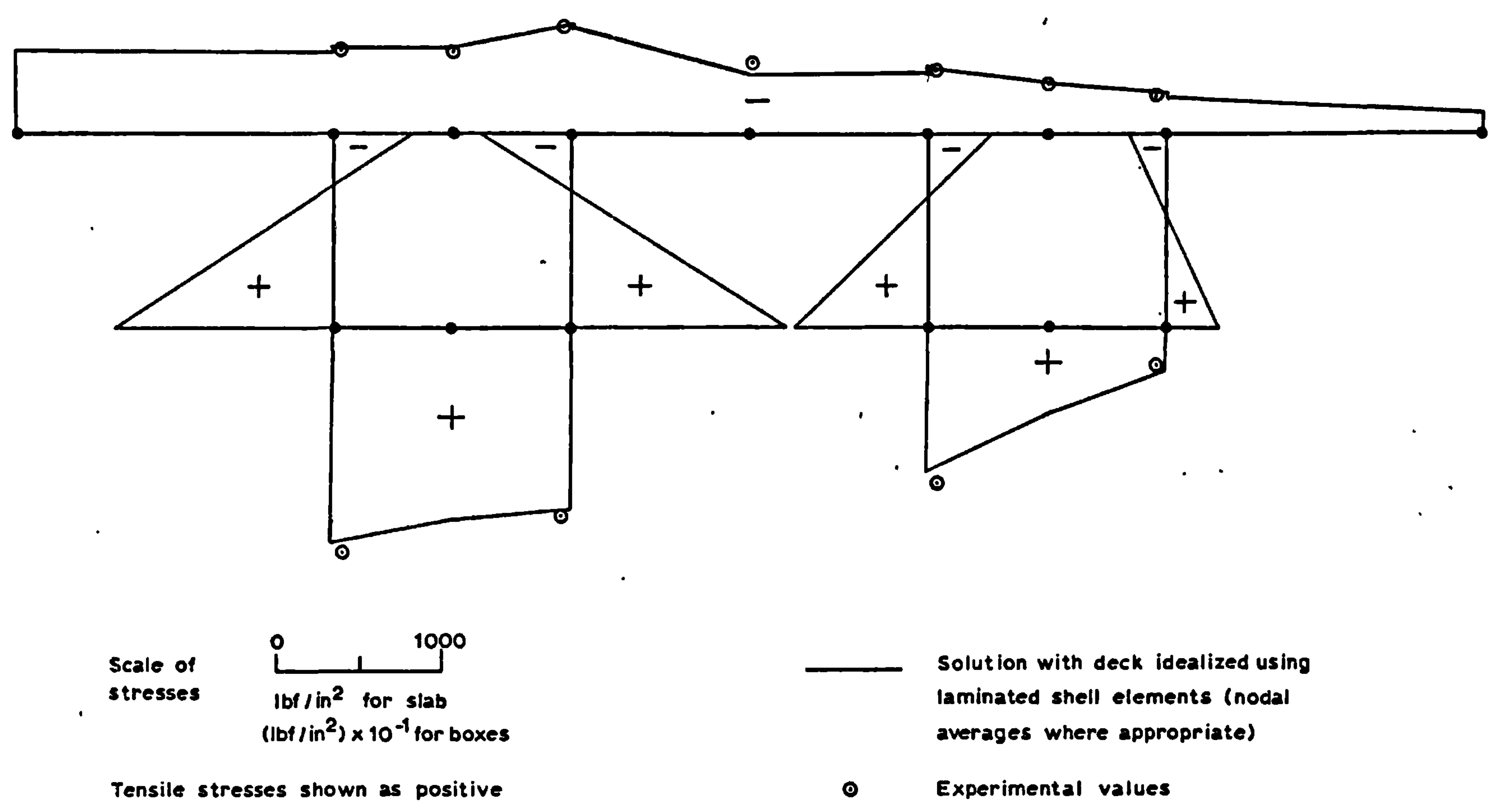

Fig. 4.7. Skewed composite twin cell box girder bridge model. Distribution of longitudinal outer surface stresses at centre cross-section for model under Type HB loading

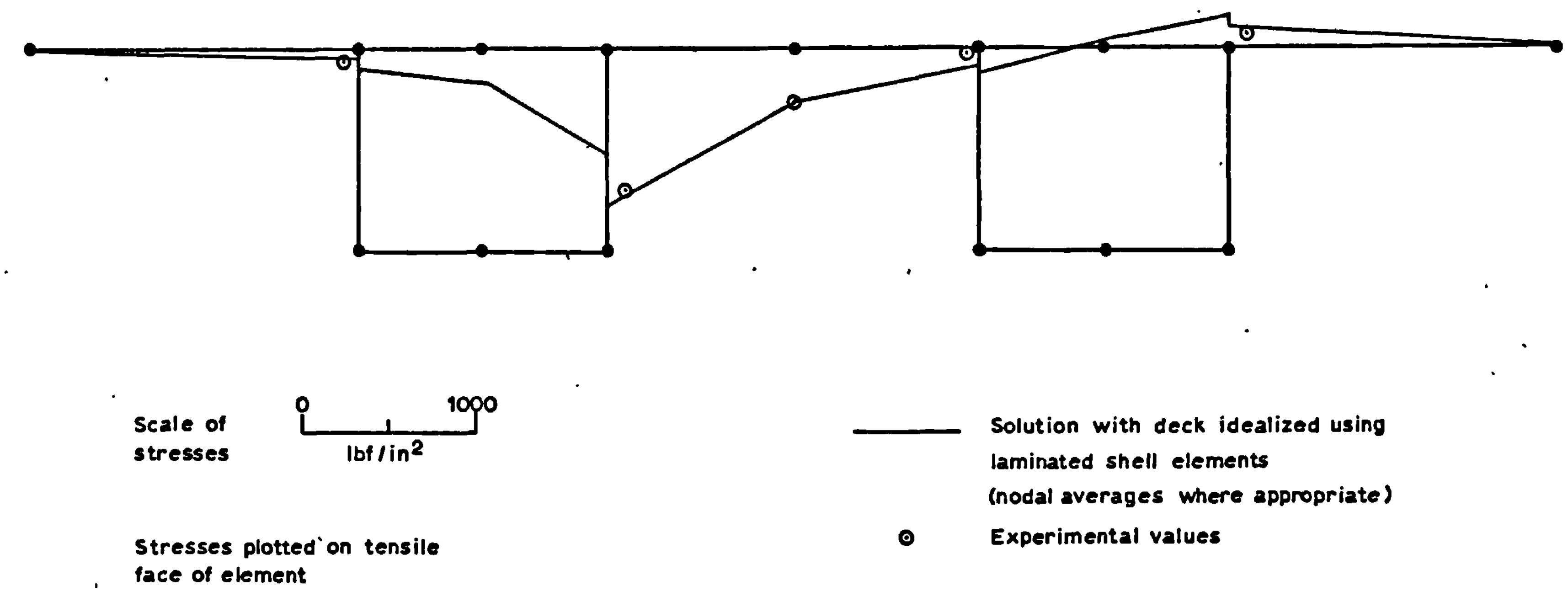

Fig. 4.8. Skewed composite twin cell box girder bridge model. Distribution of transverse flexural stresses in slab at centre cross-section for model under Type HB loading

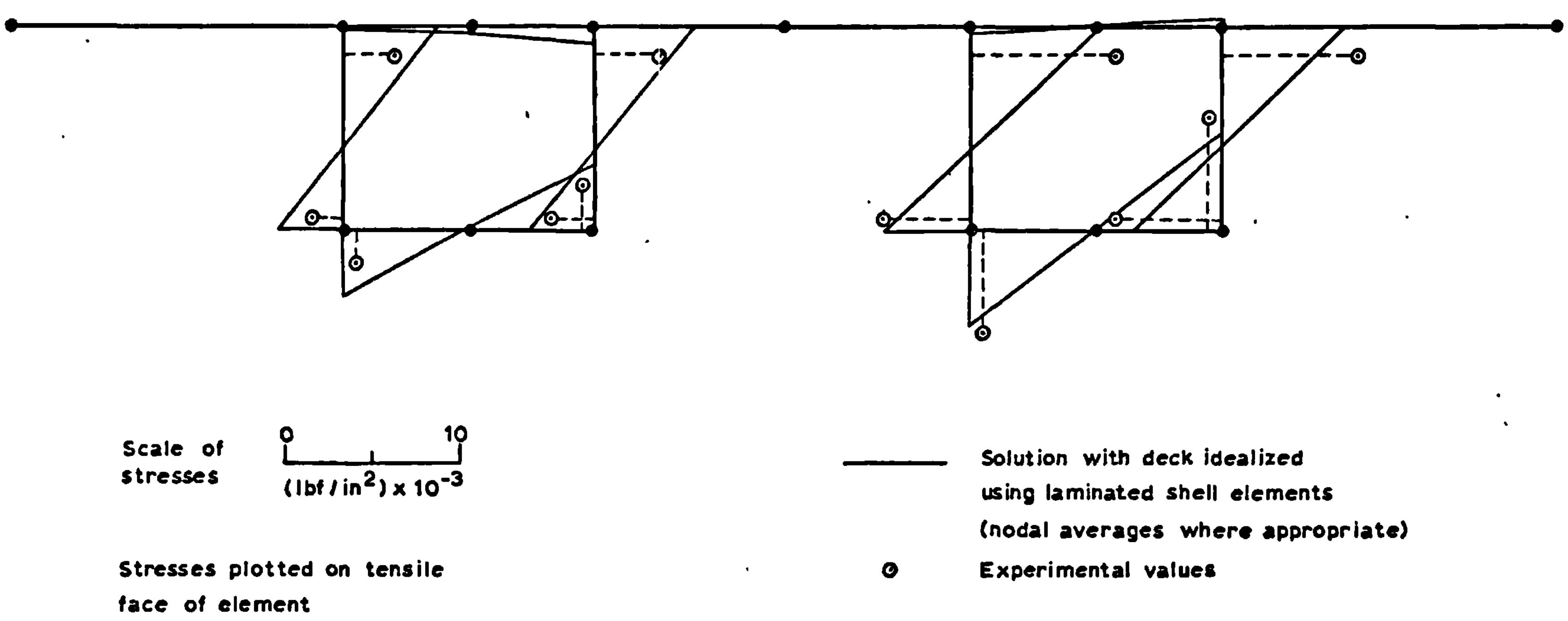

Fig. 4.9. Skewed composite twin cell box girder bridge model. Distribution of transverse flexural stresses in steel boxes at centre cross-section for model under Type HB loading

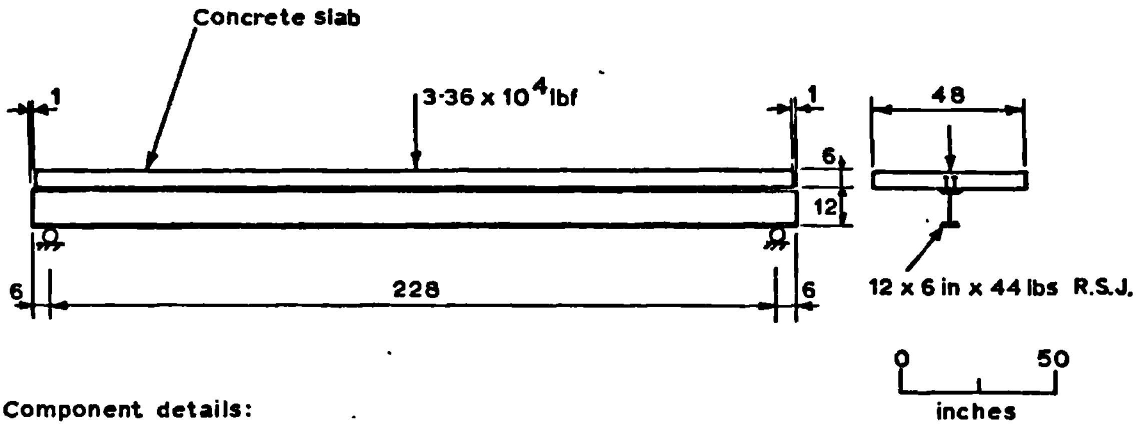

Component details:

Concrete slab	$E = 3{\cdot}3 \times 10^6$ lbf / in^2 $\nu = 0{\cdot}2$
Steel beam	$E = 30{\cdot}0 \times 10^6$ lbf/ in^2 Area = $13{\cdot}0$ in^2 $I = 316{\cdot}76$ in^4
Shear connectors	$4 \times \frac{3}{4}$ in headed studs in pairs at $14\frac{7}{8}$ in centres

Note:
The bond between the concrete and steel was broken by applying a load to the beam before testing.

Fig. 4.10. Straight composite beam model.
Details of model and loading

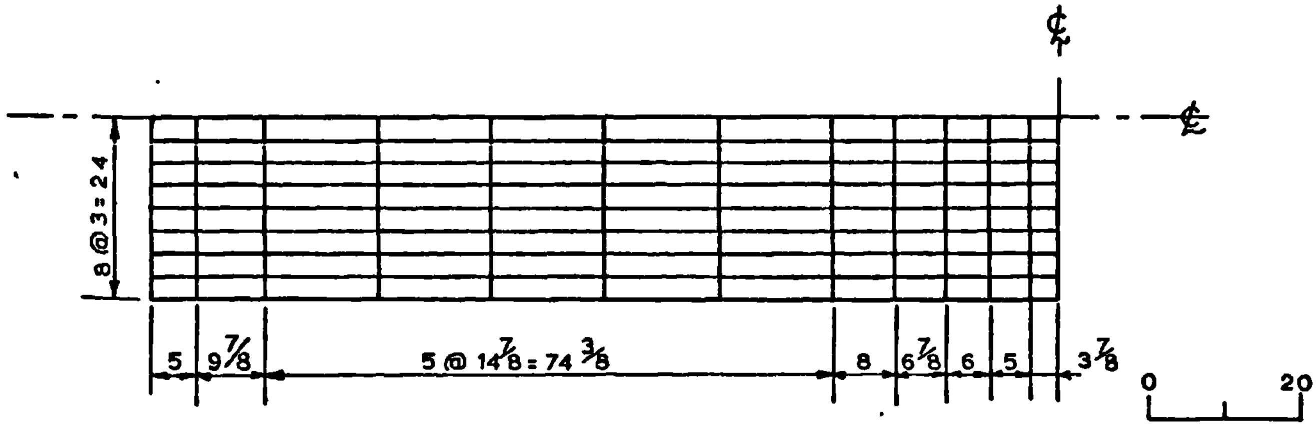

(a) Subdivision of slab into elements

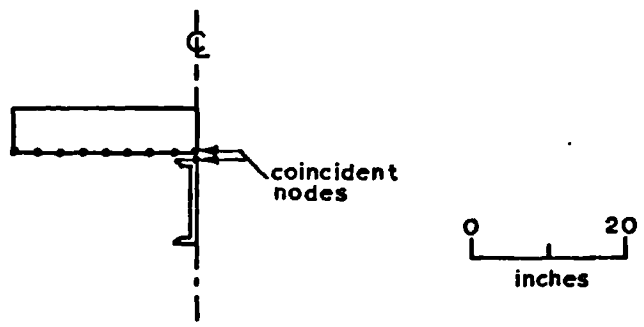

(b) Position of nodes in cross-section

Fig. 4.11. Straight composite beam model.
Finite element idealization

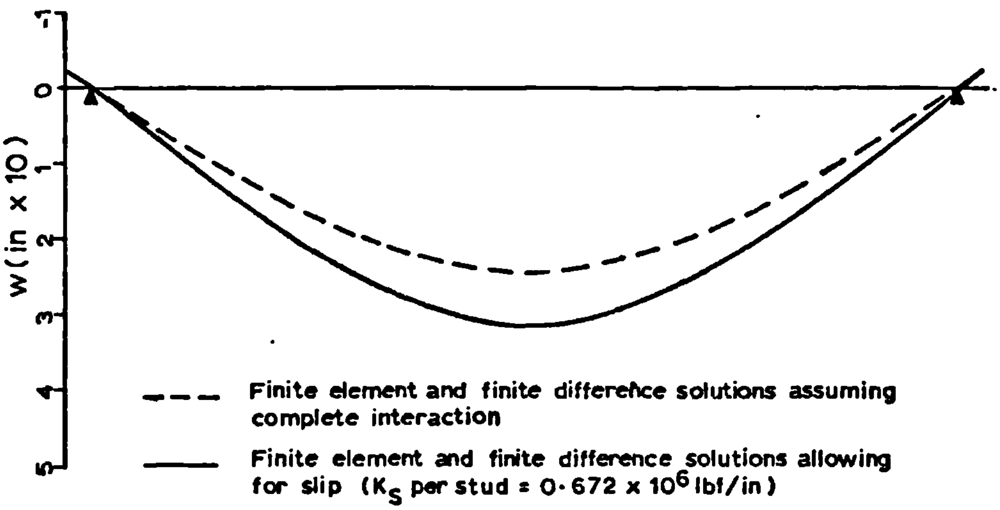

Fig. 4.12. Straight composite beam model. Central longitudinal deflexion profile for model under central point load

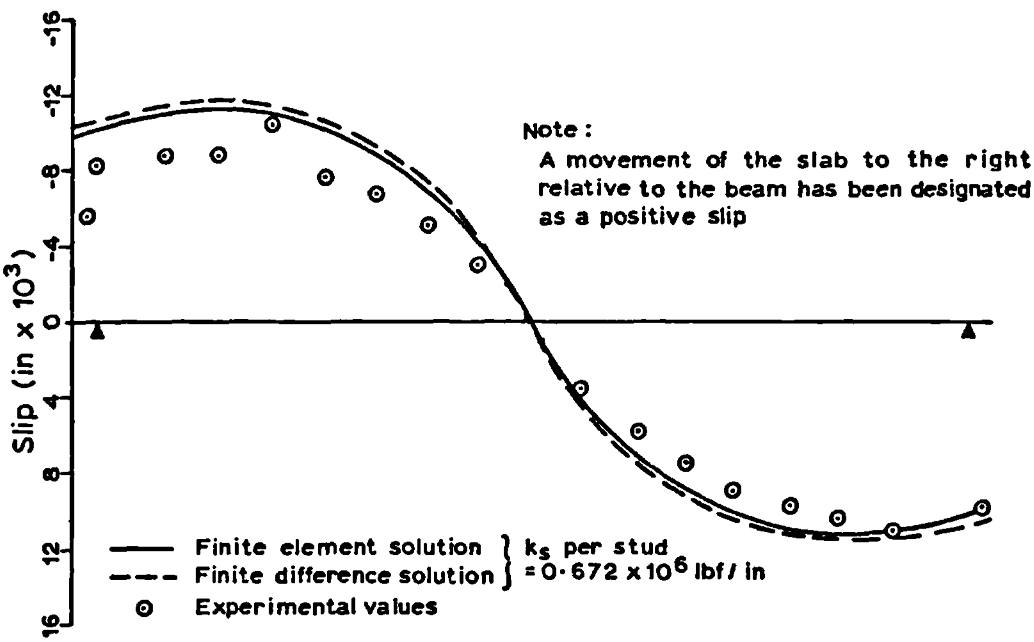

Fig. 4.13. Straight composite beam model. Longitudinal slip profile for model under central point load

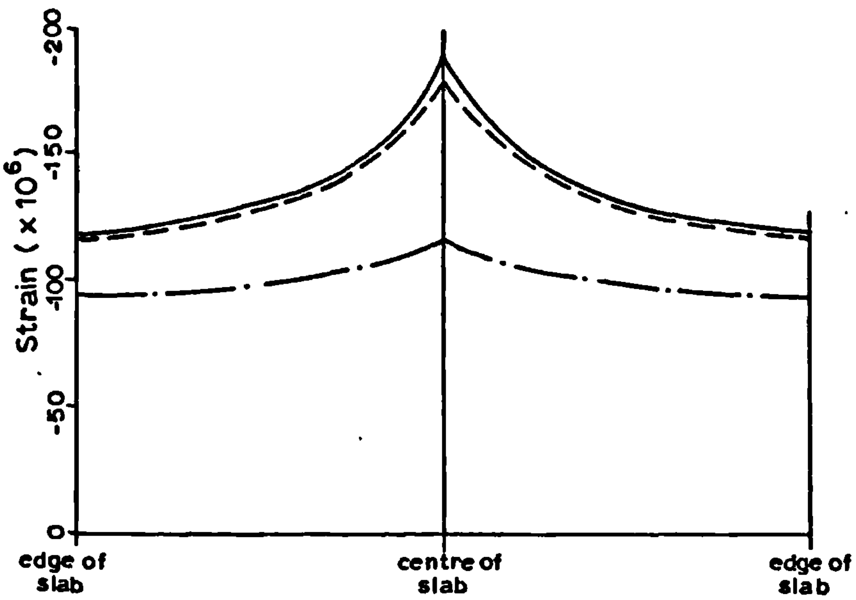

(a) Distribution of longitudinal strains across mid-plane of slab

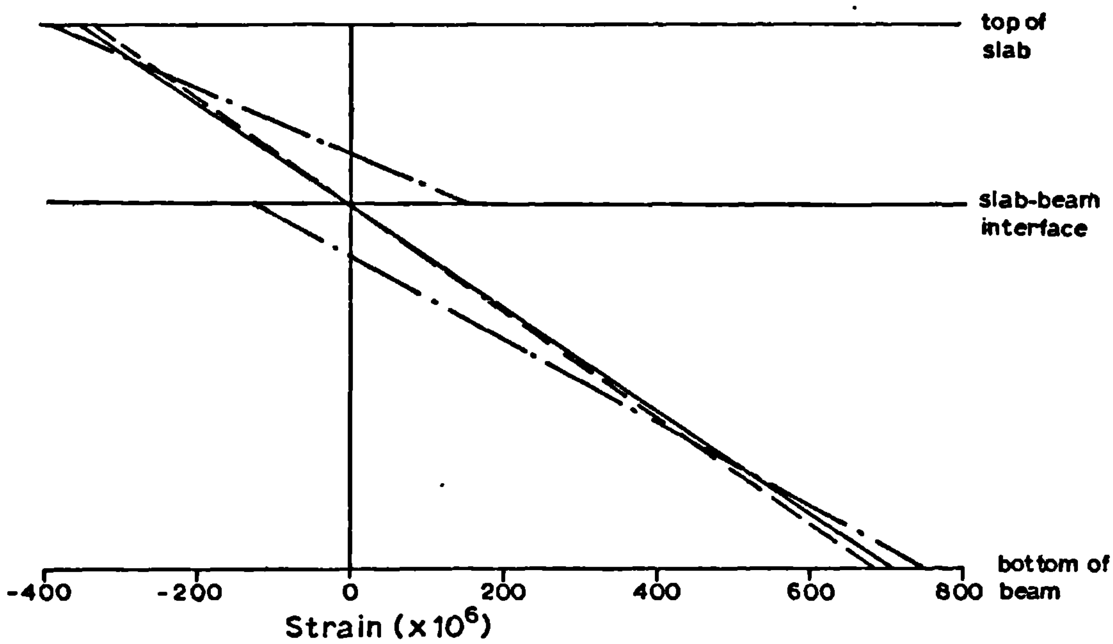

(b) Distribution of longitudinal strains down centre plane of slab and beam

——— Finite element solution } assuming complete interaction
— — — Finite difference solution }

—·— Finite element and finite difference solutions allowing for slip (K_s per stud = 0·672 x 10^6 lbf/in)

Fig. 4.14. Straight composite beam model.
Distribution of strains at centre cross-section for model under central point load

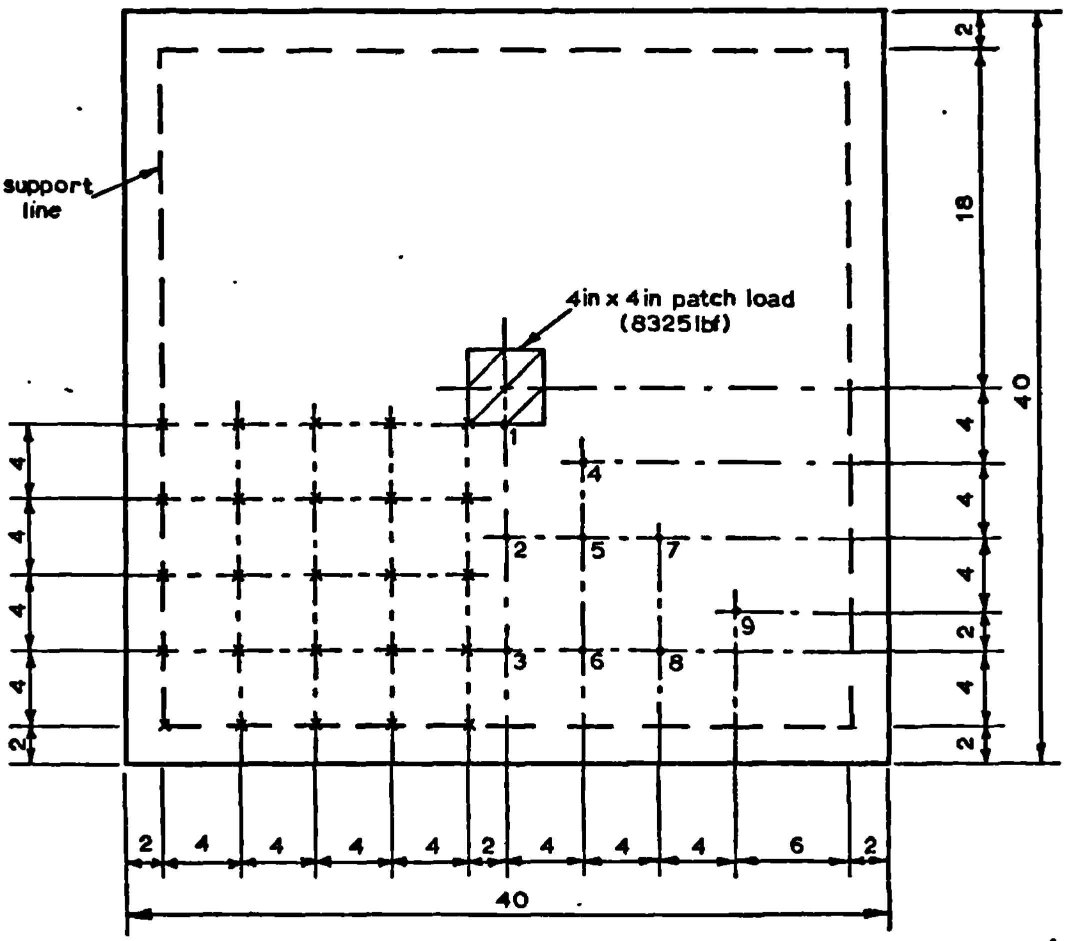

0 10
inches

• slip gauges

x shear connectors (all quadrants have identical arrangement)

Component details:

concrete slab	$E = 5{\cdot}8 \times 10^6 \, lbf/in^2$	$V = 0{\cdot}15$	$t = 2{\cdot}0$ in
steel plate	$E = 30{\cdot}4 \times 10^6 \, lbf/in^2$	$V = 0{\cdot}30$	$t = 0{\cdot}183$ in
shear connectors	$1\frac{3}{8} \times \frac{1}{4}$ in headed studs		

Note: The bond between the concrete slab and steel plate was broken by applying a load before testing.

Fig .4.15. Square composite plate model. Details of model and loading

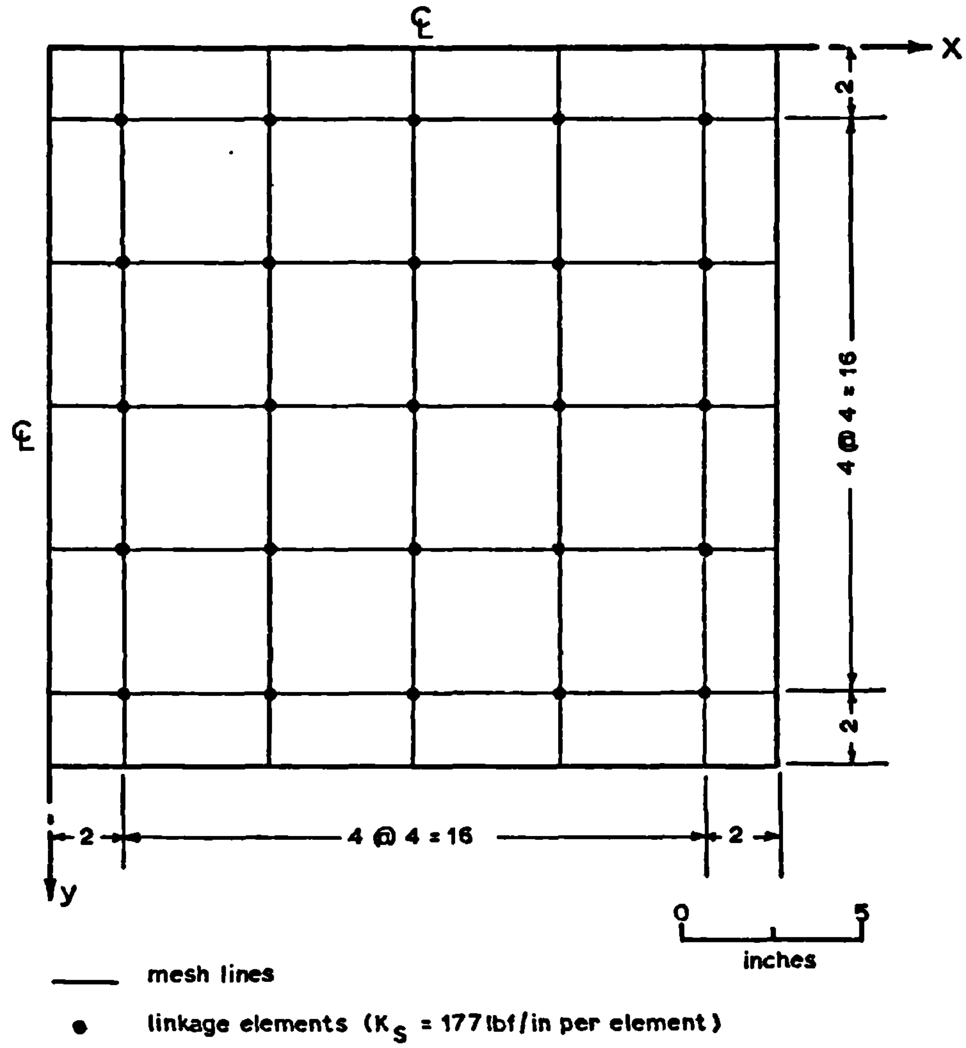

Fig. 4.16. Square composite plate model.
Finite element idealization

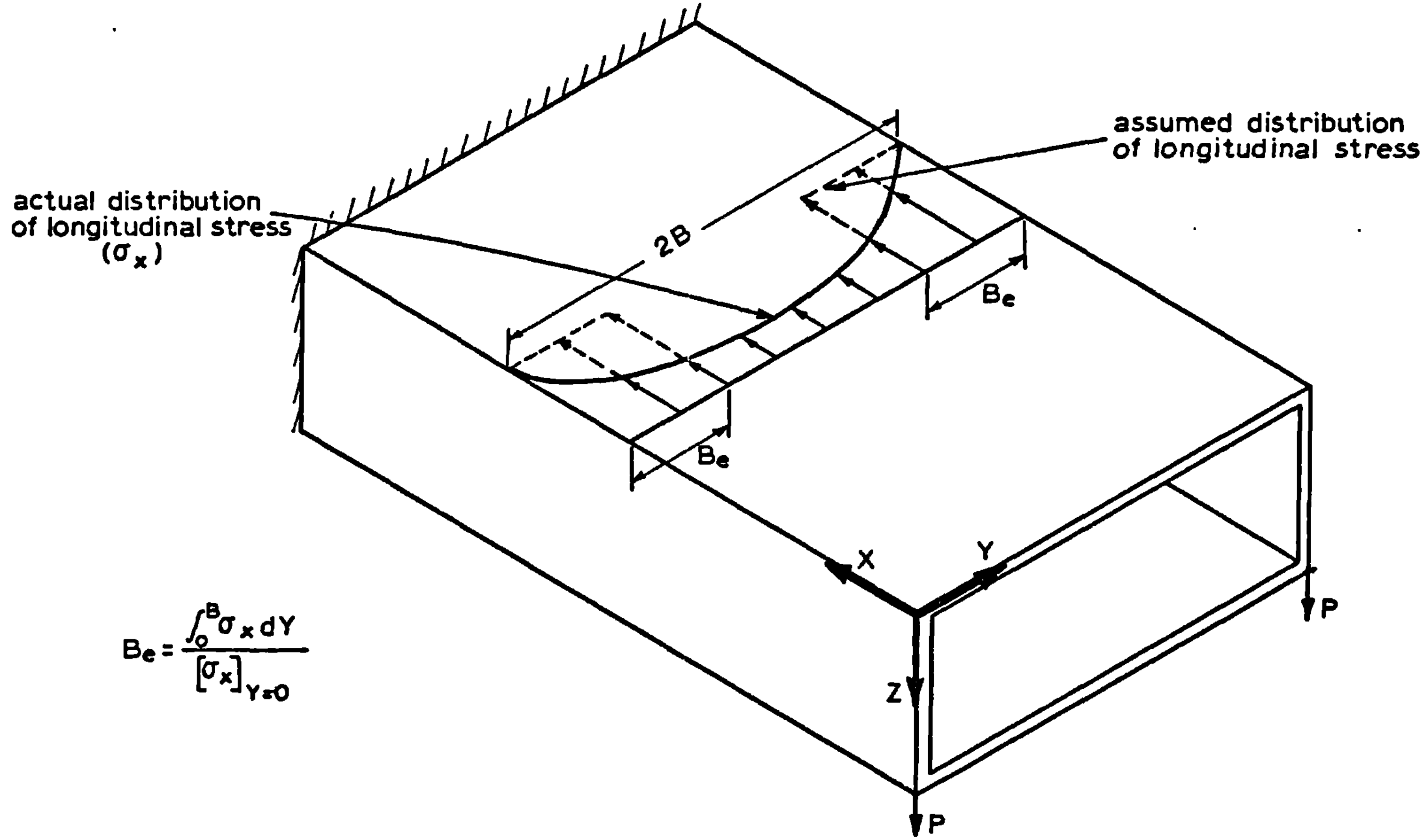

$$B_e = \frac{\int_0^B \sigma_x \, dY}{[\sigma_x]_{Y=0}}$$

Fig. 5.1. Notation relating to concept of stress effective breadth

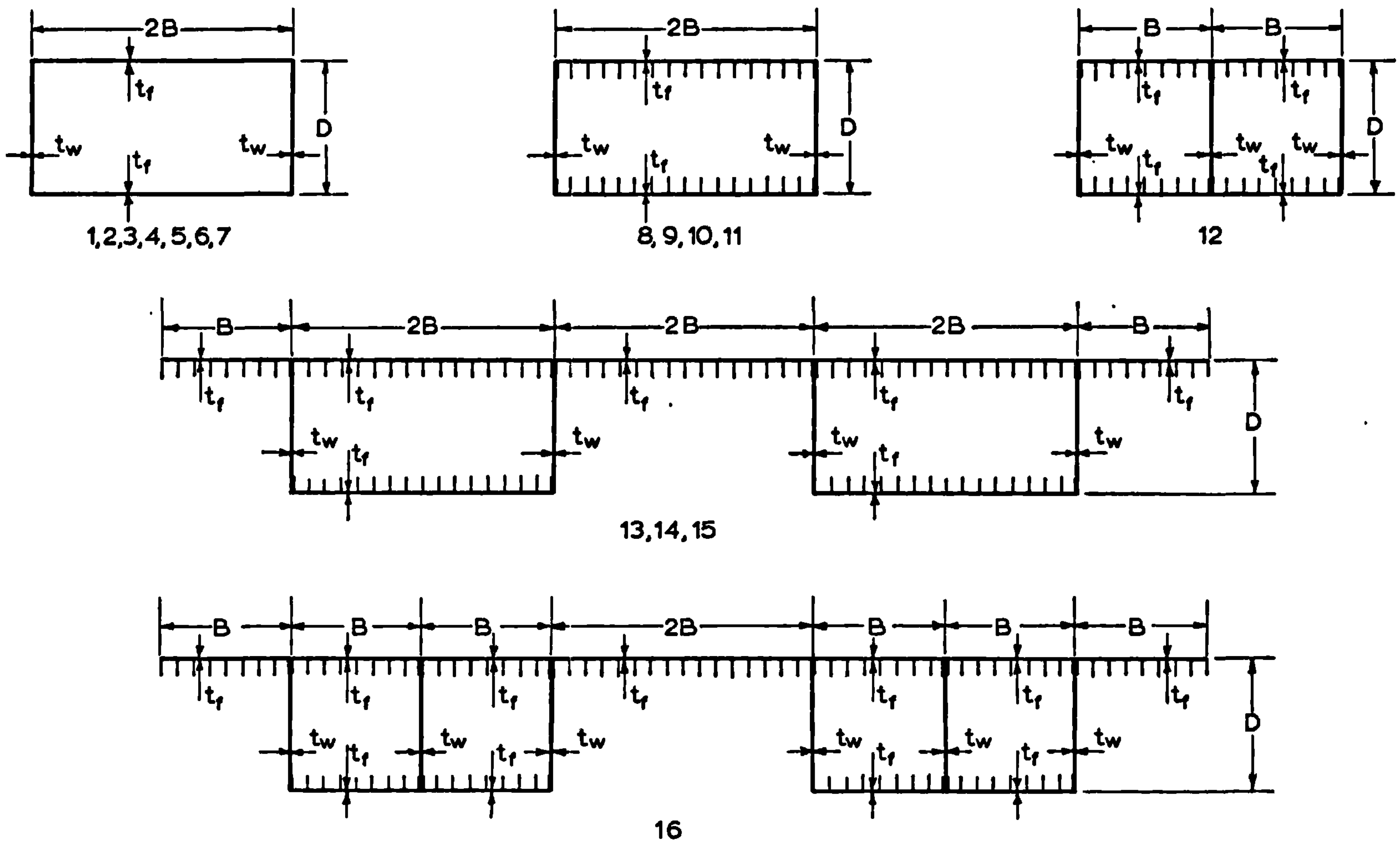

Fig. 5.2. Cross-sections of bridges used in shear lag parametric study. Dimensions are given in Table 5.1

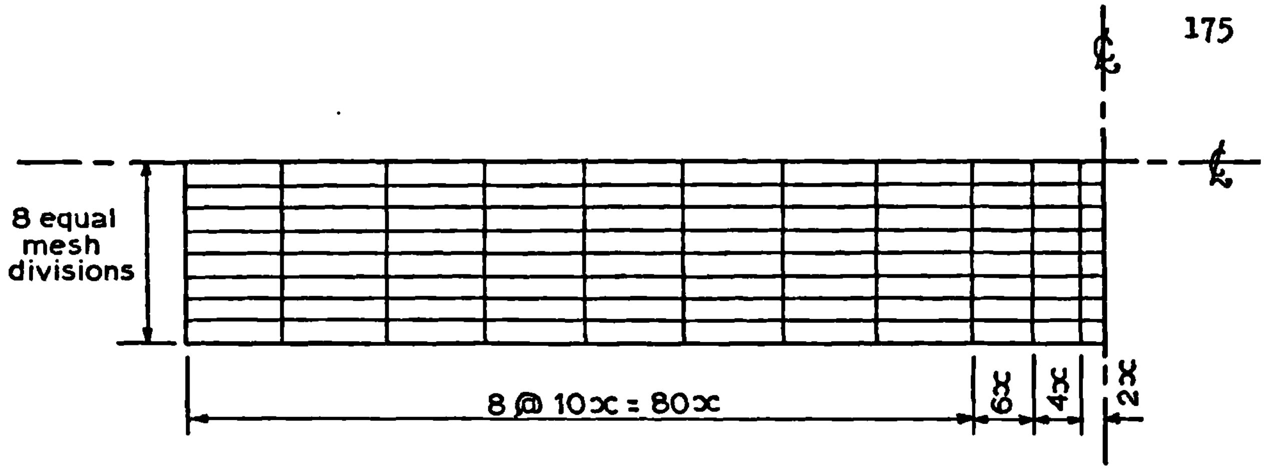

Fig. 5.3. Idealization of flange of simply supported single cell box girder showing mesh grading in region of mid-span

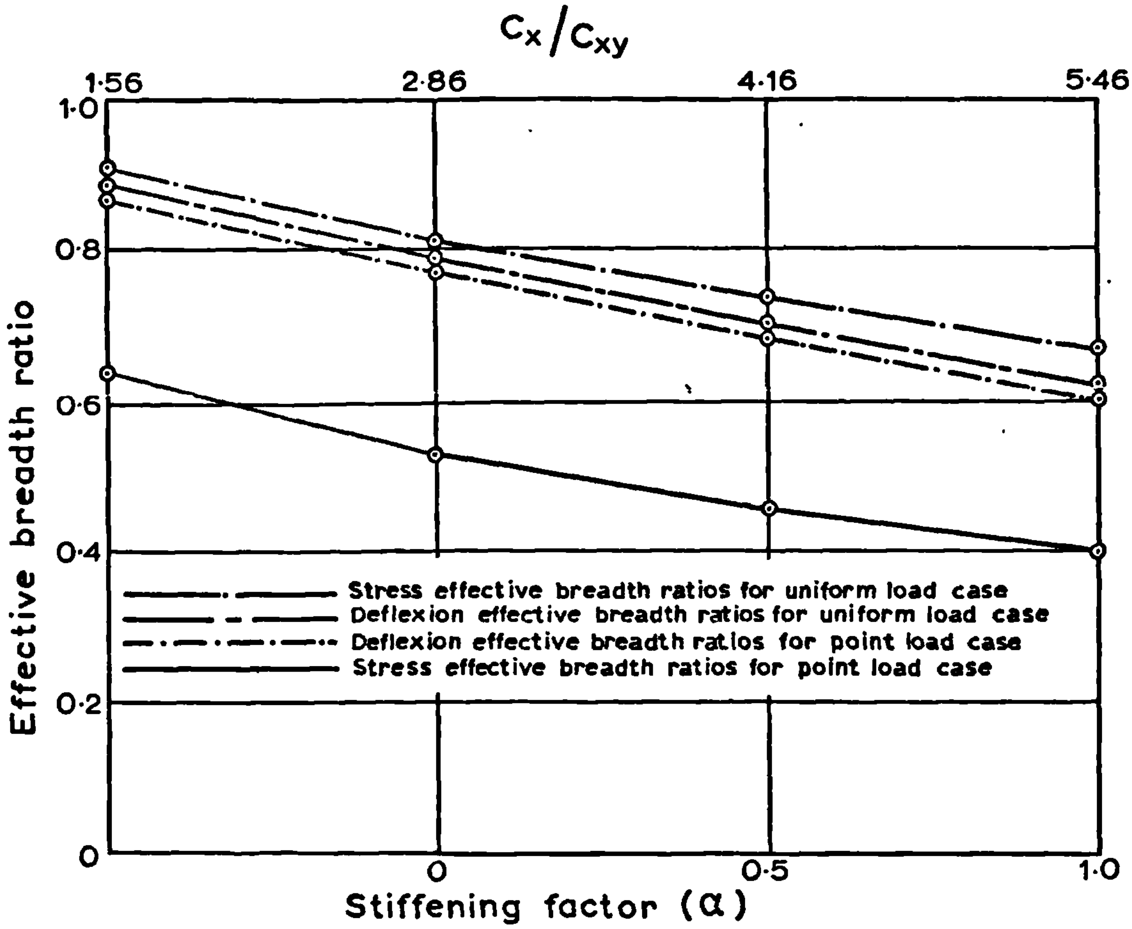

Fig. 5.4. Variation of effective breadth ratios at mid-span with stiffening factor for simply supported box girders (B / L = 0·2, cross-sections 1, 8 and 11)

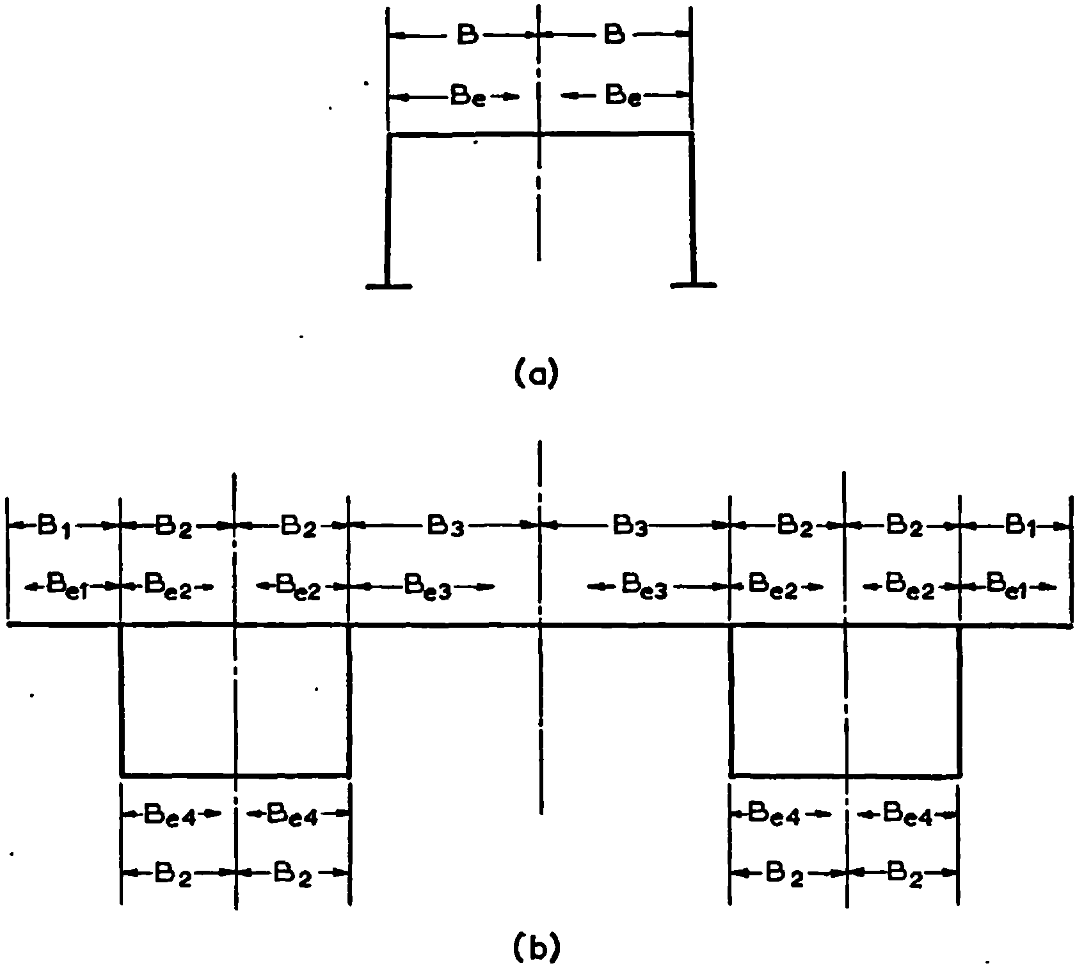

Fig. 5.5. Bridge cross-sections showing breadth of flange associated with each web for purpose of estimating effective breadths

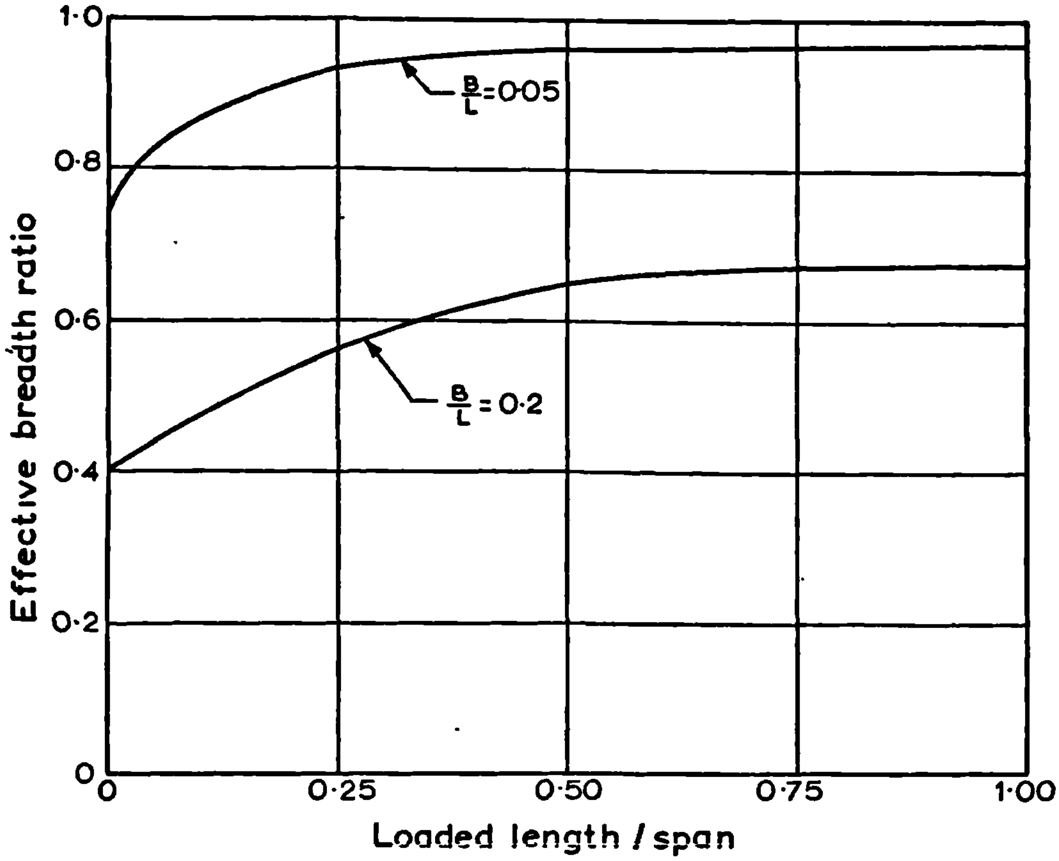

Fig. 5.6. Variation of stress effective breadth ratios at mid-span with length of uniform load over each web for simply supported box girders (cross-section 8)

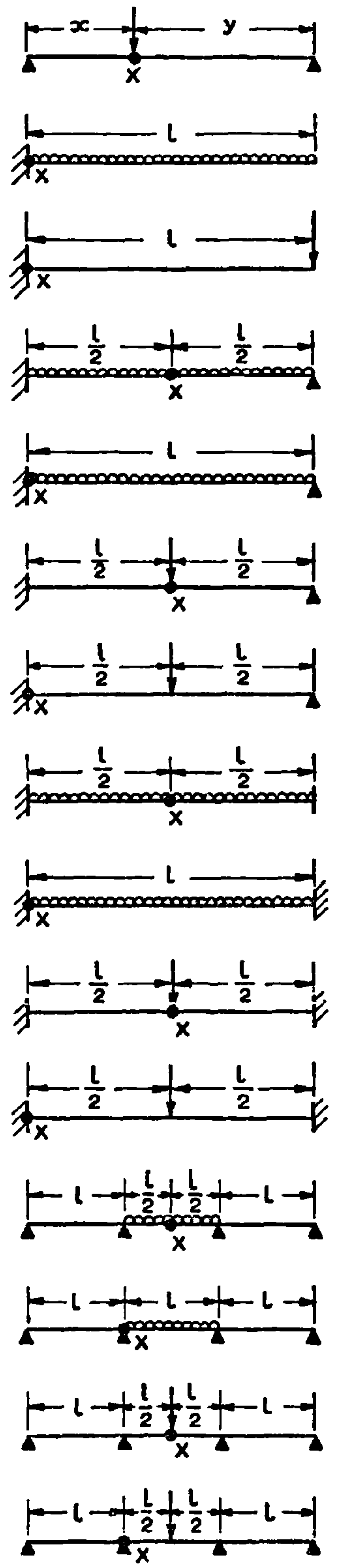

1. $\psi_x = \frac{1}{3}\left(2\psi^{P*}_{2x\dagger} + \psi^{P}_{2y}\right)$

2. $\psi_x = \dfrac{1}{\left(\dfrac{2}{\psi^{P}_{2L}} - \dfrac{1}{\psi^{U}_{2L}}\right)}$

3. $\psi_x = \psi^{P}_{2L}$

4. $\psi_x = \psi^{U}_{0.75L}$

5. $\psi_x = \dfrac{1}{\left(\dfrac{1{\cdot}25}{\psi^{P}_{0{\cdot}5L}} - \dfrac{0{\cdot}25}{\psi^{U}_{0{\cdot}5L}}\right)}$

6. $\psi_x = \frac{1}{3}\left(2\psi^{P}_{0{\cdot}45L} + \psi^{P}_{L}\right)$

7. $\psi_x = \psi^{P}_{0{\cdot}55L}$

8. $\psi_x = \psi^{U}_{0{\cdot}58L}$

9. $\psi_x = \dfrac{1}{\left(\dfrac{1{\cdot}268}{\psi^{P}_{0{\cdot}423L}} - \dfrac{0{\cdot}268}{\psi^{U}_{0{\cdot}423L}}\right)}$

10. $\psi_x - \psi^{P}_{0{\cdot}5L}$

11. $\psi_x = \psi^{P}_{0{\cdot}5L}$

12. $\psi_x = \psi^{U}_{0{\cdot}774L}$

13. $\psi_x = \frac{1}{3}\left(2\psi^{P}_{0{\cdot}226L} + \psi^{P}_{2L}\right)$

14. $\psi_x = \psi^{P}_{0{\cdot}7L}$

15. $\psi_x = \frac{1}{3}\left(2\psi^{P}_{0{\cdot}3L} + \psi^{P}_{2L}\right)$

* Indicates applicable load condition in Table 5.7.
P for point load condition U for uniform load condition

† Indicates value of equivalent simply supported length (L) to be used when referring to Table 5.7.

Fig. 5.7 Formulae for estimating stress effective breadth ratios (ψ) using mid-span values of Table 5.7

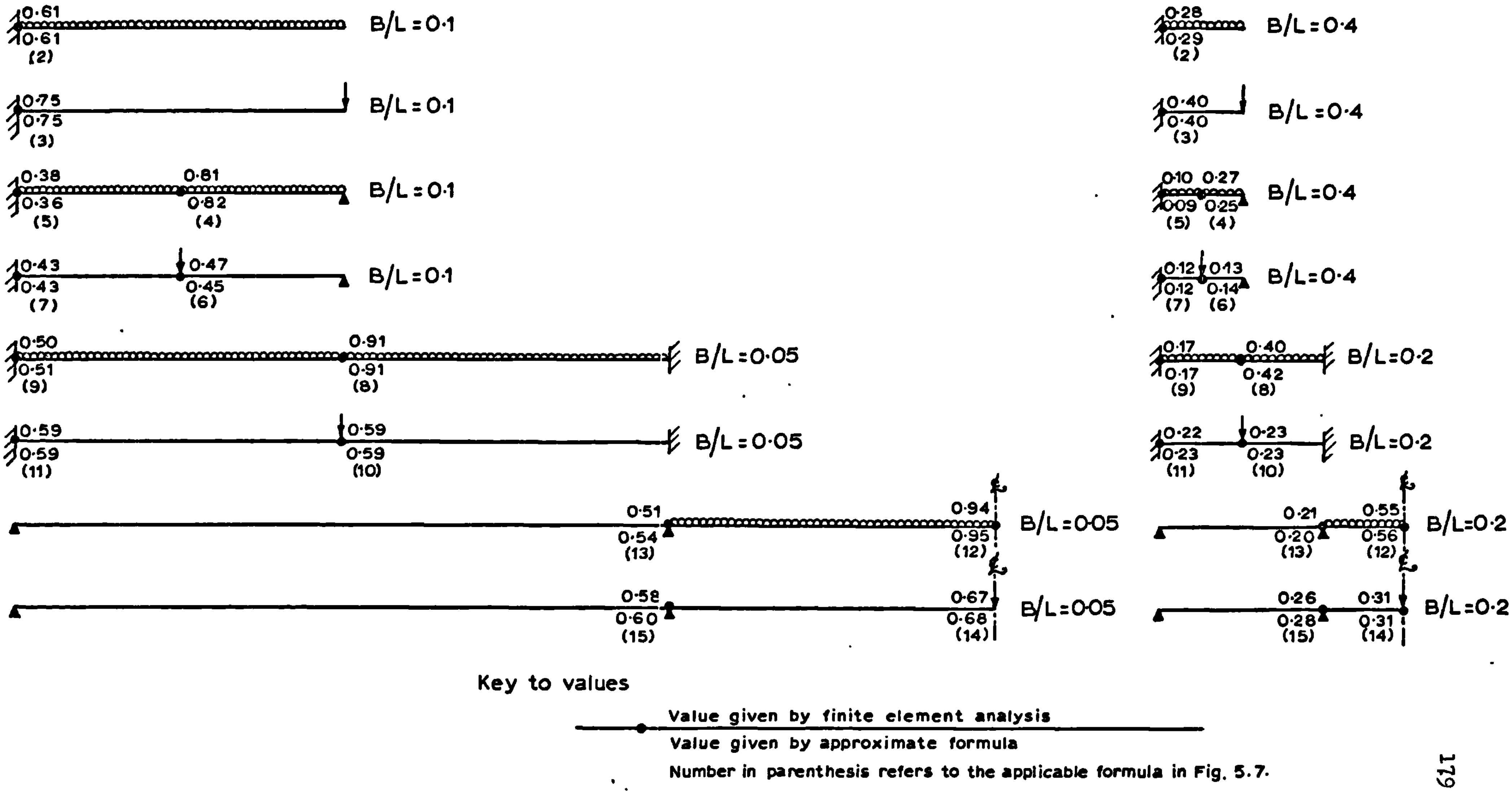

Fig. 5.8. Comparison of stress effective breadth ratios for box girders (cross-section 8) obtained using finite element and approximate methods

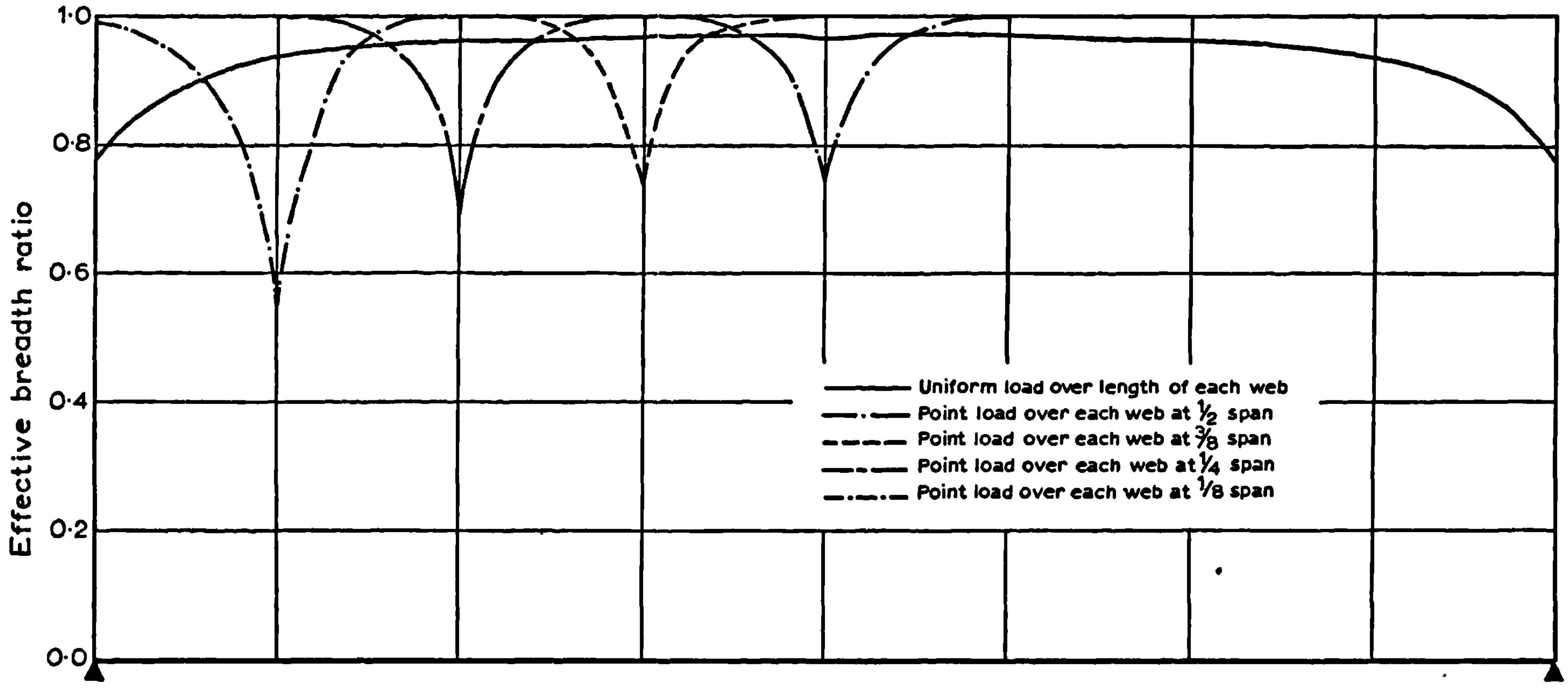

Fig. 5.9. Variation of stress effective breadth ratios along span of simply supported box girder (B/L = 0·05, cross-section 8) for uniform load and point loads at various positions

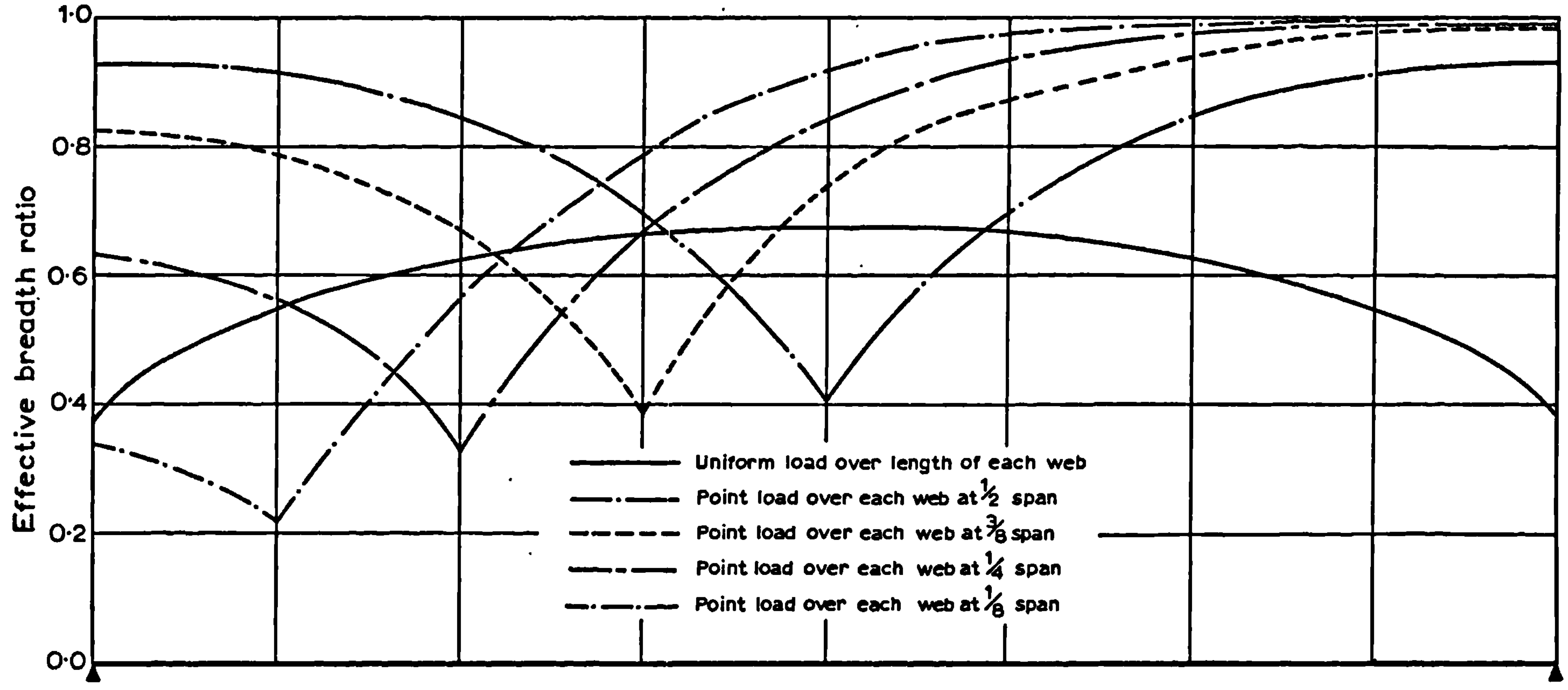

Fig. 5.10. Variation of stress effective breadth ratios along span of simply supported box girder (B/L = 0·20, cross-section 8) for uniform load and point loads at various positions

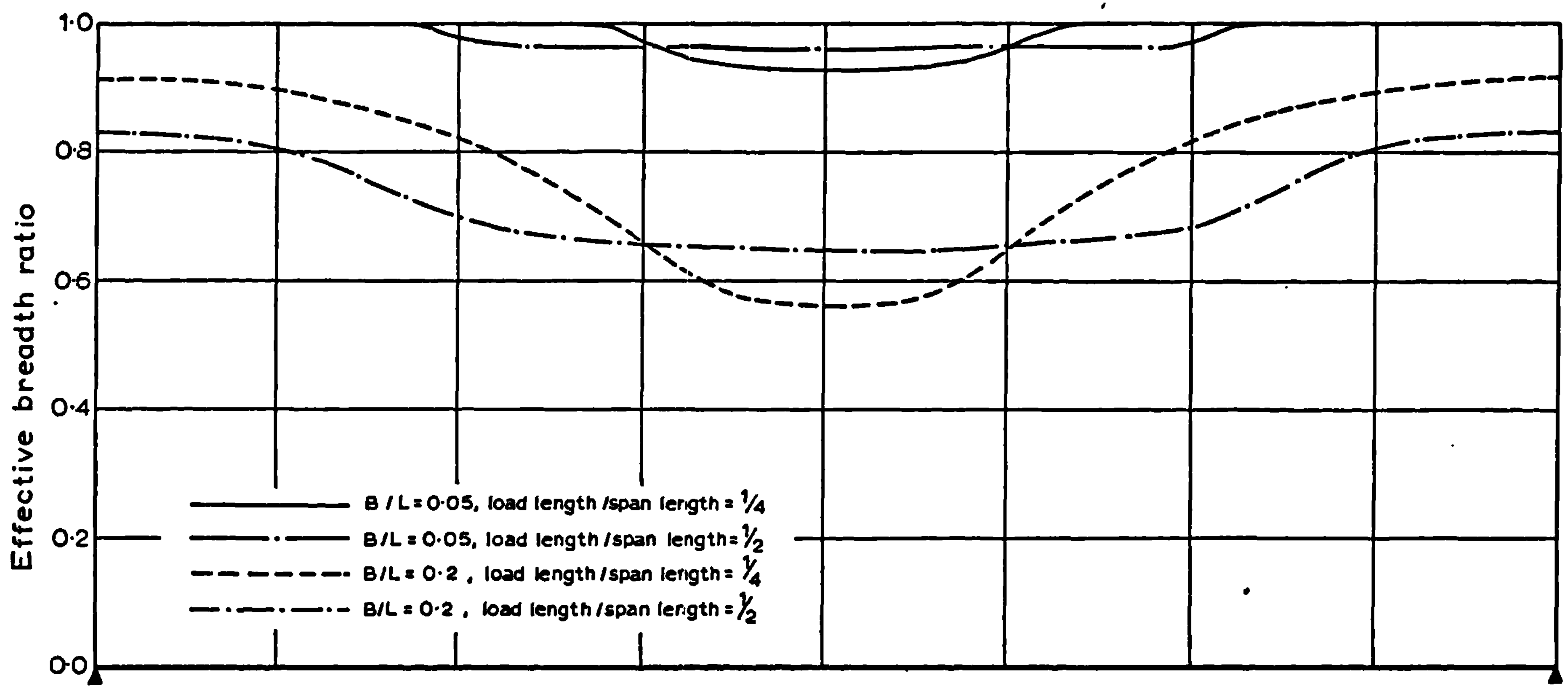

Fig. 5.11. Variation of stress effective breadth ratios along span of simply supported box girders (cross-section 8) for various lengths of uniform load positioned centrally about mid-span

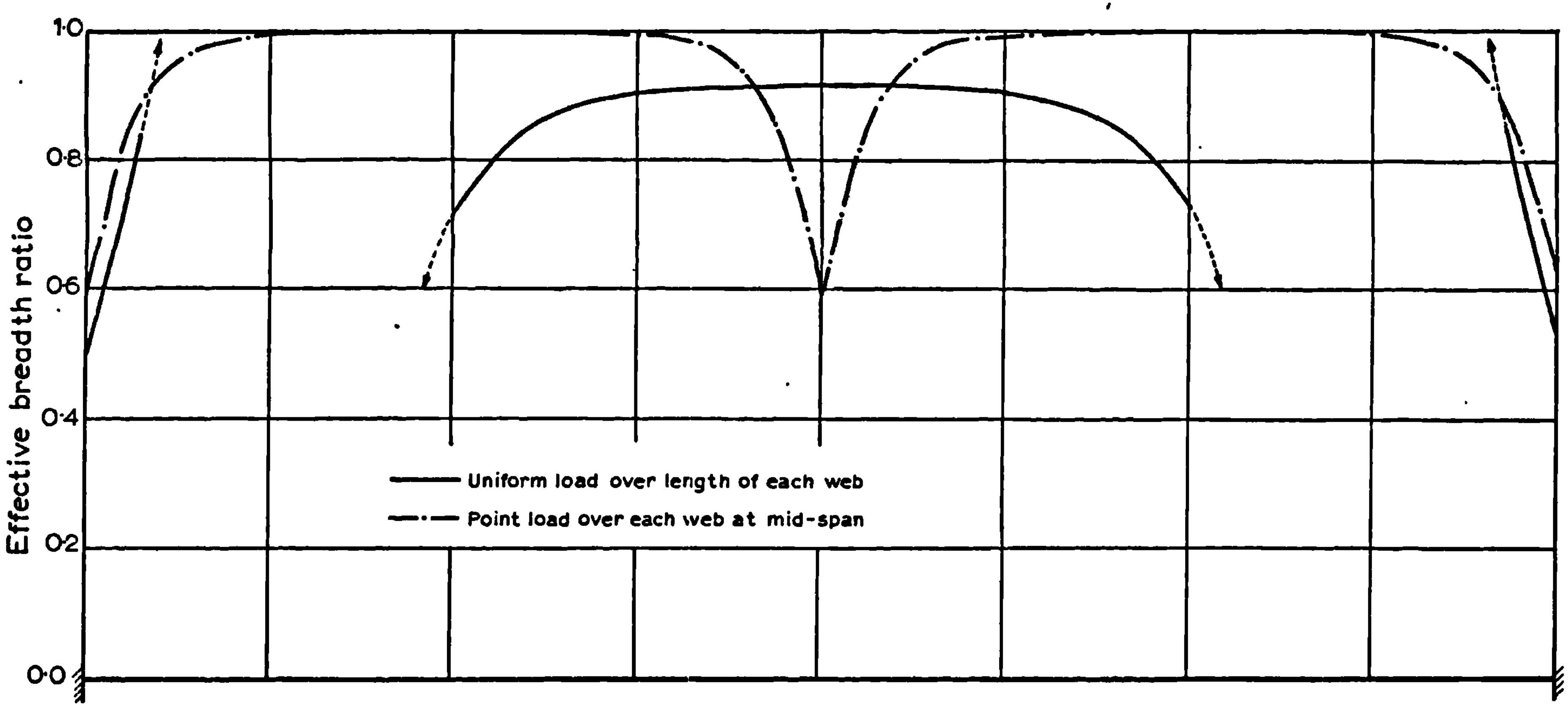

Fig. 5.12. Variation of stress effective breadth ratios along span of fixed ended box girder (B/L = 0·05, cross-section 8) for uniform load and point loads at mid-span

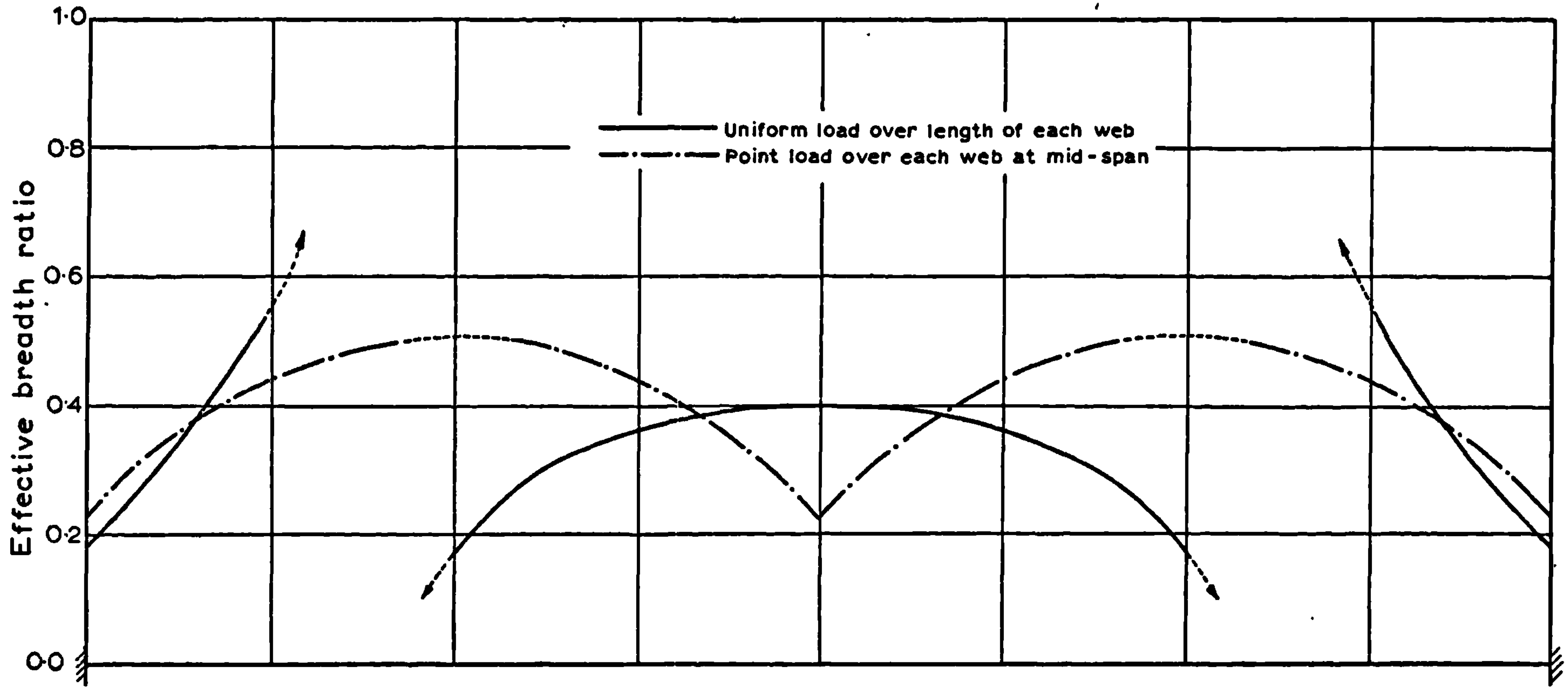

Fig. 5.13. Variation of stress effective breadth ratios along span of fixed ended box girder (B/L = 0·20, cross-section 8) for uniform load and point loads at mid-span

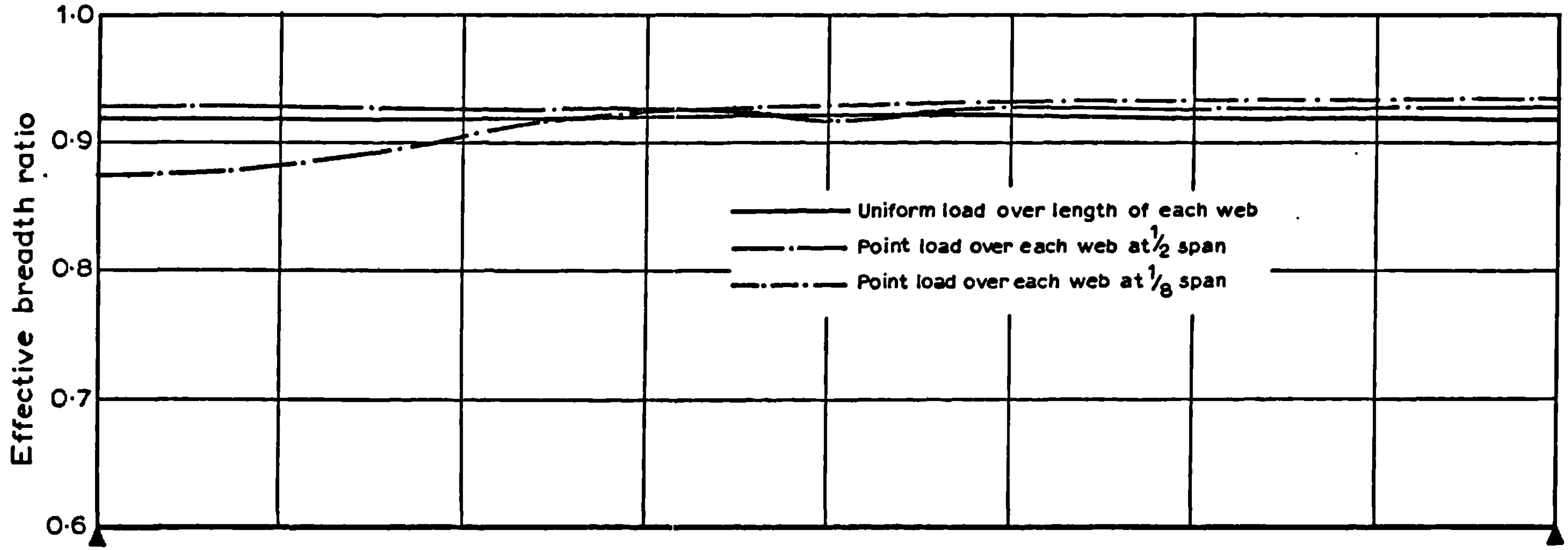

Fig. 5.14. Variation of deflexion effective breadth ratios along span of simply supported box girder (B / L = 0·05, cross-section 8) for uniform load and point loads at various positions

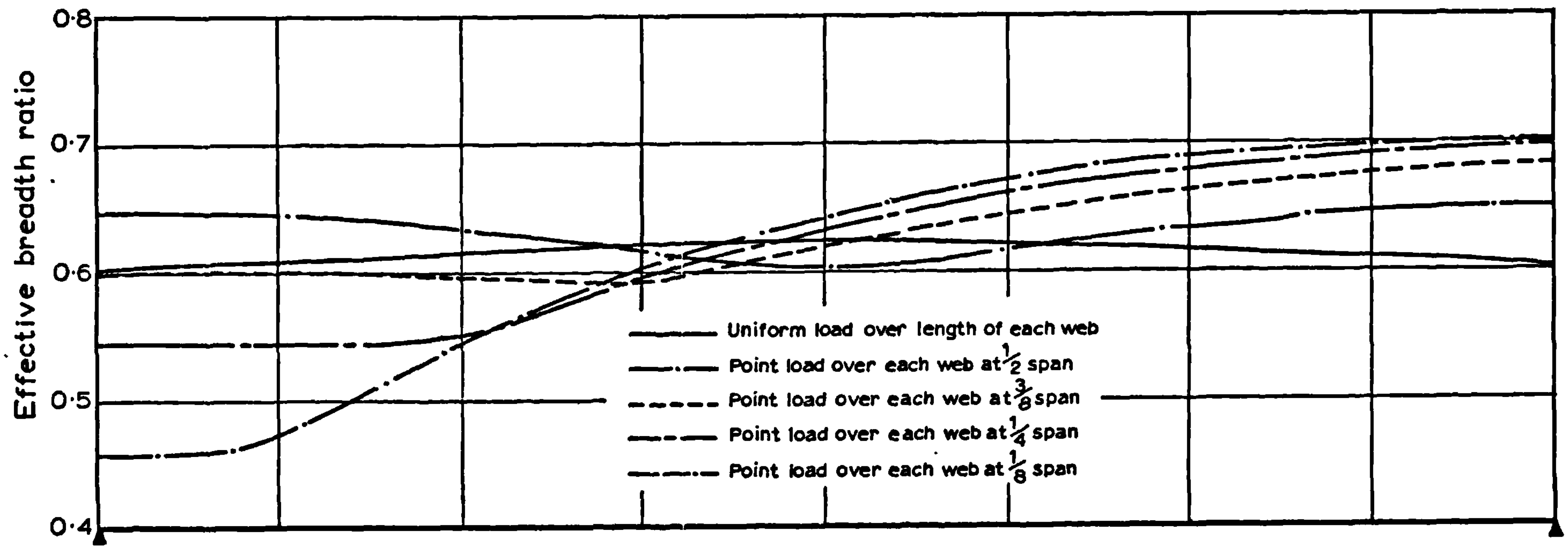

Fig. 5.15. Variation of deflexion effective breadth ratios along span of simply supported box girder (B/L = 0·20, cross-section 8) for uniform load and point loads at various positions

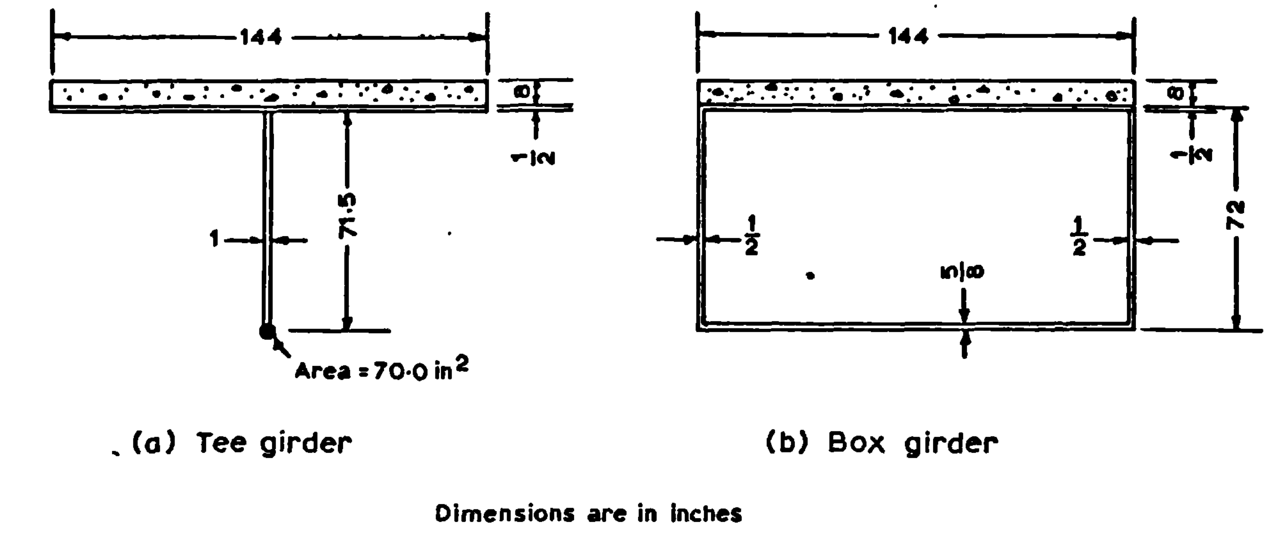

Fig. 6.1. Cross-sections of girders used in incomplete interaction parametric study

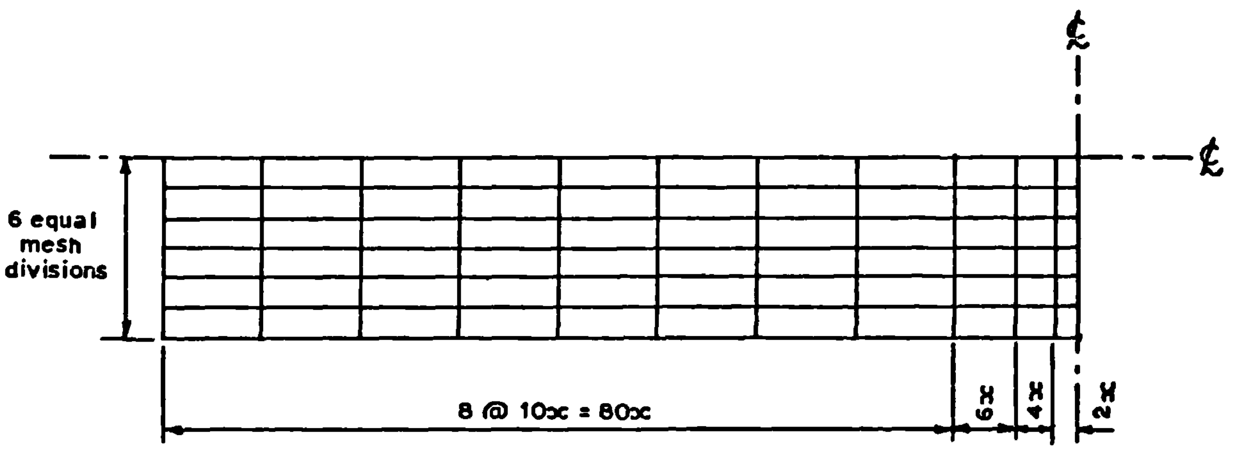

Fig. 6.2. Subdivision of composite girder flange into elements

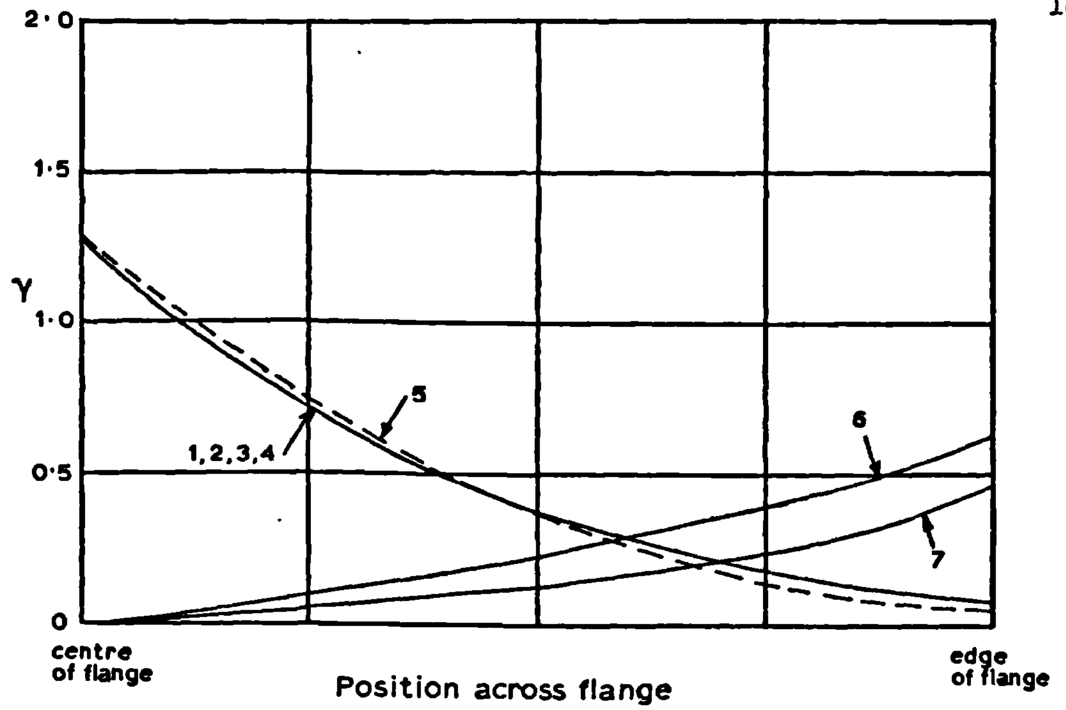

(a) B/L= 0·05

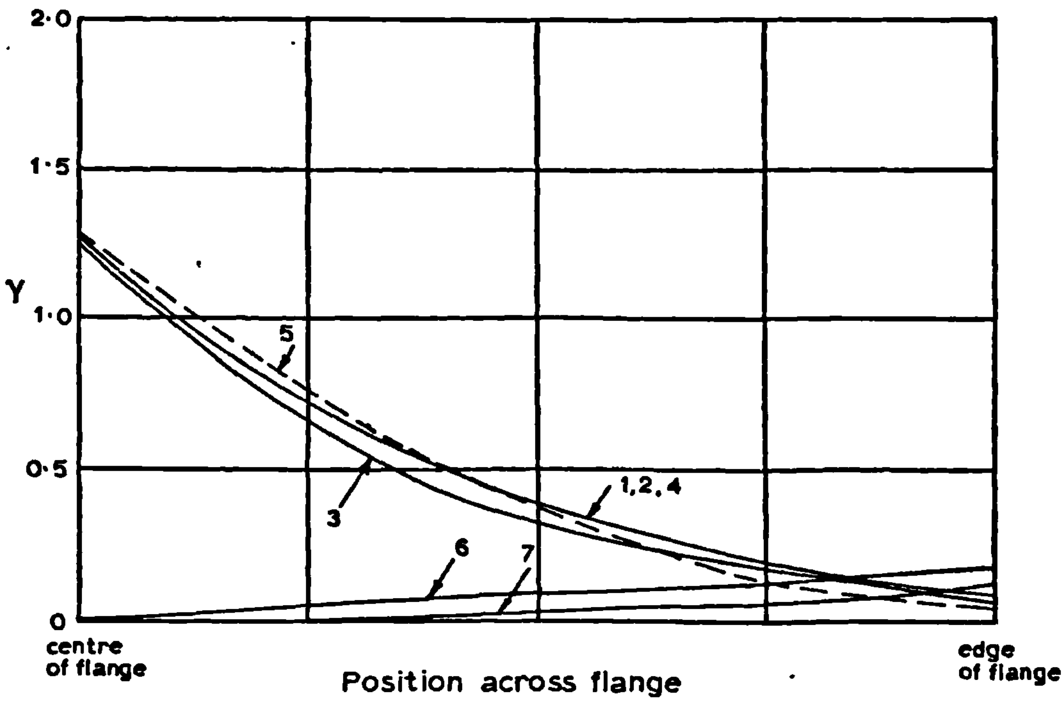

(b) B/L=0·20

Curve 1 : Longitudinal forces at quarter-span section for uniform load case
Curve 2 : Longitudinal forces at quarter-span section for point load case
Curve 3 : Longitudinal forces at support section for uniform load case
Curve 4 : Longitudinal forces at support section for point load case
Curve 5 : Proposed design curve for longitudinal forces
Curve 6 : Transverse forces at quarter-span section for uniform load case
Curve 7 : Transverse forces at quarter-span section for point load case

Fig. 6.3. Variation of shear connector forces with position across flange of simply supported tee girders having shear connexion I2

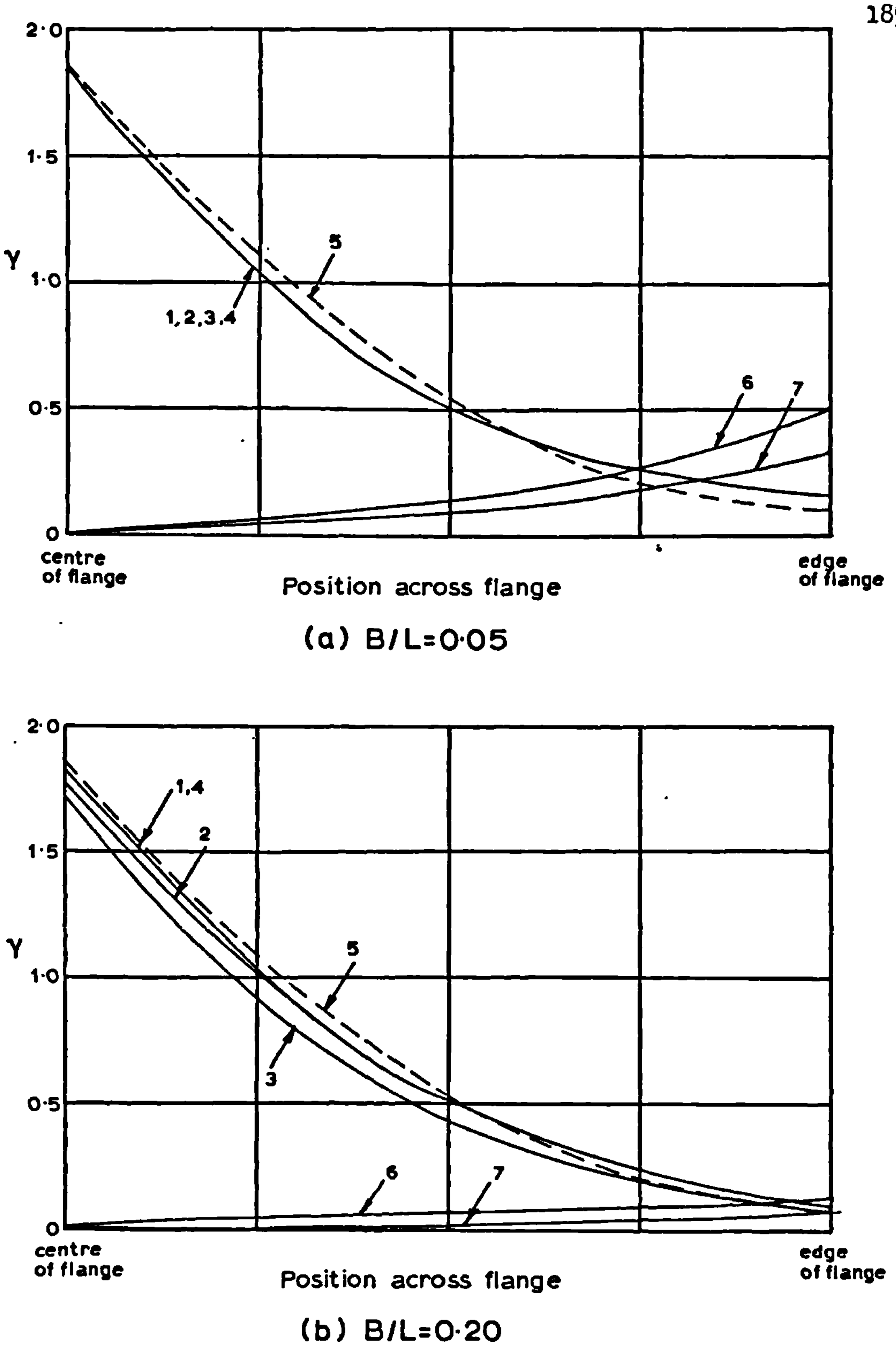

Curve 1 : Longitudinal forces at quarter-span section for uniform load case
Curve 2 : Longitudinal forces at quarter-span section for point load case
Curve 3 : Longitudinal forces at support section for uniform load case
Curve 4 : Longitudinal forces at support section for point load case
Curve 5 : Proposed design curve for longitudinal forces
Curve 6 : Transverse forces at quarter-span section for uniform load case
Curve 7 : Transverse forces at quarter-span section for point load case

Fig. 6.4. Variation of shear connector forces with position across flange of simply supported tee girders having shear connexion I 3

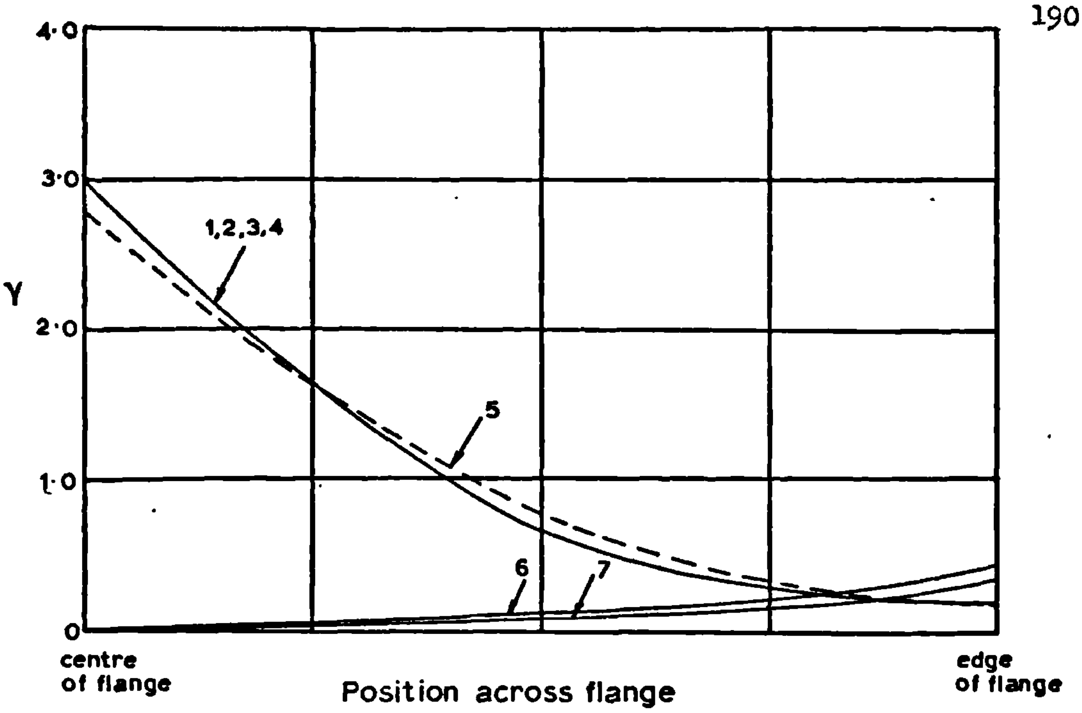

(a) B/L=0·05

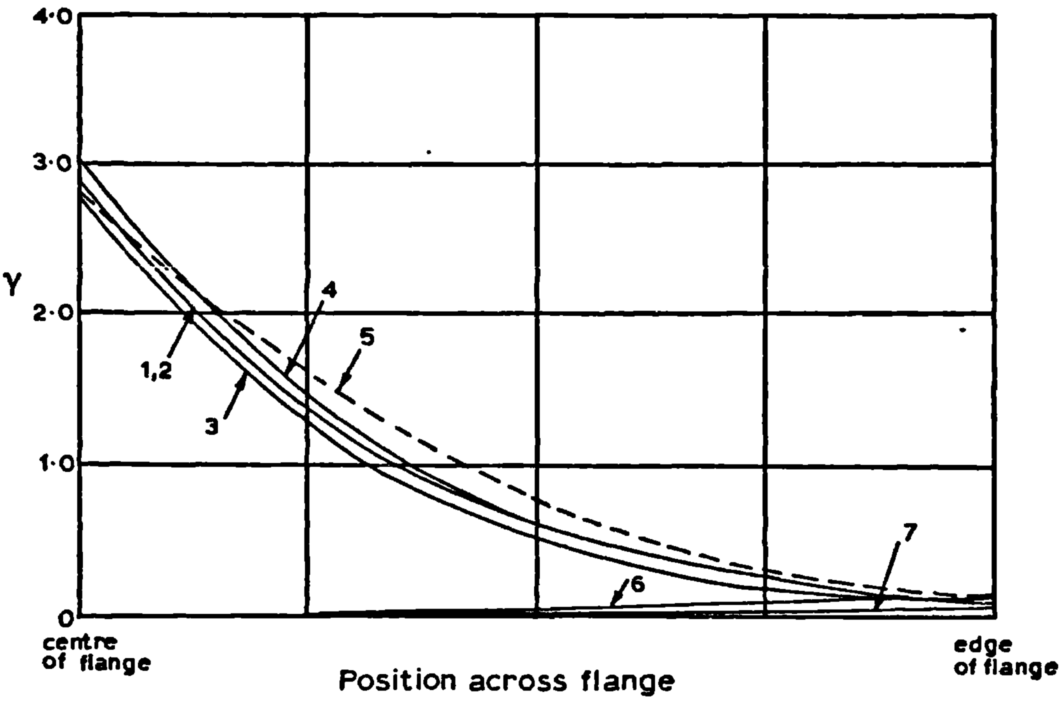

(b) B/L=0·20

Curve 1 : Longitudinal forces at quarter-span section for uniform load case
Curve 2 : Longitudinal forces at quarter-span section for point load case
Curve 3 : Longitudinal forces at support section for uniform load case
Curve 4 : Longitudinal forces at support section for point load case
Curve 5 : Proposed design curve for longitudinal forces
Curve 6 : Transverse forces at quarter-span section for uniform load case
Curve 7 : Transverse forces at quarter-span section for point load case

Fig. 6.5. Variation of shear connector forces with position across flange of simply supported tee girders having shear connexion I4

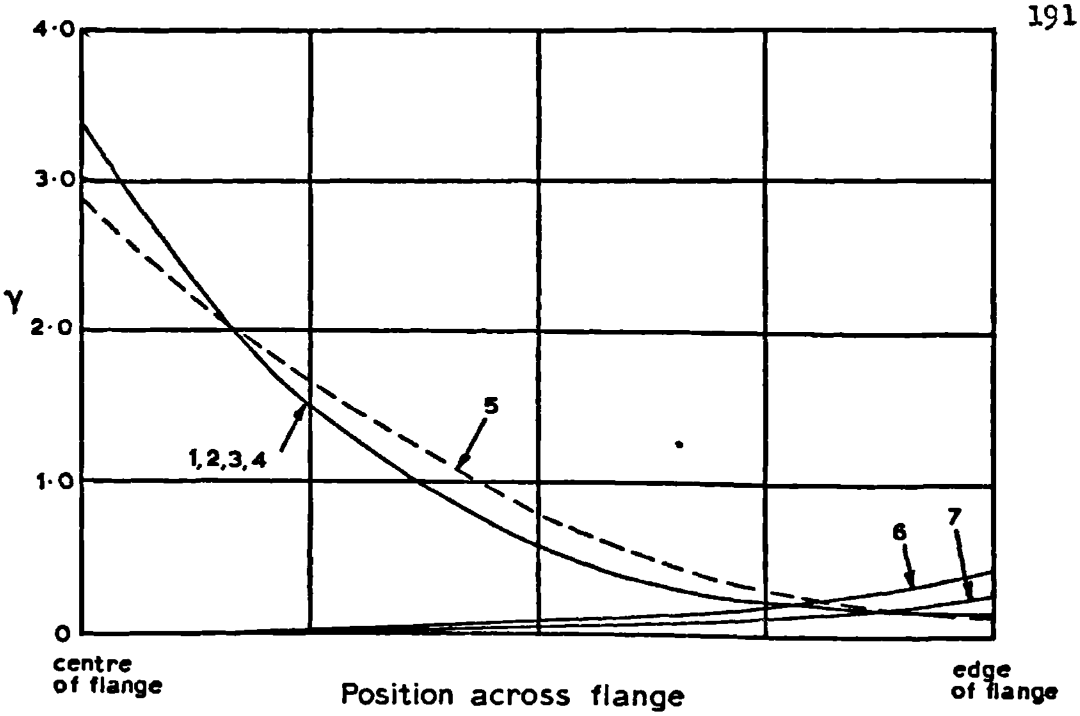

(a) B/L=0·05

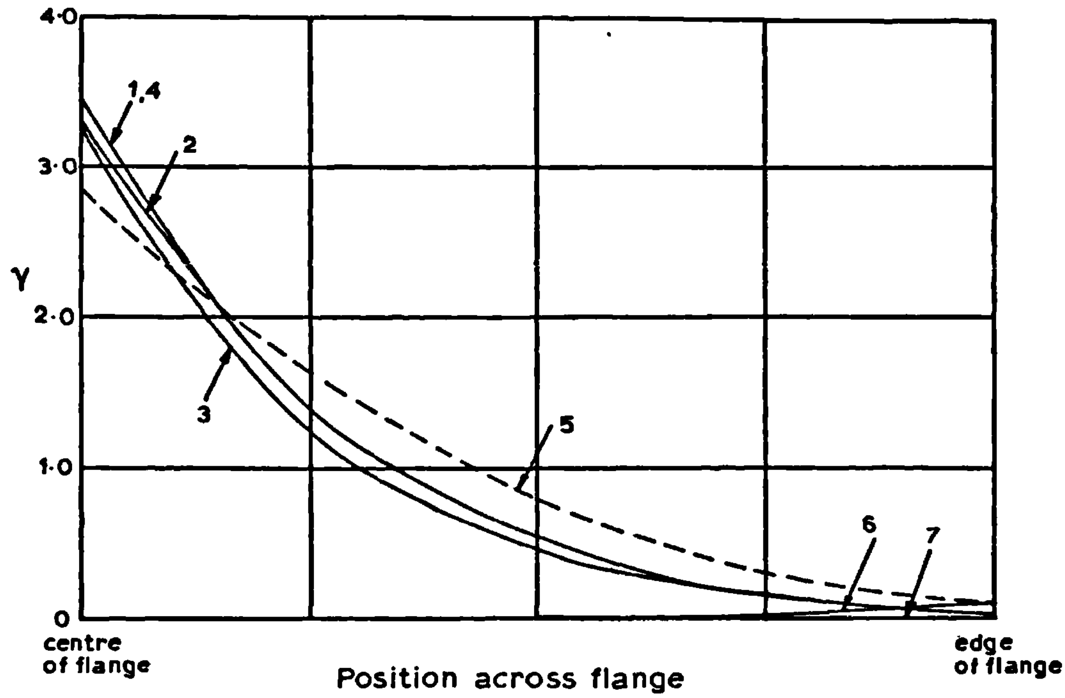

(b) B/L=0·20

Curve 1 : Longitudinal forces at quarter-span section for uniform load case
Curve 2 : Longitudinal forces at quarter-span section for point load case
Curve 3 : Longitudinal forces at support section for uniform load case
Curve 4 : Longitudinal forces at support section for point load case
Curve 5 : Proposed design curve for longitudinal forces
Curve 6 : Transverse forces at quarter-span section for uniform load case
Curve 7 Transverse forces at quarter-span section for point load case

Fig. 6.6. Variation of shear connector forces with position across flange of simply supported tee girders having shear connexion I5

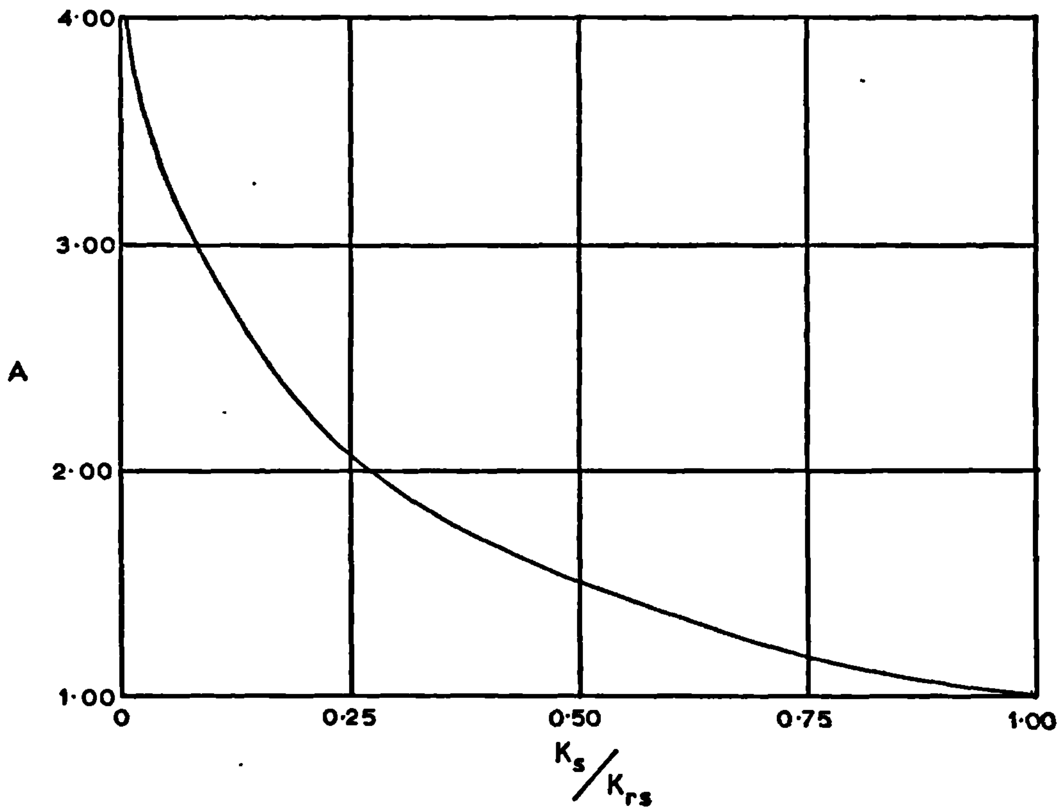

Fig. 6. 7. Curve for estimating value of A to be used in equation describing distribution of longitudinal connector forces across composite girder flanges

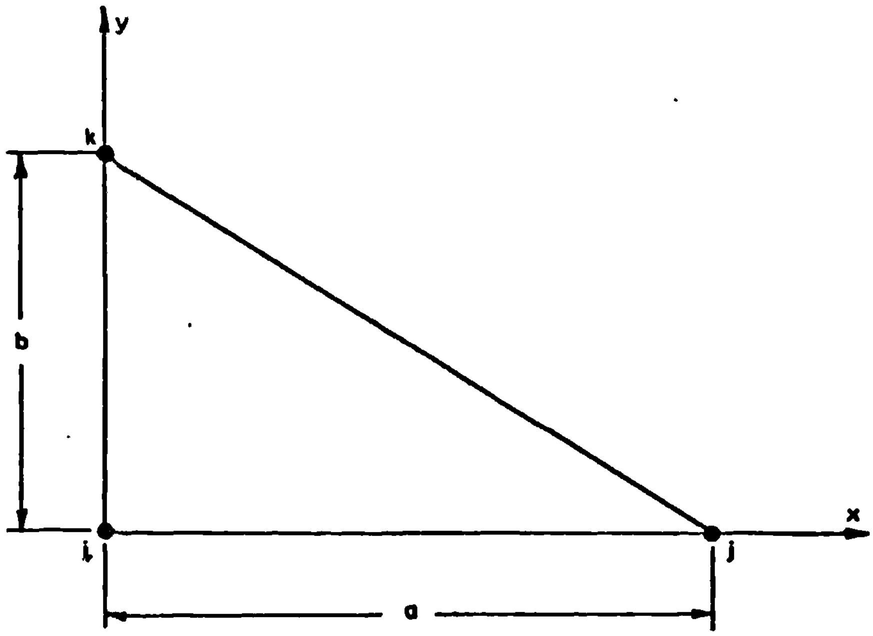

Fig. B.1. Triangular element

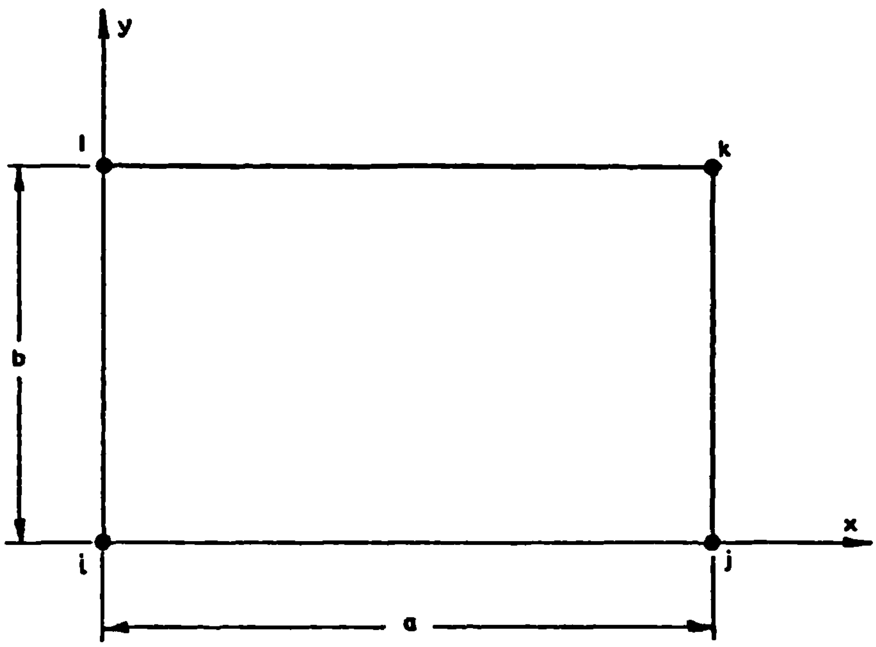

Fig. C.1. Rectangular element

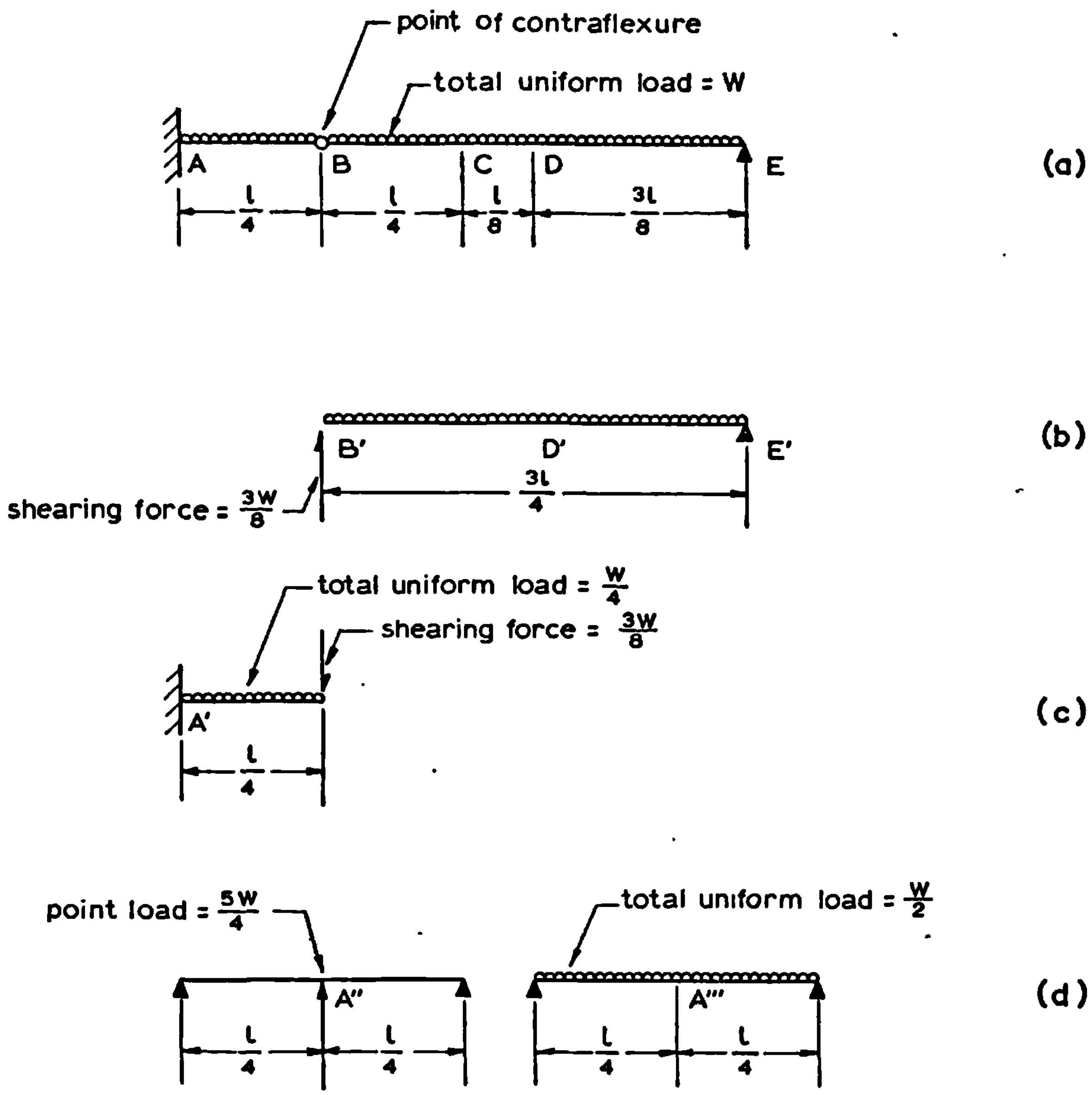

Fig. D.1. Representation of propped cantilever under uniform load as simply supported girders for purpose of estimating effective breadths

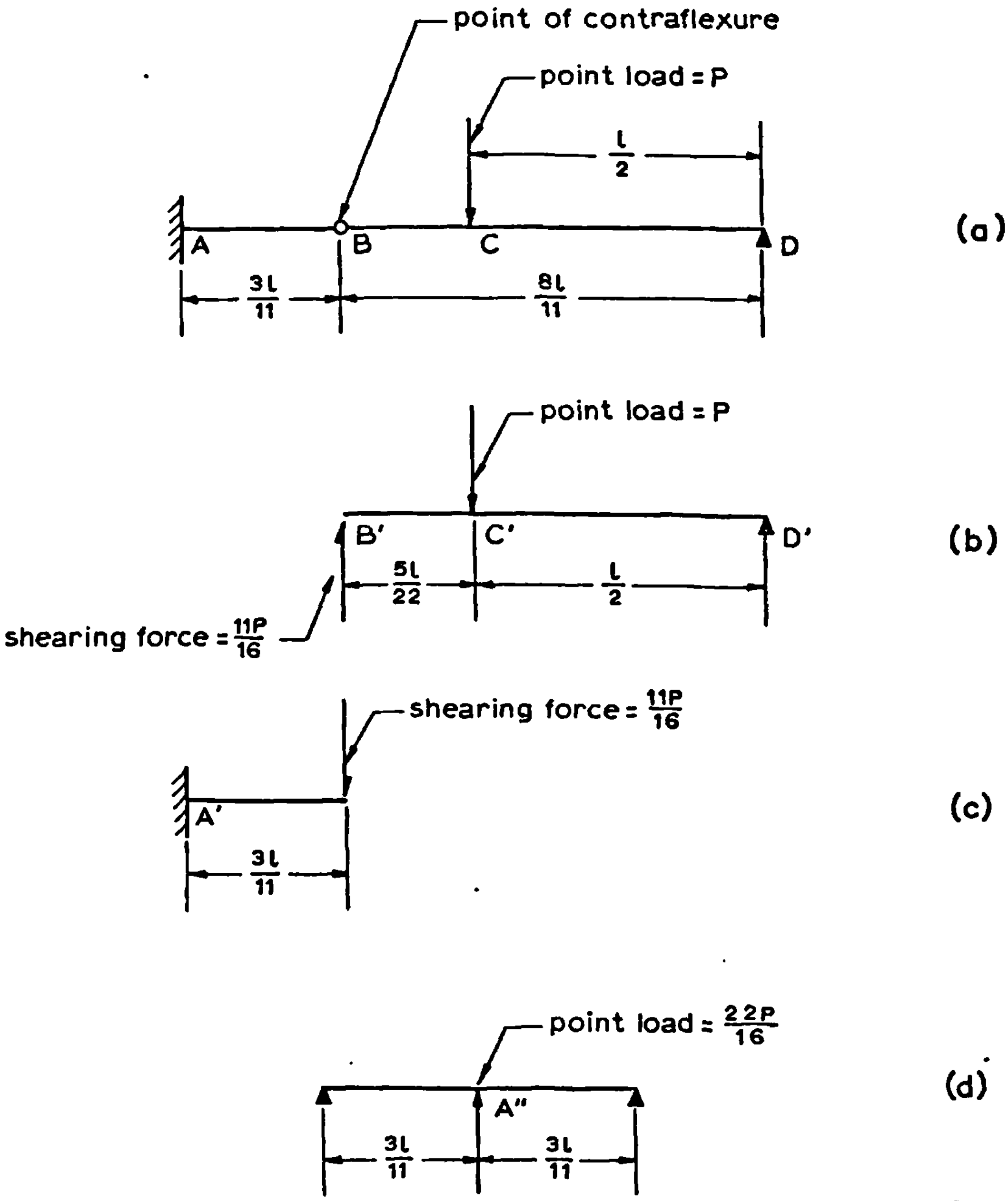

Fig. D.2. Representation of propped cantilever under point load as simply supported girders for purpose of estimating effective breadths